Università
Ca'Foscari
Venezia

PhD course in:

Science and Technology of Bio and Nanomaterials

in agreement with Centro di Riferimento Oncologico di Aviano

XXXIV CICLO

PhD Thesis

A metabolomics approach to predict trabectedin pharmacokinetic and pharmacodynamic variability in advanced soft tissue sarcoma patients

SSD: BIO/11

Coordinatore del Dottorato
Prof. Flavio Rizzolio

Supervisore
Dott. Giuseppe Corona

Supervisore cotutela
Prof. Flavio Rizzolio

Dottorando
Emanuela Di Gregorio
Matricola 956454

CONTENTS

ABSTRACT

Trabectedin is an anticancer drug mainly used in the treatments of patients with advanced or metastatic soft tissue sarcomas (STSs). Despite its recognized activity, a great variability in the pharmacological response is still observed among patients. So far, no effective and specific biomarkers have been identified, making challenging the assessment of the clinical outcome of trabectedin treatment. This metabolomics study aimed to find pre-dose serum metabolic signatures able to predict the individual variations in trabectedin pharmacokinetics (PK) as well as the overall clinical response to the treatment of STSs patients.

The study enrolled 40 metastatic STSs patients receiving trabectedin intravenously as single agent. For all patients pre-dose serum targeted metabolomics profiles, encompassing 51 amino acids and 16 bile acids, were determined by LC-MS/MS together with the plasma trabectedin PK profile up to 48 hours, measured by a novel validated HILIC-MS/MS method. Multivariate partial least square regression (PLS) and univariate statistical analyses were used to find correlations between pre-dose metabolites and PK as well as with the clinical response to trabectedin treatment. A risk prediction model for the overall survival of the patients was built by Cox multivariate regression analysis integrating metabolomics and clinical data.

Individual trabectedin exposure, expressed as area under the curve (AUC), showed a great coefficient of variation of 34% among patients. Multiple regression model, encompassing citrulline, cystathionine, phenylalanine/tyrosine ratio, taurocholic acid and haemoglobin, exhibited good predictive ability for AUC (bias of 5.16%; precision 16.85%) explaining up to 70% of the AUC variability. The PLS-discriminant analysis of the pre-dose metabolomic profile distinguished patients in stable (n=16) and progressive disease (n=20) and identified cystathionine and haemoglobin as specific metabolic signatures of trabectedin response. Moreover, the Cox risk prediction model, based on performance status, haemoglobin and citrulline, allowed to distinguish patients in high risk with low overall survival (OS $\leq$2.1 months) from those with long-medium survival (OS $\geq$19.1 months).

This translation study supports the use of metabolomics as potential tool to explain and manage the PK variability of trabectedin in STSs patients. The pre-dose metabolomics profile was found also useful to predict the clinical response to the trabectedin treatment as well as the overall survival of patients. The predictive and prognostic metabolomics signatures raised from this investigation may contribute to improve trabectedin therapy by the early identification of the patients who may receive the best benefit from the treatment.

ABBREVIATIONS

ESI	Electrospray ionization
GC-MS	Gas chromatography-mass spectrometry
HILIC	Hydrophilic interaction chromatography
IS	Internal standard
LC-MS	Liquid chromatography-mass spectrometry
LC-MS/MS	Liquid chromatography-tandem mass spectrometry
LIT	Linear ion trap
NMR	Nuclear magnetic resonance
OS	Overall survival
PCA	Principal components analysis
PD	Progressive disease
PFS	Progression-free survival
PK	Pharmacokinetics
PLS	Partial least squares-regression analysis
OPLS-DA	Orthogonal-Partial least squares-discriminant analysis
QQQ	Triple quadrupole
QTOF	Quadrupole Time-of-Flight
RP	Reversed phase
RT	Retention time
SD	Stable disease
STSs	Soft tissue sarcomas
VIP	Variable importance for the projection

1. INTRODUCTION

1.1 Metabolomics

Metabolomics refers to the comprehensive study of small molecules (<1 kDa) in biological cells, tissues, organs or organisms [1,2]. The term came from the analogy with the other omics sciences, indeed just as genomics studies the DNA, transcriptomics the RNA gene expressions and proteomics the proteins, metabolomics analyses the end products of cellular metabolism, which is influenced by both genetic and environmental factors. Being the downstream product of cellular regulatory processes, the metabolomic profile incorporates the complex interactions among gene transcription, protein expression and environmental factors such as age, sex, lifestyle and physio-pathological conditions (**Figure 1**). Moreover, unlike genome and proteome, the metabolome instantaneously reacts to the external stimuli allowing to immediately catch such temporal dynamic changes in biological fluids. For these characteristics, the metabolome can provide a reliable snapshot of the current individual phenotype [3], which is useful to reveal host metabolic alterations induced by the disease or by treatments as well as to discover novel biomarkers for diagnosis and prognosis [3–8]. The study of metabolome is however very complex. Metabolomics profiling analysis involves countless molecules deriving from disparate endogenous molecular pathways besides those from diet, xenobiotics and the gut microbiome activity. All these metabolites belong to several classes, such as amino acids, lipids, carbohydrates, and present completely different chemical structures. This makes the analysis of the whole metabolome very challenging, and currently, there is not a unique analytical method able to detect with large coverage the metabolites present in biological matrices [9].

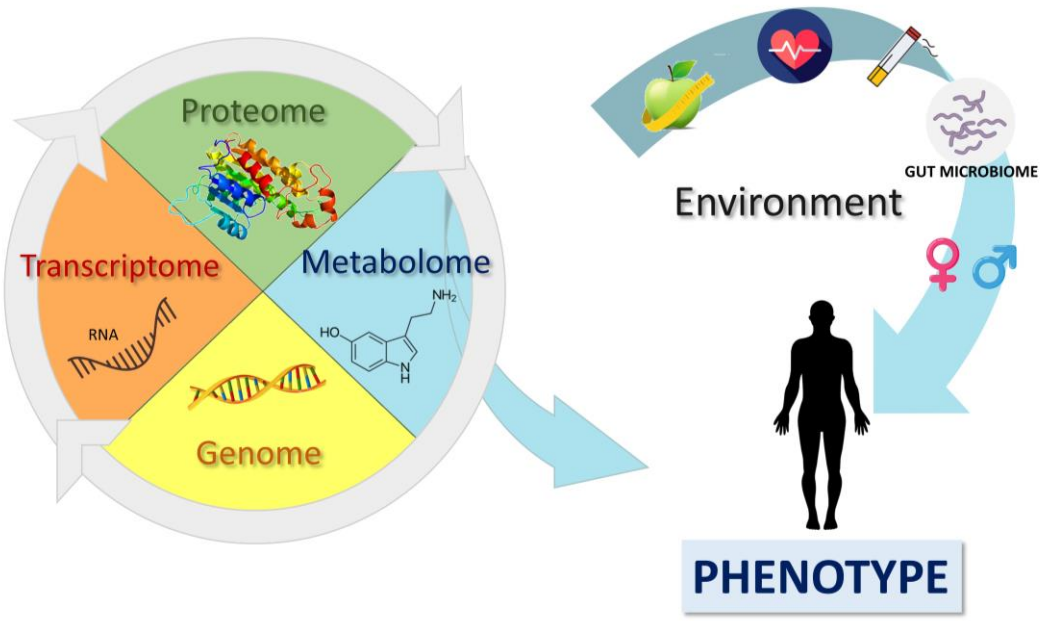

Figure 1. Overview of the omics flow from genes to phenotype. Metabolomics represents the downstream result of the genome, transcriptome and proteome but also the upstream input from the environment and therefore it is the most representative of the individuals' phenotype.

1.1.1 Metabolomics workflow

Two main approaches are generally used in metabolomics studies, untargeted and targeted. The first refers to the comprehensive analysis of all known and unknown metabolites in a sample, and it is usually applied in hypothesis-generating studies, such as novel biomarkers discovery or for elucidating metabolic pathways [10]. In an untargeted metabolomics profiles analysis, both the sample extraction and chromatographic separation methods are set to minimize the selectively and instead ensure the widest metabolites coverage. The analytical platform usually includes proton nuclear magnetic resonance (^{1}H-NMR) or mass spectrometry (MS) coupled with separation systems such as liquid (LC) and gas chromatography (GC). The ^{1}H-NMR is a non-destructive technique able to detect a great span of metabolites, being the detection based on the C-H proton resonance signals. This analytical platform has the advantage to be intrinsically quantitative and not to require samples' processing steps, thus ensuring a very high reproducibility in the analysis. However, the main drawback of ^{1}H-NMR is the low sensitivity with a detection limit in the mM - μM range, which narrows its application to specimens with high abundant metabolites [11,12]. Conversely, MS allows the quantification of metabolites with higher sensitivity, although, compared to NMR it shows lower reproducibility, being pre-analytical sample preparation and chromatographic separation steps required. The MS instruments of choice for untargeted investigations are the high-mass resolution mass spectrometer (HRMS), such as Orbitrap, which has a very high resolution (70,000-280,000) and mass accuracy (1-5 ppm), and quadrupole time-of-flight (QTOF) with a bit lower resolution (30,000-40,000) but faster scan speed [10]. HRMS usually couples the full scan spectra with tandem mass spectra measurements (MS/MS) to facilitate compound identification. Two main tandem data acquisition approaches are generally used: *a)* data-dependent acquisition (DDA) consists of a full MS scan followed by selection and fragmentation of the most intense ions to obtain their MS/MS spectra [13]; *b)* data-independent acquisition (DIA) integrates the full scan MS with tandem MS/MS fragmentation for all precursor ions detected within a narrow masses' window either simultaneously (all-ion fragmentation, AIF) or in sequential mass ranges (sequential window acquisition of all theoretical fragment-ion spectra, SWATH) [14,15].

Targeted metabolomics requires *a priori* knowledge of the metabolites of interest and it finds application in the investigation of specific metabolic pathways or to validate biomarkers resulted from untargeted experiments [16]. The advantage of the targeted approach is the absolute quantification of the compounds, obtained thanks to the use of pure standards and labelled internal standard (IS) (e.g. ^{13}C, ^{2}H, ^{15}N). Moreover, unlike the untargeted approach, the chromatographic separation and the MS parameters are optimized in order to isolate specific molecules and exclude signals from the background matrix, thus yielding high sensitivity and selectivity. Triple quadrupole (QQQ) or the hybrid QQQ-linear ion trap (QTrap) are the MS instruments mainly used due to their high sensitivity and selectivity, especially when used in multiple reaction monitoring (MRM) mode. The main drawback of this targeted approach is the reduced metabolite coverage, however research

efforts have led to the creation of targeted large-scale metabolic profiles allowing the simultaneous detection of hundreds of compounds [17–19]. Finally, it is worthy to mention that data obtained from targeted investigations can be immediately used and do not need of complex and time-consuming processing steps, required instead by untargeted analyses [20].

1.1.2 Targeted metabolomics

For the above-mentioned advantages, the present research project adopted the targeted approach. The typical metabolomics workflow is depicted in the schematic figure (Figure 2). The main steps consisting of sample preparation, chromatographic separation, detention, quantification, and data analysis, will be discussed with main focus on the LC-QQQ system used in this thesis work.

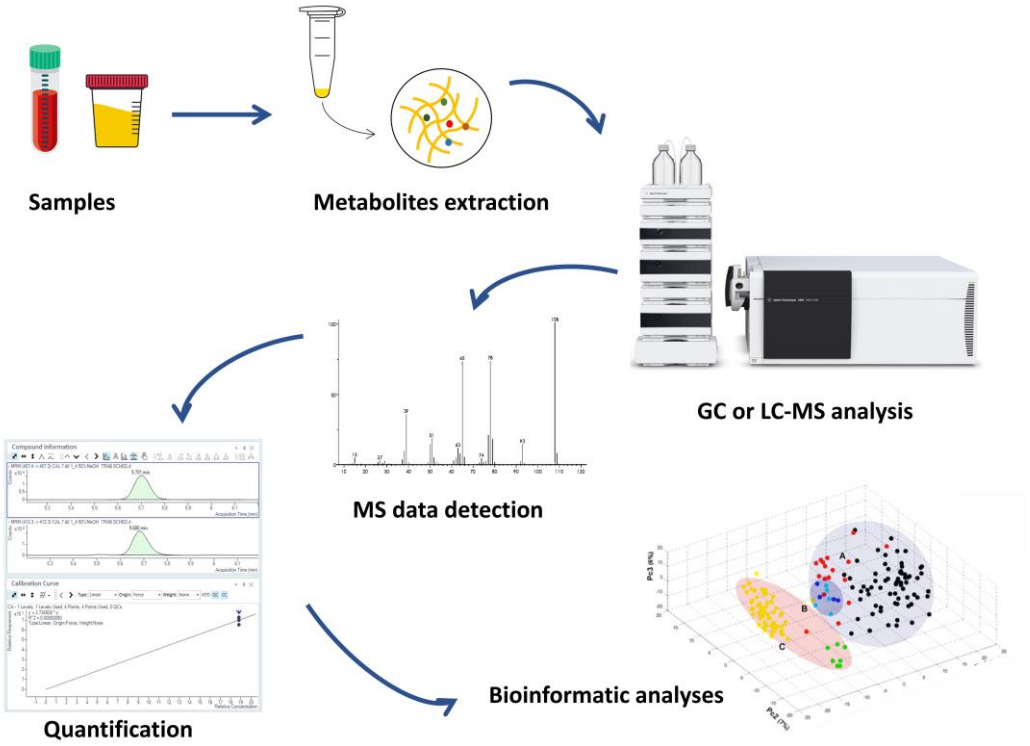

Figure 2 Targeted metabolomics workflow. Metabolites are extracted from the sample biological matrix followed by chromatographic separation and MS detection. Raw data are then converted into quantitative data and subjected to bioinformatic analyses using univariate and multivariate statistical approaches.

Pre-analytical sample preparation

Specimens mostly analysed in metabolomics clinical studies include whole blood, serum, plasma, urine, saliva and cerebrospinal fluid. Many samples processing techniques can be performed to ensure efficient extraction of the metabolites of interest, and the protocols can be tailored according to the physicochemical properties of the analytes, their abundance, and the available sample volume. Besides metabolites extraction, sample preparation is also extremely important to improve chromatographic performance. The removal of proteins and other constituents of the matrix can avoid the clog of the chromatography column, moreover, the organic solvent and the pH of the

injected extract can have a profound effect on peak shapes, peak separation and retention times (RT), consequently affecting the selectivity and sensitivity of the assay. Among the sample processing techniques, the protein precipitation with organic solvents is the most simple and fast method, though it does not allow to have totally purified extract and to concentrate analytes. Conversely, liquid-liquid (LLE) or solid-phase extraction (SPE) ensure a clearer and concentrated extract solution but are more labour intensive. Indeed, the LLE consists of multiple steps including analytes partitioning between the aqueous and organic phases, evaporation, and reconstitution of the extract in a solvent miscible with the LC mobile phase. The SPE has a similar procedure, but the analytes are captured in a selective stationary phase and after several washing steps, are eluted with an opportune solvent mixture. Instead of classic solid phase with cartridges or plates, the online SPE uses a "trap" column before the LC system, thus minimizing the hands-on time of the protocol.

Chromatographic techniques

A separation step is usually performed prior to MS detection mainly using chromatography either GC or LC. The GC technique is popular for the analysis of volatile compounds. Analytes are separated on the basis of their intrinsic evaporation properties using temperature gradients generated by an inert gas flowing on the stationary phase [21]. However, GC presents some pitfalls generally linked to the possible degradation of thermolabile compounds and to the cumbersome and time-consuming sample preparation, that requires the derivatization of the non-volatile analytes [22].

In respect to GC, LC enables the analysis of thermolabile and not-derivatizable molecules. Several LC stationary and mobile phases can be chosen according to the chemical-physical properties of the analytes to measure. Reversed-phase (RP) chromatography is the commonly used technique for nonpolar or weakly polar compounds since the separation is based on the hydrophobic interactions between the analytes and the hydrophobic stationary phase such as C18. One of the main advantages of RP is represented by its high reproducibility and resolution, that have contributed to its wide application in many metabolomics and lipidomics studies [23–27]. However, over the last decades, numerous metabolomics investigations have exploited the hydrophilic interaction liquid chromatography (HILIC) [28–33]. This technique allows to better retain polar and hydrophilic metabolites thanks to the use of a highly hydrophilic stationary phase on which the aqueous-organic mobile phase forms a water layer. The retention mechanism in HILIC is the result of the analytes partitioning between such water layer and the mobile phase mainly occurring by hydrogen bonds and electrostatic interactions. This technique shows the advantage to provide enhanced MS signals due to the use of high percentage of organic phase that favours the ions desolvation. Moreover, the possibility to directly inject organic extract significantly simplify the sample preparation, making HILIC an interesting technique for metabolomics high-throughput analyses [29,34].

Mass-spectrometry detention

Chromatography separation is followed then by MS detection, which is considered the gold standard technique for metabolomics investigations requiring high sensitivity. The latter is significantly affected by the ionization step since the analyte MS signal is directly proportional to the number of ionized molecules. Among the ionization MS sources, electrospray ionization (ESI) is commonly used in LC-MS metabolomics studies since it produces efficient molecules ionization directly in the liquid phase. However, the main drawback is the ion suppression occurring when, analysing complex matrix, co-eluting compounds can compete for charge in the ionization process quenching the MS signal of the analyte of interest [35]. Atmospheric pressure chemical ionization (APCI) less suffers from ion suppression and it is very helpful to analyse non-polar compounds poorly ionized by ESI; indeed ionization occurs in a mixture of liquid and gas that, at atmospheric pressure, has high collision frequency [36]. For the ions' separation, the most commonly used mass analysers in targeted metabolomics, are those arranged in tandem (MS/MS). Among them, the QQQ and the QTrap are widely employed [37], since they allow the concomitant identification and quantification of the metabolites. A high degree of specificity is obtained when used in MRM mode [38]. In MRM the first quadrupole (Q1) operates as first filter of the precursor ion, which is then fragmented in the second quadrupole (Q2) by collision-induced dissociation (CID) and finally, the resulting product ions are accelerated into the third quadrupole (Q3) that further filters a particular selected m/z fragment [16]. The specificity of the assay derives from fact that generated fragment ions are strictly dependent on the chemical structure of the precursor molecule and not on its mass, thus allowing to distinguish also isobaric compounds on the base of their fragmentation pattern. The QTrap combines the QQQ and linear ion trap (LIT) technologies that enables the absolute identification of unknown compounds. Indeed, the Q3 can work either as a quadrupole or ion trap, and by scanning secondary product ion (MS^3), it can provide additional qualitative structural information on the analyte [39].

Quantification

The quantification in targeted MS metabolomics investigations strictly requires the use of pure standards to build calibration curves and corresponding labelled IS, necessary to control analytical variability. The chromatographic and MS performance may decrease over time, matrix ion suppression and RT drifts can occur, creating differences among batches of analyses or even in the same analysis. The normalization of the peak area of the analyte for that of its IS can control such analytical bias and ensure reliable and robust measurements. Moreover, in order to verify whether the reproducibility and accuracy of measurements among batches is within the accepted range of tolerance, multiple injection of quality controls (QCs) with known nominal concentration, are usually run along the analytical batch.

Data analysis

The outcome of a targeted metabolomics analysis is generally a complex data matrix with hundreds of variables, that require pre-treatment steps and multivariate statistical analyses before extracting information. Data pre-processing consists of normalization, transformation and scaling of the raw data [40]. Normalization prevents that systemic biases can affect data reliability. Beyond IS normalization, other methods can be applied according to sample type or the analytical method. For instance, creatinine concentration normalization is commonly used to correct the variability among individuals' urine volumes [41], while the total ion current (TIC) area normalization is the approach used mainly in semiquantitative methods. Data transformation is generally performed to correct for heteroscedasticity and allow parametric test, whereas scaling permits to adjust the fold differences among variables and fit them within the same range [40].

Data pre-treatment is followed by statistical analysis. Univariate methods alone cannot meet the requirements of a complex metabolomics dataset, hence, multivariate statistical approaches, able to reduce the dimensionality of the dataset, are necessary to make the understanding of the data simpler and faster. Principal component analysis (PCA), partial least square-discrimination analysis (PLS-DA) and orthogonal PLS-DA (OPLS-DA) are some of the most commonly used multivariate analyses to identify differences between groups. PCA is an unsupervised technique where input data are unlabelled (no classes are given, e.g., case-control). PCA separation occurs only if the intragroup variability is smaller than the intergroup variability, a very rare situation in real clinical samples [42]. On the other hand, supervised PLS-DA and OPLS-DA can better highlight differences among groups, however, they tend to overfit the data, especially when the high dimensionality data correspond to small sample size. This over-fitting issue can be verified by model validation tests, ideally splitting the dataset into a training set, used to build the model, and a testing set used to estimate the predictability [43]. When the number of samples is too small, an alternative approach can be the cross-validation method or leave-n-out, where the dataset is divided into n subsets, and each one is in turn removed from the model and used as a testing set [42]. Results of the cross-validation tests are the quality parameters R^2 and Q^2 values that indicate the goodness of fit and predictability of the model respectively, with $R^2 = 1$ indicating perfect description of the data by the model, and $Q^2 = 1$ perfect predictability. A model with $Q^2 > 0.5$ is admitted for good predictability, however, it is difficult to assign a general threshold in the biological context, and many models have been published with a Q^2 below 0.4 or even below 0.3 [44,45]. In these cases to better assess the quality of the model, permutation test is performed, where samples are randomly permutated to generate and compare new (O)PLS-DA models [43].

1.1.3 Clinical metabolomics: potentiality and challenges

Despite metabolomics clinical studies have been emerged relatively recently, the detection of metabolites as source of information about disease precedes the introduction of metabolomics itself.

Ancient Chinese doctors used ants as "biosensors" to evaluate the "sweetness" of urines and recognize what is now known as diabetes, as well as Egyptians observed changes of urine taste and smell during certain medical conditions [46]. However, the introduction of the modern concept of "individual metabolic profile" can be tracked back of 80 years, when Roger Williams using more than 200,000 paper chromatograms fingerprinted the profiles of patients affected by different diseases, showing that each one has a characteristic metabolic pattern [47]. The term "metabolic profile" was officially coined some decades later by Horning, Pauling and Robinson, that developed the first GC-MS-based method to measure hundreds of metabolites in human breath and urine [48,49], launching the basis for the application of metabolomics in clinical chemistry [50–52].

Nowadays, metabolomics is finding large application in clinical research with the great perspective to work as a translation tool and a bridge between pre-clinical and clinical results [3,53–55]. The analysis of metabolome has been shown to provide remarkable insights about the disease mechanism, the pathological conditions and also to improve the diagnosis and prognosis of patients [4,56,57]. Its application in cancer research has been significantly growing; as cancer cells have a characteristic metabolic phenotype, metabolomics may help to disclose mechanisms underlying the uncontrolled cellular proliferation and identify novel potential targets for drugs as well as to improve the assessment of therapeutic interventions [54,58,59]. However, the exponential number of metabolomics investigations in clinical studies has been rising in parallel with the methodological challenges, since paradoxically the more sophisticated and advanced technologies, have led to the accumulation of big data difficult to manage. Moreover, many analytical pitfalls may be occurred in the entire workflow and potentially affect the biological interpretation, likely contributing to the quite common trouble to translate metabolomics findings into clinical application [60,61]. One of the problems is the difficulty to compare the results of independent research studies because of the lack of standardized metabolomics methods and protocols. For instance, the different sample collection and storage rules as well as sample analytical processing, have a significant impact on the metabolites detection mainly because of compounds' stability issues or not efficient or non-selective extraction procedures [62,63]. Another source of variability is the choice of the analytical instrumentation and chromatography technique, which determine the span of the covered metabolome and the degree of reliability of the data. This is particularly true for untargeted analyses where semiquantitative data of unknown molecules are obtained [60]; conversely, the absolute quantification allows to have more meaningful and inter-labs comparable results and it is an unavoidable requirement for clinical metabolomics translation and application. Last but not least, the post-analytical processes play a crucial role in determining the results' accuracy. First of all, analytical errors such as instrumental drift, ion suppression or batch effects, that can jeopardize the quality of the data, has to be assured before data analyses and opportunely solved [64,65]. Afterwards, the different pre-treatment methods (data normalization and scaling) can greatly affect the final statistical metabolomics model [66] thus scientists should ensure that the observed results are not an artifact of the statistical data

processing but truly reflects a biological phenomenon. Finally, the compound identification is the bottleneck of untargeted metabolomics, and despite the big number of tools and available databases, only 2% of human metabolites have been currently annotated with the remaining 98% falling into the "dark metabolome" [67]. The future of metabolomics can be revolutionized by artificial intelligence (AI) and machine learning (ML). AI is referred to the technology able to simulate human thinking capability and behaviour, whereas ML is a subfield of AI which enables a computer system to automatically learn from historical data and make decisions without being previously programmed [68]. The use of computational approaches rather than human intervention would allow to analyse metabolomics complex data faster and more accurately accelerating the translations of the metabolomic results from the bench to the clinics [69–71].

Although metabolomics still suffers from some issues, the scientific community is working to overcome them and enhance the effectiveness of metabolomics studies. So far, metabolomics represents the most powerful tool for clinical research with the great potentiality of improving the clinical management of severe diseases such as cancer, not only by providing predictive and prognostic biomarkers but also allowing to assess the response to drug treatments. In this context, a specific application of metabolomics in clinical pharmacology, called pharmacometabolomics, has been revealing interesting in precision medicine. Indeed, pharmacometabolomics could predict drug effectiveness and/or toxicity based on the individual phenotype, thus guiding physicians in the achievement of personalized therapy [72].

1.1.4 Pharmacometabolomics

Personalized medicine has the ambitious goal to tailor the drug treatment for the single individual maximizing the therapeutic effect with the least adverse effects. Many factors including genotypes, gut microbiota, lifestyles, pathophysiological status, gender, age, etc. [73] determine the drug PK and pharmacodynamics variations thus leading to different drug response and making challenging the prediction of the patients' clinical outcome. Pharmacometabolomics profile can assess the sum of all these factors and help to predict such inter-individual drug variability overcoming the "trials and error" medical approach, currently used to establish the therapeutic plan of patients. This is remarkably important for cancer treatments where the used chemotherapy agents have a narrow therapeutic index, and the variability in the drug exposure can translate into over-dosing and side effects, or into under-dosing and therapeutic failure. Hence, the identification of markers predictive of the drug response would avoid wasting precious time and ensure therapeutic continuity. Many pharmacometabolomics studies aimed to identify biomarkers predictive of PK parameters useful to optimize drug dosing regimens [74–77]. One of the first investigations regards the immunosuppressant tacrolimus, characterized by a narrow therapeutic index and a high degree of individual variation in blood drug concentration. In the study, the pre-treatment urine metabolomics profile was correlated with the area under the curve (AUC) of tacrolimus and four

endogenous metabolites were found able to predict patient's drug exposure allowing to select the individual dose before administration [76]. Pharmacometabolomics can be also applied to study the metabolism of drugs, whose high variability among patients can lead to big differences in drug clearance [73,78–81]. Such variability is mainly associated with alterations in the activity of metabolizing enzymes, that can significantly be affected by other drugs, such as in the case of co-therapies, or by endogenous metabolites. An example is the investigation of Rahmioglu et al. that identified urine metabolic markers associated with the induction or inhibition of cytochrome CYP3A4, allowing the prediction of midazolam clearance [79]; another is the study on paracetamol whose sulphation metabolism was found to be competitively decreased by p-cresol produced by gut microbiome [73]. Besides PK prediction, pharmacometabolomics has been employed to monitor the pharmacodynamic response to treatment, providing biomarkers of drug efficacy or even elucidating mechanism of action [4,82]. These studies collectively, demonstrate that pharmacometabolomics has the potential to improve treatment strategies, guiding physicians in the selection of the optimal drug dose as well as in the establishment of the best therapeutic program by *a priori* prediction of the clinical outcome. In this context, the present research work focused on the anticancer drug trabectedin to search for metabolomics signatures associated with its high PK and pharmacodynamics variability among STSs patients. To date, this disease lacks both predictive and prognostic biomarkers, making challenging the assessment of the clinical outcome and highlighting the need to improve the knowledge about the factors implicated in such high inter-patient variability to treatments.

1.2 Trabectedin in STSs treatment

STSs are rare group of tumours of mesenchymal origin accounting for about ≈ 70-80% of sarcomas and 1% of all malignancies [83]. The World Health Organization (WHO) reported an incidence rate of 5 cases per 100,000 people [84] with a higher incidence in men in elderly age [84,85]. About 100 different STSs histotypes were recognized with origin from disparate anatomical sites, such as smooth muscle (leiomyosarcoma), adipocyte (liposarcoma), fibroblast (dermatofibrosarcoma), striated muscle (rhabdomyosarcoma), peripheral nerve tissues (malignant peripheral nerve sheath tumour), endothelium (angiosarcoma) and the other unknown origins (undifferentiated pleomorphic sarcoma) [84]. Leiomyosarcoma and liposarcoma (L-sarcoma) are the most frequent subtypes accounting for about 26.2% and 16.1% respectively [86].

Conventionally, surgery is the standard treatment for localized STSs tumours, in some cases preceded by radiotherapy [87], while chemotherapy is reserved for patients with locally advanced or metastatic STSs. The first-line treatment usually includes the anthracycline doxorubicin as single agent or in combination with the alkylating agent ifosfamide [88]. Trabectedin is used as second-line treatment for metastatic STS patients unsuited for anthracycline chemotherapy. It is a tetrahydro-

isoquinoline initially isolated from the marine tunicate *Ecteinascidia turbinata* and currently semi-synthesised from the secondary metabolite cyanosafracin-B, derived from fermentation media of bacteria *Pseudomonas fluorescens* [89]. Trabectedin has been shown to have higher efficacy in L-sarcoma [90] and translocation related-STSs [91–93], although, a great response variability still exists and prognosis for metastatic patients remains poor [94].

1.2.1 Pharmacodynamics and pharmacokinetics of trabectedin

The antitumor activity of trabectedin is explained through a complex mechanism action that affects biological processes both in tumour cells and in the tumour microenvironment (TME). Unlike other anticancer drugs, trabectedin covalently binds DNA in the minor groove by alkylation of the N2 guanidine, inducing the bending of the DNA towards the major groove with consequent double-strand break [95]. A part of the drug molecule protrudes out of the DNA and probably interacts with several proteins and transcription factors, triggering a cascade of events that cease the activated transcription and poison DNA nucleotide excision repair (NER) mechanisms [96–98]. In particular, trabectedin can inhibit the transcription by direct induction of RNA polymerase II degradation [97,99] or indirectly by two different mechanisms [100]. The first one is linked to DNA structural modification induced by trabectedin itself that hinders the recognition of transcription factors to DNA site [101,102]. A representative example regards the myxoid liposarcoma, where trabectedin was found to promote differentiation by displacing from targeted promoters, the abnormal transcription factor responsible of the tumour pathogenesis [91,101,102]. The second indirect mechanism is associated with the formation of a trabectedin-DNA adduct, stabilized by covalent bond with one DNA strand and by van der Waals forces and hydrogen bonds with the opposite strand. Such stable structure was found to mimic an interstrand crosslink, a type of DNA lesion, which results highly effective in blocking transcription [97,103]. Besides these molecular mechanisms, trabectedin displays the antitumor activity by affecting key processes in the TME. The latter is a complex system of multiple cells such as inflammatory leukocytes, activated fibroblasts, endothelial cells, that are able to promote tumour survival and progression [104]. Trabectedin was found to induce apoptosis of mononuclear phagocytes (monocytes and macrophages) through activation of caspase 8 by membrane signalling TRAIL receptors expressed in these cells [105–107] and in addition, to cause a significant decrease of pro-inflammatory mediators secreted by both monocytes/macrophages and tumour cells, with consequent reduction of angiogenesis [105–107].

For the treatment of STSs, trabectedin is administered at the dose of 1.5 mg/m^2 body surface area as an intravenous infusion over 24 hours every three weeks. PK studies demonstrated large values of volume of distribution, that range from about 1000 to 4000 L, reflecting the extensive tissue distribution of the drug and high plasma proteins binding (94% to 98%) [108]. The dose-time trabectedin PK profile suggests multiexponential elimination kinetics, since plasma levels drop

rapidly at the end of the infusion and then slowly decline in the terminal phase with a long terminal half-life of about 180 hours [109]. Elimination of trabectedin mainly occurs in the faeces and less than 1% in urines, where only a negligible amount of unchanged drug was measured, indicating an extensive liver metabolism [110,111]. Many cytochrome (CYP) enzymes metabolize trabectedin, but *in vitro* studies indicated that CYP3A4 is the main responsible of the oxidative metabolism [112,113] as further confirmed in patients treated with trabectedin co-administered with rifampin (CYP3A4 inducer) or ketoconazole (CYP3A4 inhibitor) [114]. The trabectedin plasma clearance is approximately 31.5 L/h with a large inter-and intra-variability of 51% and 28%, respectively, and neither age nor gender were found associated with such variability [115]. Considerable inter-patients variability was reported also for the other PK parameters [109,115–117] hampering the total control of total drug exposure. Since the pharmacodynamics effect (efficacy and toxicity) of a drug depends also on its bioavailability, the inter-individual variability in PK may contribute to the differences in the response to trabectedin treatment among patients. However, so far no effective biomarkers to assess trabectedin efficacy and the prognosis of STSs patients are available; further investigations are strongly necessary to guide physicians in trabectedin therapy management.

1.2.2 Prognostic biomarkers in STSs

Patients with metastatic STSs experience a poor prognosis with a median survival of approximately one year from the first-line therapy. Currently, very few prognostic factors are used for STSs such as tumour size, tumour grade, histologic subtype, and age at diagnosis [118,119]. However, the prediction of the patients' outcome remains sub-optimal and only about 50% of people survive within 5 years from diagnosis [85,120], underlying the need of more accurate prognostic biomarkers. Different research studies have explored blood markers, mapping genome and transcriptome to assess genetic and epigenetic variations associated with STSs response to treatments [121–125]. For instance, the mutations in tumour suppressor genes *PTEN*, *RB1* and *TP53* were identified in patients in progression disease [126], as well as molecular signatures of microRNA were found associated with a more proliferative and invasive tumour [127,128]. A small number of studies used metabolomics to search for potential novel prognostic markers for STSs, but they mainly involved *in vitro* investigations [129,130], and only one was a clinical study [131]. The latter identified some AAs, γ-aminobutyric acid (GABA) and carnosine, whose serum decrease was found correlated with a better response to the chemotherapy treatment [131]. However, none of these studies was specifically designed to identify prognostic markers of trabectedin treatment and to date, few retrospective studies have been published. Their results highlighted some common clinical data such as low performance status (PS), tumour grade and absence of metastasis as predictive of a good prognosis, while hyponatremia, anaemia and high blood levels of absolute neutrophil count (ANC) have been associated with a worse outcome [132,133]. Another small number of studies have focused on the nucleotide excision repair genes to identify predictive factors for trabectedin efficacy

[134–136], finding high expression of *ERCC/5*, and *BRCA1* in patients with longer survival. However, the prognostic power of these genetic and clinical factors is limited and better markers are needed to improve clinical treatment of STSs patients with advanced disease. In order to fill this gap, in this study, we attempt to search for predictive markers of trabectedin efficacy as well as of its PK variability by metabolomics, aware that the individual metabolome can provide useful insight to improve the current knowledge about those factors that contribute to the different clinical outcome among STSs patients.

2. MATERIALS AND METHODS

2.1 Design of the experiment

The present monocentric observational study enrolled 40 patients with locally advanced and metastatic STSs who were undergoing trabectedin. The first aim of the study was to find a predictive model based on pre-dose serum endogenous metabolites able to explain the trabectedin PK variability observed in the studied STSs population. For the assessment of PK, a novel analytical LC-MS/MS method was developed and validated. Blood samples were collected before treatment (baseline) for the metabolomics profile measurement, during 24h-continuous intravenous infusion and up to 48 h from the starting therapy (0, 2, 4, 8, 24, 25, 28, 32, 48 hours) for PK determination. The PK parameters, area Under the Curve (AUC_{0-48}) and maximum concentration (C_{max}), were considered for the further pharmacometabolomic analysis since AUC represents the total drug exposure, while C_{max} informs about the dose-adverse effects relationship. The second aim of the study was to look for metabolomics signatures associated with trabectedin pharmacodynamics evaluated in terms of clinical outcome. Two clinical endpoints were considered as measurement of the treatment efficacy: a) clinical benefit, assessed at the third chemotherapy cycle, defined as the proportion of subjects with stable disease (SD) or with increase tumour size and progressive disease (PD); c) OS calculated from the date of starting trabectedin chemotherapy to death or last follow-up (**Figure 3**).

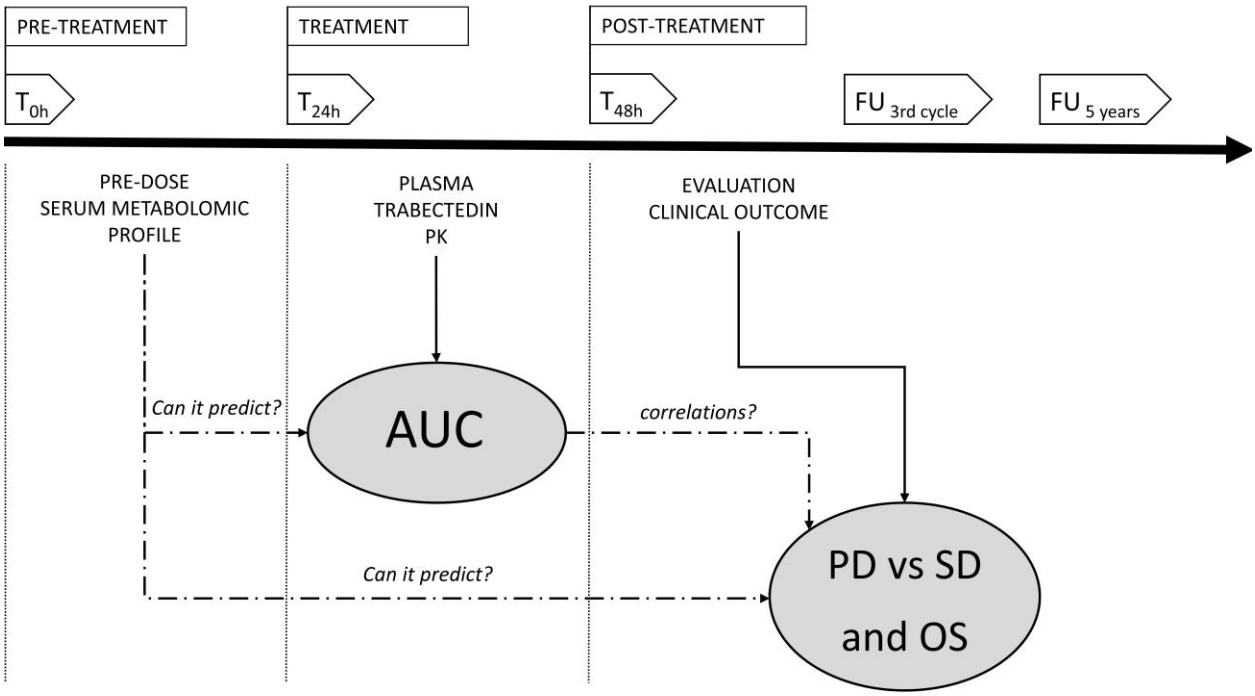

Figure 3. Schematic representation of the study design.

2.3 Patients' population

Forty patients with locally advanced and metastatic STSs undergoing trabectedin treatment were enrolled between 2016 and 2019 at the Centro di Riferimento Oncologico (CRO) in Aviano. Trabectedin was administered by 24h-intravenous infusion at a dose of 1.5 mg/m^2 body surface area every 21 days for 6 cycles after premedication with dexamethasone 20 mg. to reduce liver and bone marrow toxicity. Normal haematological, renal and liver functions, as well as the performance status (PS) ≤2, were verified to establish whether patients could receive trabectedin therapy. Participants were required to have received previous chemotherapy a minimum of 3 weeks before enrollment in the study and had to have measurable disease according to Response Evaluation Criteria in Solid Tumours (RECIST). The presence of neuropathy, central nervous system metastases, cardiovascular disease or pregnancy were considered as exclusion criteria. At the baseline, clinical data were recorded, including age, sex, body mass index (BMI), PS, tumour histotypes and grade, haematological parameters as well as toxicity grading classified according to Common Toxicity Criteria.

The investigation was carried out in accordance with the principles of the Declaration of Helsinki and approved by the CRO Institutional Ethical Committee (no. 2015.004CE, 09/04/2015, NCT04394728). All subjects gave written informed consent.

2.3 Chemicals

Acetonitrile and methanol (LC-MS grade) were purchased from Carlo Erba Reagents (Milan, Italy). Ultrapure water was generated by a Milli-Q Plus system (Millipore, Billerica, MA, USA). Formic acid, ammonium formate, ammonium acetate and dimethyl sulfoxide (DMSO) were purchased from Sigma-Aldrich (Milan, Italy). Analytical standards of trabectedin and its deuterium-labelled derivative d_3-trabectedin were provided by PharmaMar (Colmenar Viejo, Madrid, Spain). Trabectedin-free human plasma used for calibration curves and QCs preparation was obtained from healthy volunteers at CRO, Aviano. The AbsoluteIDQ® Bile Acids kit, consisting of five calibrators, three levels of QCs and labelled IS, was acquired from Biocrates Life Sciences (Innsbruck, Austria). Analytical reference standards and labelled IS for amino acids quantification were purchased from Toronto Research Chemicals (North York, ON, Canada) and Jasem (Istanbul, Turkey).

2.4 Sample collection

Time- serial blood sampling for PK analysis, was performed collecting whole blood in 5 ml tubes containing EDTA as anticoagulant. Plasma was separated from blood cells by centrifugation at 4 °C for 10 min at 3200 rpm (Thermo Scientific Heraeus Megafuge 16R centrifuge). Pre-dose serum samples for metabolomics analysis were obtained from whole blood collected in glass tubes (5ml) let to clot for 30 minutes at room temperature and then centrifuged for 15 min at 3200 rpm. Both

serum and plasma samples were immediately transferred into polypropylene tubes and stored at −80 °C until analysis.

2.5 LC-MS/MS Analyses

The measurement of plasma trabectedin and the metabolomics profile, encompassing amino acids (AAs) and derivatives and bile acids (BAs), were carried out by ultra-performance liquid chromatography coupled with tandem MS (UPLC-MS/MS). The UPLC system consisted of a 1290 Infinity II binary pump equipped with an integrated degassing unit, a column thermostat, and a refrigerated auto-sampler (Agilent Technologies, Santa Clara, California). The tandem MS was an Ultivo triple quadrupole mass spectrometer (Agilent Technologies, Santa Clara, California) with orthogonal Jet Stream ESI source.

2.5.1 Trabectedin Pharmacokinetics: method development and validation

Preparation of calibrators, QC solutions and plasma samples

Trabectedin and d_3-trabectedin stock solutions were prepared in DMSO at a concentration of 100 µg/mL. Two independent series of working solutions, each for plasma calibrators and QCs, were obtained diluting the trabectedin stock solution in acetonitrile–0.1% formic acid in water (70:30, v/v) at the nominal concentration of 100, 10 and 1 ng/mL. The IS working solution was diluted till 100 ng/mL in acetonitrile–0.1 % formic acid in water (70:30, v/v) and stored at −30 °C. Calibrators were prepared diluting working solutions in drug-free plasma at eight different concentrations: (A) 2.5 ng/mL, (B) 1.0 ng/mL, (C) 0.5 ng/mL, (D) 0.25 ng/mL, (E) 0.1 ng/mL, (F) 0.05 ng/mL, (G) 0.025 ng/mL, and (H) 0.01 ng/mL. Each batch of analysis included also three levels of drug-free plasma QCs at high (0.80 ng/mL, QC-H), medium (0.16 ng/mL, QC-M) and low (0.04 ng/mL, QC-L) concentrations, a double blank (plasma without IS) and a blank (plasma with IS).

Pre-analytical sample processing consisted of protein plasma precipitation using as solvent acetonitrile containing 1 % formic acid and 0.1 ng/mL d_3-trabectedin. Briefly, 200 µL of this solution were added to 50 µL of plasma/calibrators/QCs and vigorously vortexed. After centrifugation at 20,800 g for 10 min 4°C (5430R Eppendorf centrifuge), the supernatant was transferred into UPCL glass vials and 3 µL were injected into the UPLC-MS/MS system.

LC conditions

Chromatographic separation was performed on a HILIC Acquity BEH Amide 2.1 × 100 mm, 1.7 µm column (Waters, Mil-ford, MA, USA) maintained at 25 °C. The mobile phases (MP) consisted of acetonitrile–0.1% formic acid (MPB) and water–0.1 % formic acid (MPA) flowed at a rate of 0.2 mL/min. Separation was carried out using gradient elution program, starting with 1.5 min of isocratic

step at 80% of MPB followed by a rapid drop to 50% B at 5 min and another 1 min isocratic step before re-equilibrating at initial conditions of 80 % B.

MS conditions

The LC system was coupled to Ultivo QQQ equipped with ESI source working in positive polarity. Samples were quantified in MRM mode using the following transitions m/z 762→234 and m/z 765→234 for trabectedin and d_3-trabectedin, respectively. The MRM transitions m/z 762→206 and m/z 762→557 for trabectedin, and m/z 765→206 and m/z 765→560 for d_3-trabectedin were used for further qualification (**Table 1**). The ESI source conditions were optimized to have the best ionization and the selected parameters were: gas temperature, 350 °C; gas flow, 10 L/min; nebulizer gas, 30 psi; sheath gas temperature, 400 °C; sheath gas flow, 12 L/min; capillary voltage, 4000 V; and nozzle voltage, 50 V. Data were processed with Mass Hunter Quantitative Data Analysis software.

Table 1. MRM transitions of trabectedin, d_3-trabectedin and optimized parameters of the ESI source

	Precursor (m/z)	**Product (m/z)**	**CE (V)**	**Fragmentor (V)**
Quantifier MRM				
Trabectedin	762	234	30	150
d_3-trabectedin	765	234	30	150
Qualifier MRM				
Trabectedin	762	206	30	150
Trabectedin	762	557	25	150
d_3-trabectedin	765	206	30	150
d_3-trabectedin	765	560	25	150

MS Jet Stream ESI Source Parameters	
Gas Temperature	350 °C
Gas Flow	10 L/min
Nebulizer gas	30 psi
Sheath gas temperature	400 °C
Sheath gas flow	12 L/min
Capillary voltage	4000 V
Nozzle voltage	50 V

MRM, multiple reaction monitoring; CE, collision energy; ESI, electrospray ionization source

Method validation

The method was validated according to the Food and Drug Administration guidelines [137] with respect to linearity, low limit of quantification (LLOQ), selectivity, intra- and inter-day accuracy and precision, matrix effect and recovery, stability [137].

Linearity was evaluated on three independent plasma calibration curves by plotting the relative peak area ratio (area trabectedin/ area d_3-trabectedin) against the analyte concentration. The calibration curves were built by weighted (1/X) least-squares linear regression and the accuracy and precision of back-calculated concentrations of calibrators were considered valid when ≤15 %. Accuracy was calculated as relative error (RE), that is the absolute error divided to the real nominal concentration (eq. 1); while precision was expressed as relative standard deviation (RSD) also known as coefficient of variation (CV) (eq.2).

Eq. 1 $$RE\ (\%) = \frac{\text{back calculated concentration} - \text{nominal concentration}}{\text{nominal concentration}} \cdot 100$$

Eq. 2 $$CV\ (\%) = \frac{\text{standard deviation}}{\text{mean}} \cdot 100$$

LLOQ is the lowest quantifiable concentration of the analyte with a CV (precision) and accuracy (RE) ≤20 %. LLOQ was determined by comparing the signal from samples with known low concentrations of analyte and by selecting that with a signal-to-noise ratio (S/N) of 5.

Selectivity of the method was assessed to exclude the presence of endogenous compounds in the matrix interfering with the trabectedin quantification. It was investigated by analysing six different plasma samples added with trabectedin at the LLOQ concentration. The absence of peaks at the RT of trabectedin, CV and RE ≤ 20 % were the criteria used to establish method selectivity.

Intra-day and inter-day accuracy and precision were determined over three different days by analysing QCs samples processed in the same way of calibrators and plasma samples. Intra-day precision and accuracy were assessed calculating CV and RE for 12 replicates of QCs samples in one day, while the inter-day validation was carried out using 6 QCs run over three consecutive days. Accuracy and precision were required to be ≤15 %.

The extraction overall recovery was determined by comparing trabectedin peak areas in triplicates between plasma samples spiked with the analyte ($Plasma_{spiked}$) and neat solution spiked with the analyte ($Neat_{spiked}$) at QCs concentrations (eq.3). Matrix effect was evaluated by comparing in triplicates the peak area of post-preparation plasma samples spiked with trabectedin at three QC levels ($Plasma_{post\text{-}spiked}$)concentrations and d_3-trabectedin with those of $Neat_{spiked}$ (eq. 4) [138].

Eq. 3 $Overall\ recovery(\%) = \frac{\text{Plasma spiked}}{\text{Neat spiked}} \cdot 100$

Eq. 4 $Matrix\ effect\ (\%) = \frac{\text{Plasma post spiked}}{\text{Neat spiked}} \cdot 100$

Stability of trabectedin was assessed using QCs plasma samples in triplicates at different experimental conditions: a) 4 hours at 4°C or room temperatures (short-term stability); b) 24 hours at 4°C in the autosampler injector to verify plasma extract stability; c) after three freeze-thaw cycles, for samples frozen at – 30° C for 24h and kept 1 h at room temperature after thawing (freeze-thaw stability); d) after 3 months of storage at -30°C (long-term stability). Stability was verified whether RE values of samples at each condition were ≤15 %.

PK parameters

PK parameters were calculated using a non-compartmental model with no assumptions about body compartments. The C_{max} was directly obtained from the plasma concentration-time plot of measured data. The AUC up to 48 hours (AUC_{0-48}) was calculated by trapezoidal method, while the normalized AUC (AUC_{norm}) by dividing the AUC_{0-48} for the administered dose of trabectedin (mg). The area under the moment curve ($AUMC_{0-48}$) was calculated through the trapezoidal method using the plasma concentration multiplied by time. The mean resident time (MRT), the average time the drug stays in the body, was calculated as $AUC_{0-48}/AUMC_{0-48}$ ratio.

2.5.2 Targeted metabolomics analysis of amino-acids and bile acids

Metabolomics profile was carried out in baseline serum and targeted to 51 AAs and derivatives (Appendix 1). For the samples preparation, 10 µL of serum was mixed with 20 µL of a water solution containing 34 ^{2}H or ^{13}C- or ^{15}N-labeled amino acids. Serum proteins were then precipitated by adding 150 µL of acetonitrile–0.1% formic acid (75:25, v/v), followed by vigorous vortex and centrifugation at 20,800 g for 15 min at 4 °C. The supernatant was transferred to glass vials and 6 µL were injected into the UPLC-MS/MS system. Calibration curves were prepared for each batch of analysis using a standard mix of 43 AAs (Jasem, Turkey) integrated with another standard mix solution with creatine, urea, serotonin, asymmetric dimethylarginine (ADMA) and symmetric dimethylarginine (SDMA). These stock solutions were stored at – 30°C and serially diluted with 50% acetonitrile to generate working solutions at five different concentrations (Appendix 2). QCs solutions in synthetic serum (Jasem, Turkey) were used at two concentration levels for method validation. Chromatographic separation was performed on XBridge Amide column 3×100 mm, particle size, 3.5 µM (Waters, Milford, MA, USA) operating in HILIC mode. The column was kept at 10°C and equilibrated with 20% MPA (20 mM ammonium formate pH 3) and 80% MPB (acetonitrile containing 10% water and 20 mM ammonium formate pH 3) delivered at a flow rate of 0.2 mL/min. Chromatographic gradient changed from 80% B to 65% B in 10 min, then it rapidly dropped at 20% for 1 min washing step and

at 12.1 min it returned at the initial condition of 80% B for 5 min re-equilibration before the next injection. The QQQ was set in MRM mode and the ESI Jet Stream source in positive polarity with the following optimized parameters: capillary, 2000 V; nozzle voltage, 0 V; gas temperature, 150 °C; gas flow, 10 L/min; nebulizer, 40 psi; sheath gas temperature, 400 °C; and sheath gas flow, 10 L/min. Intra- and inter-day accuracy and precision were evaluated by analyzing QCs samples in six replicates in one day and three different days, respectively.

Serum was also profiled for 16 BAs, encompassing primary BAs (cholic acid, chenodeoxycholic acid), secondary bile acids (deoxycholic, lithocholic, hyodeoxycholic and ursodeoxycholic acids) and 10 taurine- or glycine-conjugated derivatives (Appendix 3). Briefly, 20 µL of serum were mixed with 5 µL of labelled IS solution (Biocrates Life Sciences). After adding 40 µL of acetonitrile, tubes were vigorously vortexed and centrifuged at 20,800 g for 10 min at 4 °C. The extract was then diluted with 1.5 volume of ultrapure water and 10 µL were injected into the LC-MS/MS system. Five-points calibration curves were built using the standard mixture solution (Biocrates Life Sciences) and analytical performance was checked by running three QCs levels in each batch of analysis. Chromatography was performed in RP mode using a C18 column (Biocrates Life Sciences) kept at 50 °C and equilibrated with 35% MPB (10 mM ammonium acetate 0.02% formic acid in 65% acetonitrile and 35% methanol) and 65% MPA (10 mM ammonium acetate 0.02% formic acid in water). Chromatographic separation was performed according to manufacturer's instruction by the following gradient: (a) 35% to 40% B in 0.7 min; (b) 40% to 45% in 2.3 min; (c) 45% to 55% B in 0.2 min; (d) 55% to 65% B in 2.3 min; and (e) 65% to 100% B in 1 min. A 2 min washing step with 100% B and 3 min of equilibration to the initial condition (35% B) preceded the next sample injection. The MS parameters were optimized in order to have the highest signal for each MRM transition and for ESI source parameters: polarity, negative; capillary, 3000 V; nozzle voltage, 0 V; gas temperature, 200 °C; gas flow, 12 L/min; nebulizer, 40 psi; sheath gas temperature, 200 °C; and sheath gas flow, 10 L/min. Raw data were analysed using MassHunter Quantitative Analysis software (Agilent). Intra-assay and inter-assay variability for each bile acid was accepted whether <15%.

2.6 Statistical analyses

The statistical power of this pivotal clinical study was investigated to assess the proper number of participants required to avoid type I and type II errors. The first refers to the probability of rejecting the null hypothesis when it is true, namely declaring that there are differences between groups when there are not (false positive). The type error II instead means to accept the null hypothesis when it is false, namely conclude that groups are not different when they truly are (false negative). The probability of having a type error I or II was quantified as alpha (α) and beta (β) respectively, while the likelihood of avoiding these errors as 1-β that is called statistical power [139].

The optimal sample size was calculated setting the power study at 0.8 (80%) with β at 0.2 (20%) in order to have the 80% of probability to avoid type error II. The threshold of the statistical significance was established as α = 0.05 (5%), meaning that there is a 5% risk to have type error I and that the found differences are due to chance.

Quantitative metabolomics data were pre-processed by log transformation and unit variance scaling before statistical analyses. Correlations between PK parameters and metabolites were assessed by double stage multivariate PLS analysis, selecting in each step metabolites with variable importance in projection (VIP)>1. PLS is a supervised multivariate regression that finds a linear relationship between two groups of variables, the predictors (X, metabolites) and the Y-dependent variable (AUC). The PLS was represented projecting on low dimensional hyper planes, the X-score vectors (t_a) and Y-score vectors (u_a), known as latent variables (LVs) that indicate a summary of matrix X and Y data, respectively. The PLS loading plot was built to highlight variables that most contributed to the regression model, plotting the loading coefficients for the X variables (w) and Y variable (c) as w*c for each LV. The validity of the model was tested by K-fold cross-validation, whereby the dataset is split into 7 subsets and each one was in turn left out from the model and then predicted back by using the model built with the remaining sixth of the dataset. This procedure was repeated until all subsets have been kept out at least once in order to calculate the Q^2 and R^2. The Q^2 is an indicator of the predictive ability of the model and was calculated as:

$$Q^2 = \frac{1 - \text{PRESS}}{TSS}$$

where PRESS is the sum of the squared differences between observed and predicted Y values, while SS is the total sum of the square. Good predictive ability was considered for the model with Q^2>0.4.
R^2 measures the goodness of fit, which indicates how much the model explains the variance. It was calculated as:

$$R^2 = \frac{1 - \text{RSS}}{TSS}$$

where RSS is the residual sum of the square of the data. The best model has R^2 =1 while low value indicates a large amount of noise or irrelevant information in the data [43].
In addition, permutation test was performed to assess the degree of overfitting of the model. The Y variable AUC was randomly permutated generating corresponding models, whose Q^2 and R^2 were compared with the original values. The test was considered passed when Y-axis intercepts were R^2 < 0.3 and Q^2 < 0.05.
Multiple regression analysis was applied after double stage PLS to further refine the model. Backward method was used to reduce the number of metabolites, first entering all variables with p< 0.05 and then removing the not significant with p> 0.1. Multicollinearity of highly correlated variables was checked by evaluation of Variance Inflation Factor (VIF < 2).

Multivariate supervised PLS-DA was used to find differences in baseline metabolomics profile between PD and SD patients as well as to disclose association with the toxicological response to trabectedin treatment. Models were validated by 7-fold cross-validation and permutation test. VIP and Student's t-test were used to identify significant different serum metabolites levels between groups. For data with no normal distribution, the non-parametric test Mann-Whitney U was carried out. Correlations between categorical variables were evaluated by Fisher's exact test, while Pearson correlation was used for continuous variables. *P*-values were adjusted (q) by multiple hypothesis testing based on false discovery rate (FDR). Statistical significance was accepted for $q < 0.05$ unless otherwise specified. Receiver operating characteristic (ROC) analyses were applied to evaluate the ability of selected metabolites to discriminate the groups of interest. The area under the ROC curve (AUROC), used as indicator of the diagnostic power, was obtained from the plot sensitivity (true positive rate) versus 100-specificity (false positive rate).

The OS analysis was performed in a subset of patients receiving trabectedin as second and third line (n = 24) in order to consider a homogeneous time interval in the samples group. The risk predictive OS model was obtained by application of Cox proportional hazard regression. It is a commonly used multivariate regression analysis for modelling survival data that allows the simultaneous assessment of the effect of many factors on survival [140]. Univariate Cox analysis was first used to select metabolites and clinical data significantly correlated with the OS ($p < 0.01$). Multivariate Cox regression was then applied to further screen important variables by backward method. The Cox model was expressed by hazard function as follows:

$$h(t) = h_0(t_0) \times \exp(b_1X_1 + b_2X_2 + \cdots b_nX_n)$$

where h(t) is the hazard function, $h_0(t_0)$ is the baseline hazard (the hazard value for an individual when the risk variables are equal to 0), b_n are the regression coefficients measuring the impact of the variable in the model and $\exp(b_n)$ is the relative hazard risk. Value of $\exp(b_n)$ greater than 1 belongs to covariates positively associated with the risk of death, conversely, value < 1 indicates inverse correlation. Harrell's concordance index (C-index) was calculated to evaluate the goodness of fit of the model with a value close to 1 indicating a good prediction ability for the survival event. The Cox model generated risk scores for each patient that were used to classify them into high-risk, falling into the fourth quartile, and low- medium-risk group including the first three quartiles. The Cox regression model is based on the proportional hazard assumption that the hazard function remains constant over time [141]. Schoenfeld residuals were analysed, for the selected variables, to test such assumption along with the Kaplan Meyer survival analysis between high-risk and low-moderate risk patients' groups. The univariate Kaplan–Meier analysis was also used to identify correlations between OS and clinical data including tumour type, PS, tumour grade, absolute ANC, haemoglobin, albumin and lactate dehydrogenase. The statistical significance of the differences between Kaplan-Meier curves was evaluated by

log-rank test. Martingale residuals were calculated from the Cox regression model for the variable with $q < 0.05$ to assess the significance of the correlation with the OS and to establish a possible cut-off for short and long survivors. Statistical analyses were performed using R version 4.0, SIMCA Umetrics version 14.0, MedCalc v. 19.2.1, GraphPad Prism 7, and MetaboAnalyst 4.0 tools [142].

3. RESULTS

3.1 Patient population

This monocentric study enrolled 40 metastatic STSs patients (45% females and 55% males) receiving trabectedin treatment. Patients had a median age of 66 years with equal percentage of subjects under and above 65 years (**Table 2**). Leiomyosarcoma and liposarcoma (L-sarcoma) were the most prevalent histological subtypes accounting for about 30% and 12.5%, respectively. Most of the tumours were poorly differentiated with high-grade G3, and only 25% were characterized by modest differentiation (G2). The 52.5% of patients showed good general wellbeing with a PS of 0, while the remaining 47.5% had a PS between 1 and 2. Patients received trabectedin for a median of three cycles (range, 1-48) mainly as second-third line (60%), preceded by other chemotherapy treatments based on anthracyclines or gemcitabine. The trabectedin therapy provoked modest haematological toxicities (G0-2), such as anaemia, leukopenia, neutropenia, in 60% of patients and more severe toxic effects (G3-4) in the remaining 40%. Total haematological and extra-haematological toxicities (nausea, asthenia, alopecia, mucositis) of G0-2 and G3-4 grade occurred in the 52.5% and 47.5% of patients, respectively. Because of severe adverse effects, trabectedin dose was reduced by 75% during cycles in 16 patients. After three cycles of treatment, the status of the disease was re-evaluated by positron emission tomography (PET): 20 patients showed progressive disease (PD) with an increase of tumour size and/or metastasis spread, 16 showed neither an increase nor a decrease (SD), while 4 were not evaluable because of early death. The median OS was 13 months (range, 0.8-47 months) with 20 patients already died at the data analysis and 4 still alive.

Table 2. Demographic and clinical characteristics of metastatic soft tissue sarcoma patients.

Characteristics	Value
Sex, *n* (%)	
Female	18 (45.0)
Male	22 (55.0)
Age (years), median, range	66 (37–90)
Age, *n* (%)	
<65 years	18 (45.0)
≥65 years	22 (55.0)
BMI (kg/m^2), median (range)	27.0 (17.5–41.8)
Tumor subtype, *n* (%)	
L-sarcomas[a]	17 (42.5)
Other sarcomas[b]	23 (57.5)
Tumour grade, *n* (%)	
G2	10 (25.0)
G3	30 (75.0)
Performance status (ECOG score), *n* (%)	
0	21 (52.5)
1-2	19 (47.5)
Trabectedin therapy, *n* (%)	
1st line	16 (40)
2nd line	18 (45)
3rd line	6 (15)
Hematological toxicity grade, *n* (%)	
G0-2	24 (60.0)
G3-4	16 (40.0)
Hematological and extra- toxicity grade, *n* (%)	
G0-2	21 (52.5)
G3-4	19 (47.5)
Disease status 3rd cycle, *n* (%)	
PD	20 (50%)
SD	16 (40%)
NE	4 (10)
Overall survival, median (months)[c]	13

BMI, body mass index; ECOG, Eastern Cooperative Oncology Group; PD, progressive disease; SD, stable disease; NV, not evaluable. [a] Leiomyosarcomas (*n* = 12) and liposarcoma (*n* = 5). [b] Other sarcomas include: malignant peripheral nerve sheath tumor (*n* = 3), fibrosarcoma (*n* = 4), undifferentiated pleomorphic sarcoma (*n* = 4), chondrosarcoma (*n* = 2), synovial sarcoma (*n* = 2), not otherwise specified sarcoma (*n* = 4), endometrial stromal sarcoma (*n* = 2), and desmoplastic small-round-cell tumor (n = 1), Malignant fibro histiocytoma (*n* = 1). [c] in a subset of 24 patients.

3.2 Trabectedin PK analysis

3.2.1 HILIC-MS/MS method development

The full scan of trabectedin and trabectedin-d_3 showed more intense signals when measured in ESI positive polarity, due to the presence in the chemical structure (**Figure 4**) of several hydroxylic and aminic groups able to accept a proton in presence of formic acid in the MP [143].

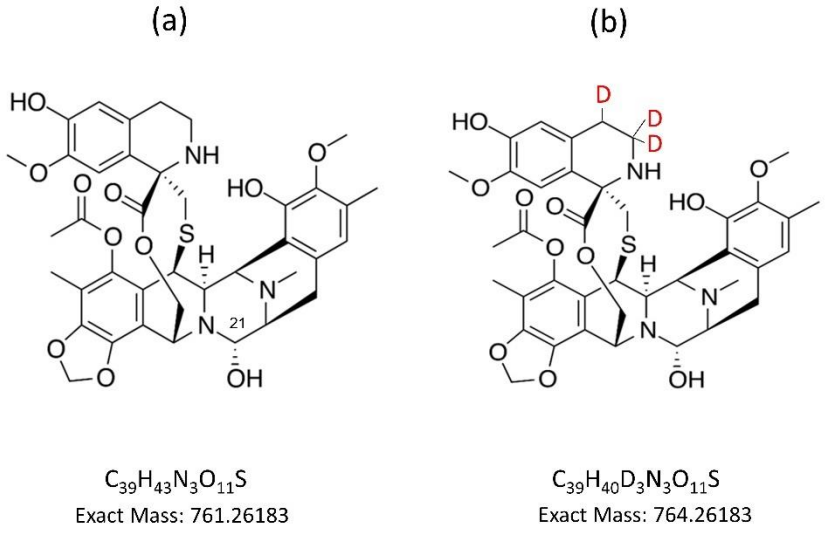

Figure 4. Chemical structures of trabectedin and the deuterated IS d_3-trabectedin.

The scan spectra of both trabectedin and d_3-labelled IS showed two main intense peak ions corresponding to the protonated drug $[M+H]^+$ at m/z 762 (trabectedin) and m/z 765 (d_3-trabectedin), and to the molecules after water loss $[M–H2O+H]^+$ at m/z 744 and m/z 747 respectively. The less intense peaks were attributed to the sodium adducts $[M + Na]^+$ at m/z 784 and m/z 787 for trabectedin and d_3-trabectedin, respectively. A very low peak corresponding to potassium adduct was observed at m/z 800 for trabectedin (**Figure 5 a, b**).

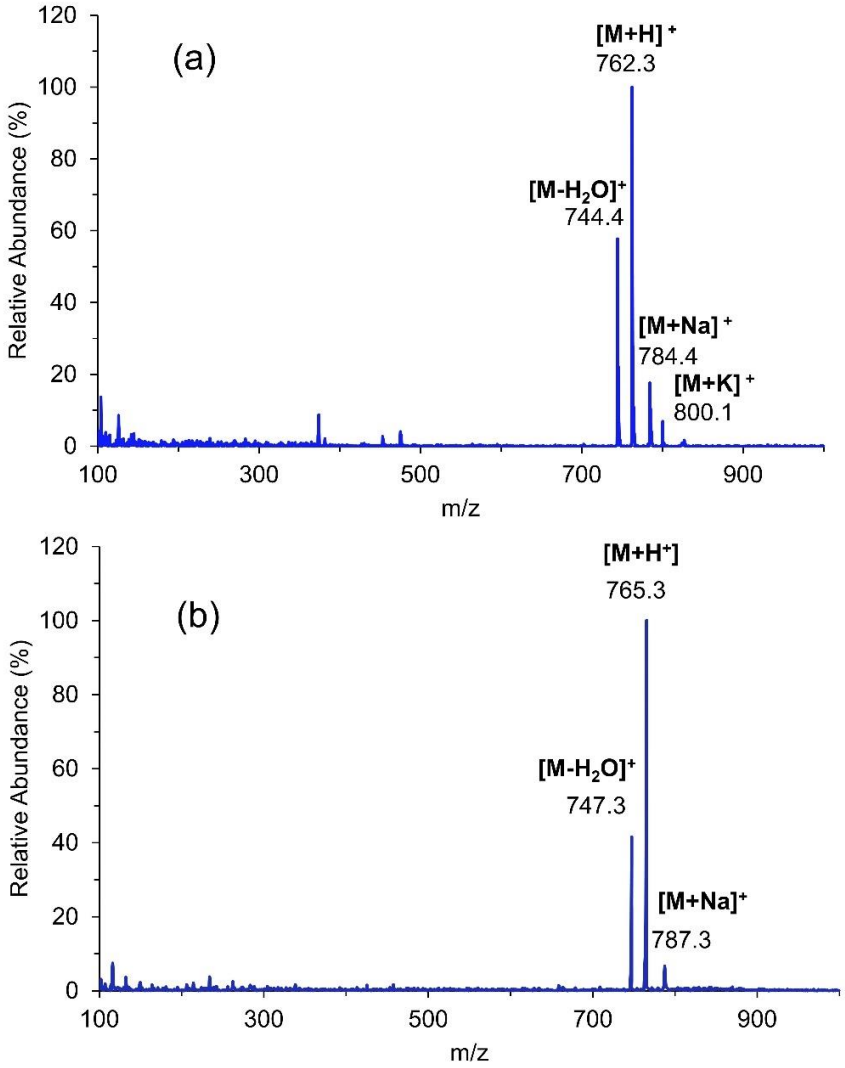

Figure 5. ESI-positive MS scan spectra of trabectedin (**a**) and d_3-trabectedin (**b**).

The precursor ions $[M+H]^+$ were filtered in the first quadrupole and sent into the collision cell where product ions were generated by fragmentation at the optimal selected collision energy (CE) and fragmentor voltage conditions. The highest signals in the product ion scan spectra were observed at m/z 234 for both trabectedin and IS (**Figure 6 a,b**) and were chosen for the quantification. The lower peaks at m/z 206, 557 (for trabectedin) and 206, 560 (for d_3-trabectedin) were used for qualification. The hypothetic chemical structures of these ion fragments were shown in **Figure 6a**.

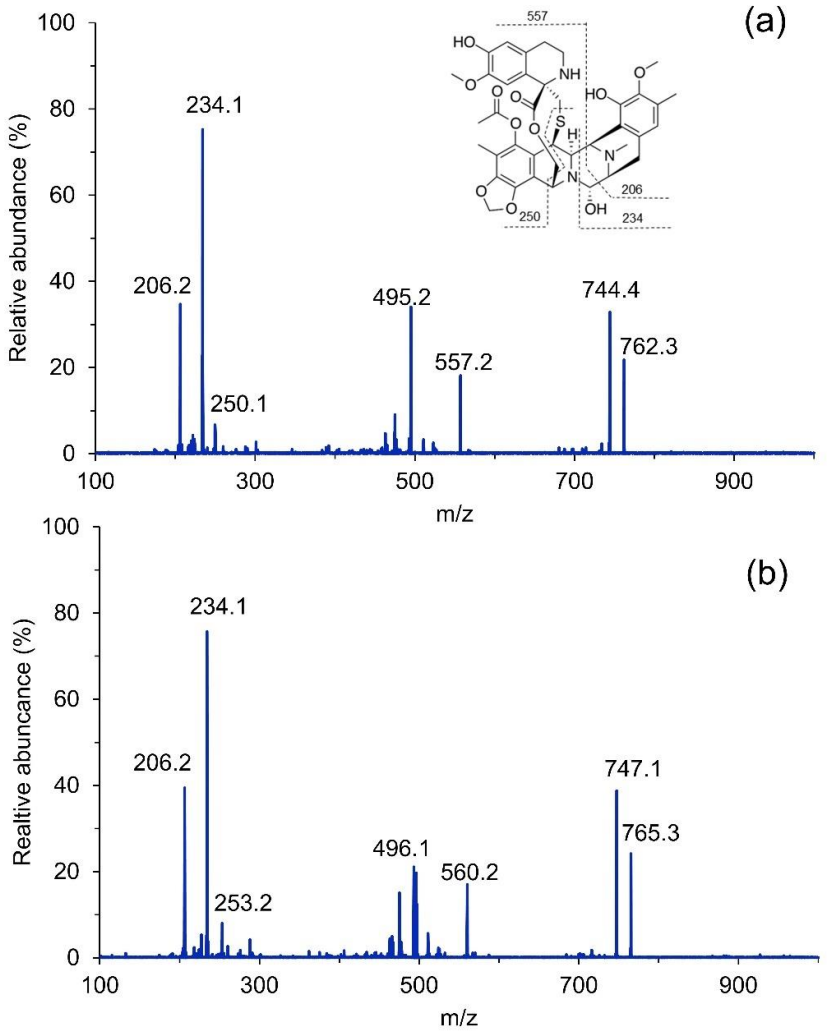

Figure 6. Product ion scan spectra of trabectedin (**a**) and d_3-trabectedin (**b**) with proposed fragmentation pattern.

After fragmentation, the selected precursor and production ions were monitored in the third quadrupole in MRM mode as reported in Table 1. The elution of trabectedin and IS from the Amide HILIC column occurred at 2.8 min with no interfering peaks deriving from the human plasma matrix (**Figure 7a**). The MRM chromatograms of the extracted human plasma spiked with trabectedin at the LLOQ (0.01 ng/mL) and that with d_3-trabectedin (0.1 ng/mL) showed an intense signal with a S/N of about 5 and 58, respectively (**Figure 7 b,c**).

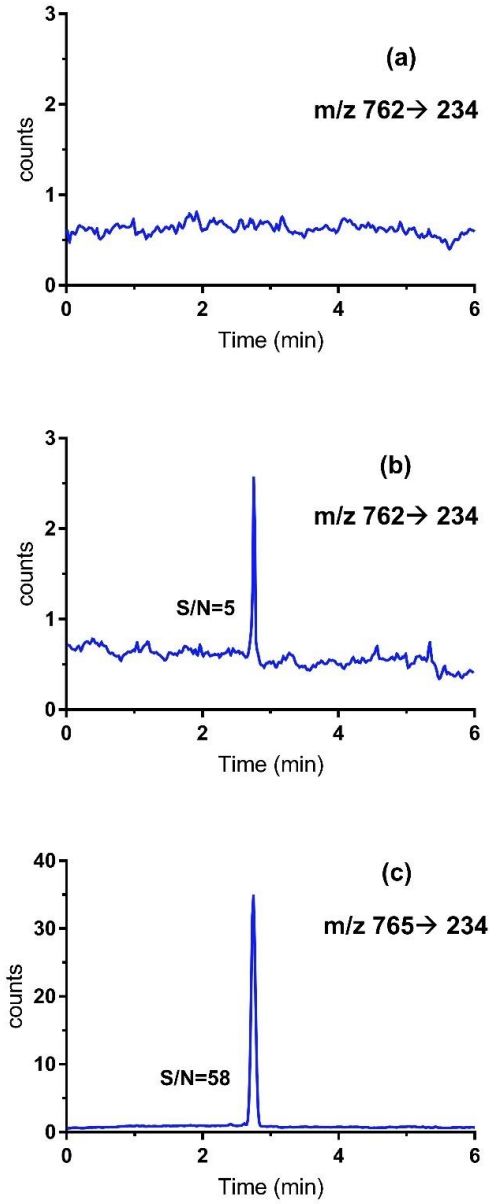

Figure 7. MRM chromatograms of human blank plasma sample (**a**); human blank plasma sample spiked with trabectedin at LLOQ (0.01 ng/mL) (**b**); human blank plasma sample added with IS (0.1 ng/mL) (**c**).

3.2.2 Method validation

Calibration curves, evaluated in three independent days in the range of 0.01-2.5 ng/mL, showed good linearity with a mean R^2 = 0.9939 ± 0.003. The precision and accuracy over the 3 days were within the 15% of error, indeed the RE ranged from -13.31 % to 10.68 %, while the CV ranged from 0.04% to 13.83 %.

The LLOQ was 0.01 ng/mL since up to such concentration both precision and accuracy resulted ≤ 20 %. In particular, the CV ranged between 9.30% and 13.83%, while RE from -7.16% to 7.80%.

The selectivity of the method was demonstrated using six different human plasma samples spiked with trabectedin at the LLOQ and as many plasma samples (double blank) and no endogenous

molecules were found to co-elute with the drug and interfere with its detection. The CV in the analysis was 7.84% and the RE between -10.59 % and 6.02 %.

Intra-day accuracy and precision resulted both < 15% at all QC levels (n=12), ranging from -8.52% to 1.19% and from 3.95% to 12.35%, respectively. The inter-day validation over three different days showed as well good RE (from -6.78% to -1.92%) and CV (from 6.57 % to 10.74 %) (**Table 3**).

Table 3. Intra- and inter-day validation for trabectedin quantification in plasma.

	Intra-day			**Inter-day**
	Day 1 (n=12)	**Day 2 (n=6)**	**Day 3 (n=6)**	**Days 1-3 (n=24)**
Nominal concentration	**Back-calculated concentrations**			
LLOQ, 0.01 ng/mL				
RSD (%)	13.83	9.30	11.22	12.49
RE (%)	-0.20	-7.16	7.80	0.72
QC-L, 0.04 ng/mL				
RSD (%)	12.35	3.95	11.66	10.74
RE (%)	-3.21	-6.24	1.19	-2.87
QC-M, 0.16 ng/mL				
RSD (%)	6.26	7.97	6.76	6.57
RE (%)	-1.50	-1.37	-3.32	-1.92
QC-H, 0.80 ng/mL				
RSD (%)	4.75	6.30	10.61	7.00
RE (%)	-7.75	-3.10	-8.52	-6.78

RSD, relative standard deviation; *RE*, relative error

The overall recovery of the extraction sample processing resulted higher when acetonitrile containing 1% of formic acid was used and it reached a mean of 54.4 ± 3.8%. The matrix effect was found to suppress the trabectedin signal of 24.54 ± 5.1%, however, such effect was controlled by adding IS during sample preparation.

The stability of QCs was successfully evaluated at different experimental conditions (**Table 4**). The short-term stability for 4h at 4°C and room temperature had good RE, indicating good stability of the drug at the condition resembling those of the sample preparation. Trabectedin resulted stable also in the extract kept at 4°C in the autosampler for 24h since RE ≤ 8.43% as well as after three freeze-thaw cycles (RE≤ 8.63%). Finally, the evaluation of the long-term storage stability at -30°C for three months showed a slight decrease of the trabectedin concentration up to -10.77%.

Table 4. Stability of trabectedin at different experimental conditions.

Experimental conditions	Nominal concentration (ng/mL)	RE (%)
Short-term stability: 4°C, 4 h	0.04	10.72
	0.16	-0.44
	0.80	-4.47
Short-term stability: room temperature, 4 h	0.04	10.39
	0.16	1.59
	0.80	9.60
Plasma extract stability: 4 °C, 24 h	0.04	2.16
	0.16	8.43
	0.80	-0.68
Freeze-thaw stability, 3 cycles	0.04	8.63
	0.16	4.83
	0.80	-2.51
Long-term stability: -30 °C, 3 months	0.04	-3.26
	0.16	-7.69
	0.80	-10.77

RE, relative error

3.2.3 Trabectedin PK profiles of patients

The plasma trabectedin concentration was measured in 40 STS patients receiving a dose of 1.5 mg/m^2 body surface, during the 24h intravenous infusion and for the following 24 h from the end of the administration. The drug showed multi-phase kinetics (**Figure 8**), initially characterized by a rapid and linear increase as a first-order PK, and then by a non-linear trend reaching the steady-state at about 8 h. The drug elimination showed as well as bi-exponential kinetics, with a rapid decline immediately after the end of the infusion, and then a slower elimination up to 48 h.

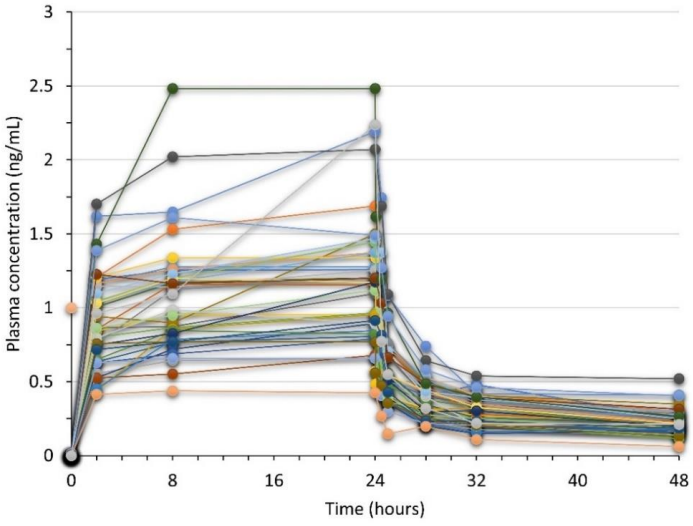

Figure 8. Plasma concentration-versus-time profile of trabectedin in 40 STSs patients undergoing 1.5 mg/m^2 dose as 24 h intravenous infusion.

PK analyses (**Table 5**) revealed a mean experimental AUC $_{0\text{-}48}$ of 33.2 ± 11.2 ng·h·mL^{-1} with a wide range from 12.7 to 63.4 and a mean C_{max} of 1.2 ng/mL (range, 0.4–2.5). The mean AUMC $_{0\text{-}48}$ and MRT were 596.8 ± 202.2 ng·h^2/mL and 18.0 ± h, respectively. The drug exposure, expressed as AUC $_{norm}$, obtained from the AUC$_{0\text{-}48}$/dose ratio, ranged from 6.33 to 31.70 with a mean of 13.6 ± 5.3 ng·h·mL^{-1} ·mg^{-1}.

Table 5. PK parameters of trabectedin in 40 STSs patients.

PK parameters	Mean	SD	Range	95% CI
AUC $_{0\text{-}48}$ (ng·h·mL^{-1})	33.2	11.2	12.7-63.4	29.6 to 36.7
AUMC $_{0\text{-}48}$ (ng·h^2·mL^{-1})	596.8	202.2	214.2-1105.1	53 to 660
MRT (h)	18.0	1.0	13.9-20.4	17.7 to 18.3
C_{max} (ng·mL^{-1})	1.2	0.5	0.4-2.5	1.1 to 1.4
AUC $_{norm}$ (ng·h·mL^{-1}·mg^{-1})	13.6	5.31	6.33-31.70	11.9 to 15.3
$C_{max\text{-}norm}$ (ng·mL^{-1}·mg^{-1})	0.50	0.21	0.22-1.24	0.43 to 0.57

SD, standard deviation; CI, confidence interval; AUC, area under the curve; AUMC, area under the first Moment curve; MRT, mean residence time; C_{max}; maximum concentration

3.4 Metabolomics analyses of AAs and BAs

The metabolomics analysis of AAs and derivatives included 51 compounds of which 12 were excluded not being detected in serum samples or being detected but not properly quantified (Appendix 1). The accuracy of the analytical AAs measurements in plasma samples, performed in two different batches, was assessed by the inclusion of QCs. The PLS-DA of all patients' samples, QC1 and QC2 from both batches showed a clear separation of the three groups indicating the good performance of the analytical method (**Figure 9a**). Moreover, the QCs of the two different batches did not show significant differences allowing to rely on quantitative data (**Figure 9b**). Among the 16 BAs, only two were excluded from the analysis being not quantifiable (Appendix 3). The single batch BAs analysis, represented in the PLS-DA, did not show any analytical bias since patients and QCs were perfectly separated (**Figure 9c**) and the QCs variations were within the indicated limits (**Figure 9d**).

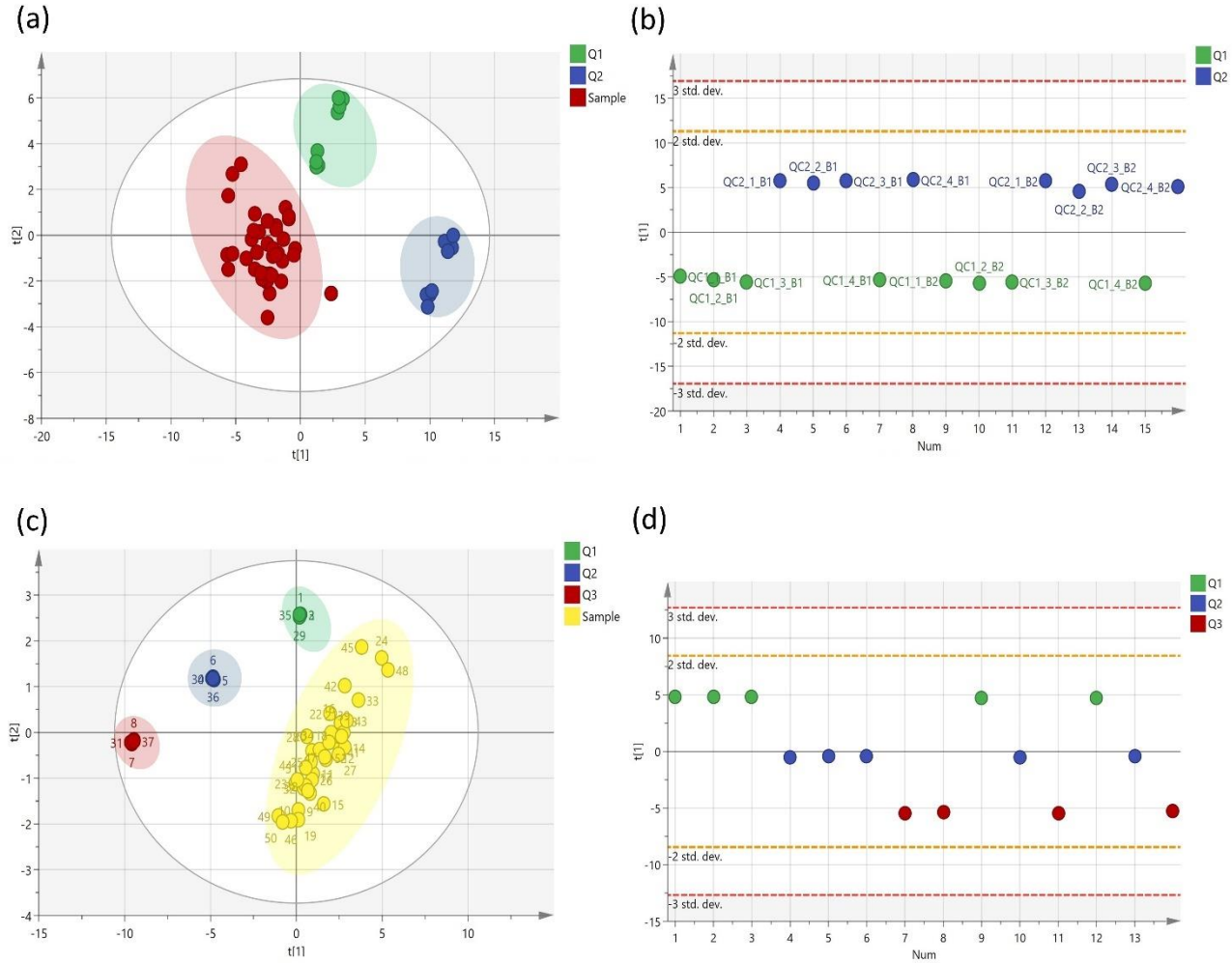

Figure 9. PLS-DA of plasma samples and QCs for the AAs (**a**) and BAs (**c**) analyses. Analysis of variance of QC samples by PLS-DA score plot with the first LV, in AAs (**b**) and BAs (**d**) LC-MS/MS analyses. The dashed yellow and red lines indicate the min and max tolerable limits of 2-fold and 3-fold standard deviations, respectively.

3.5 Power analysis

The power analysis indicated that the minimum sample size required to have a statistical power of 80% was 40. This result was obtained hypothesizing a number of 5 latent variables, a small effect size of sES=0.3, and a type error I of 5%. Moreover, since model performance, in any case, may be overestimated, internal validations were performed for the further analyses of PK or PD metabolomics associations.

3.6 Correlations between PK and baseline metabolic profiles

A predictive model for the PK of trabectedin was developed by double stage PLS regression analysis using the AUC_{norm} as representative of the total drug exposure. The initial PLS score plot, including AAs and BAs, showed a good linear relationship between the baseline metabolomics profile of patients and the AUC_{norm} with a R^2 =0.59 (Figure 10a). The PLS loading plot depicted the most

important metabolites correlated with the AUC_{norm} (Figure 10b). Metabolites in the top right quadrant with high positive coefficients showed direct relation with the AUC_{norm}, conversely, those in the bottom left with negative coefficients showed an inverse correlation (Figure 10c).

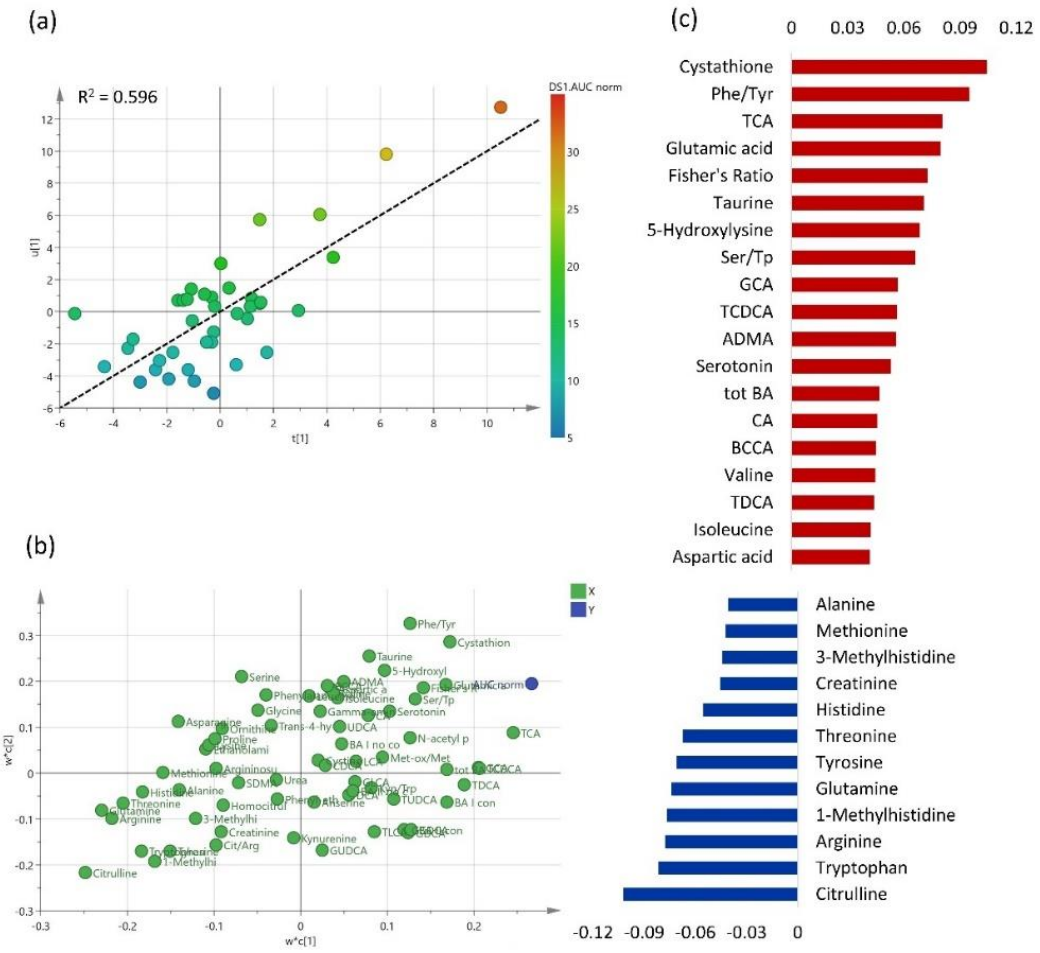

Figure 10. PLS regression analysis for AUC_{norm} prediction by serum baseline metabolites. Each dot represents a patient plotted as score from the baseline serum metabolites levels (X) versus the AUC (Y). The colour scale from blue to red indicates increasing values of AUC (**a**). PLS loading plot where each point is a metabolite plotted as loading coefficient from PLS LV1 (w*c1) vs the coefficient from LV2 (w*c2) (**b**). Metabolites mostly correlated with AUC sorted by decreasing loading coefficients (**c**).

Twenty-four metabolites contributed more to model prediction according to their VIP>1 and were included in the second PLS regression model (Figure 11a). This PLS model showed good performance when 7-fold validation was assessed with high goodness of fit (R^2 = 0.70) and predictability (Q^2 = 0.42). The result of the validation by random permutation revealed no risk of overfitting (Figure 11b) with all R^2 and Q^2 from the permutated models smaller than the original values (R^2 intercept <0.3 and Q^2 intercept<0.05). The predicted AUC_{norm} values from the PLS model plotted against the real AUC_{norm} resulted to have a good correlation as indicated by the regression coefficient line of 0.70 (Figure 11c).

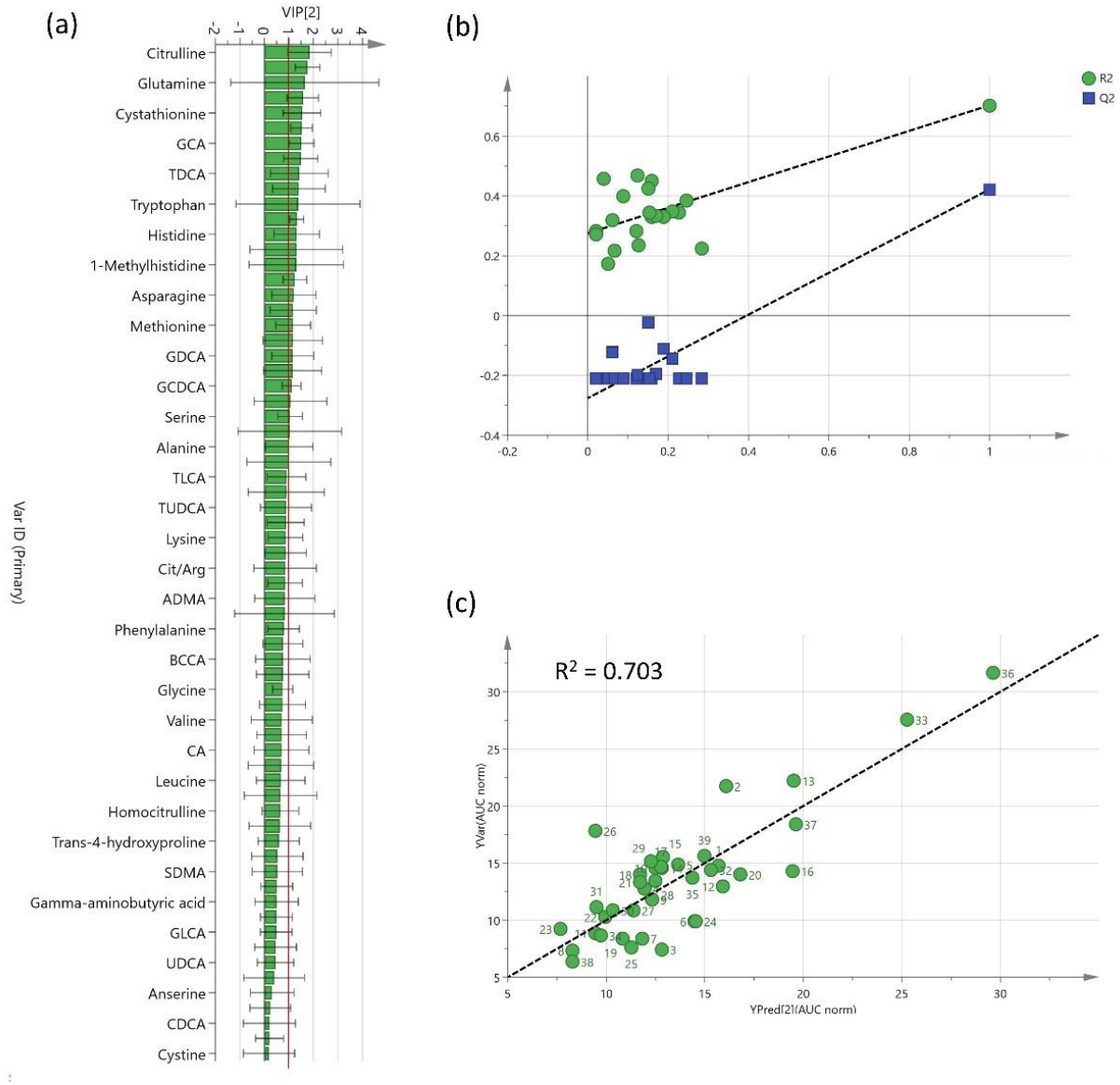

Figure 11. Variable importance projection (VIP) scores ranked by increasing values from the first PLS model based on pre-dose serum metabolites (**a**); internal validation by permutation showing goodness of fit (R^2, green) and predictability parameters (Q^2, blue) from the permuted models (intercepts: $R^2 = 0.275$, $Q^2 = -0.276$) (**b**); Predicted vs. observed AUC_{norm} plot calculated by the second PLS model (**c**).

The model was further refined to improve the clinical feasibility by backward multiple regression analysis that identified five variables as significantly associated with the AUC_{norm}: the AAs derivatives citrulline, cystathionine and the phenylalanine-tyrosine ratio (Phe/Tyr), the conjugated primary bile acid TCA and haemoglobin (Hb). These compounds showed to have an independent impact on AUC_{norm} prediction without risk of multicollinearity (VIF < 2) (**Table 6**).

Table 6. Multiple regression analysis of significant predictive variables.

Independent variables	Coefficient	*p*-value	$r_{partial}$	VIF
Cystathionine	2.69	0.036	0.35	1.44
Hb	-0.82	0.037	-0.35	1.56
TCA	15.70	0.001	0.53	1.62
Citrulline	-0.15	0.011	-0.42	1.59
Phe/Tyr	5.16	0.013	0.42	1.07
(Constant)	20.07			

VIF, Variance Inflation Factor; $r_{partial}$, partial correlation coefficient.

The final predictive model was represented by the following equation:

$$AUCnorm = -0.15\,[Citrulline] - 0.82\,[Hb] + 15.70\,[TCA] + 2.69\,[Cystathionine] + 5.16\,[Phe/Tyr] + 20.07$$

The predicted vs. observed AUC plot showed a good prediction ability of the model (R^2 = 0.73; R^2-adj = 0.69) with a bias and precision of 4.6% and 17.4%, respectively (**Figure 12**). For citrulline and Hb with negative coefficients, as their serum concentrations decrease, AUC is predicted to increase, while for variables with positive coefficients (TCA, cystathionine, Phe/Tyr), as their value increase, AUC is predicted to increase too.

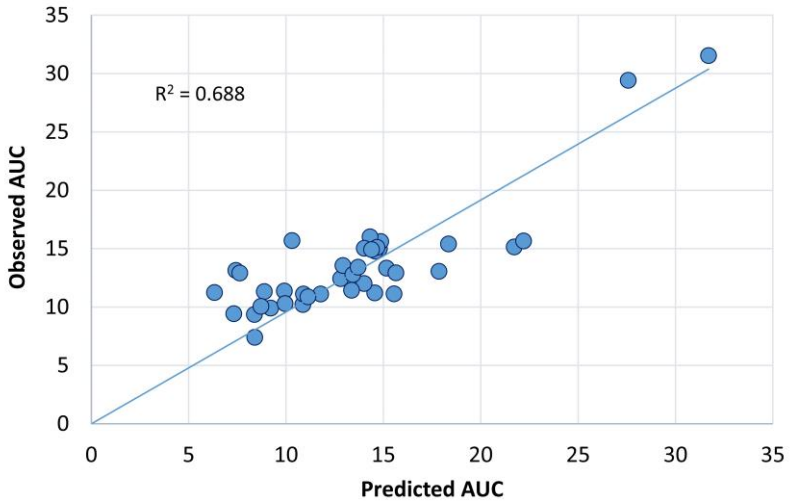

Figure 12. Predicted vs. observed AUC_{norm} plot calculated by multiple regression analysis without. The baseline showed a coefficient of regression of 0.703 and a bias of 17.4%.

Differences in the trabectedin AUC_{norm} were also investigated as function of the baseline patients' clinical and demographic characteristics (**Figure 13**). Patients with L-sarcomas showed significantly lower AUC_{norm} compared to those having other sarcomas (p = 0.008, t-test) as well as tumour grade G2 patients compared to G3 (p = 0.001) had 1.4-fold higher AUC_{norm}. PS was also found associated

with PK, indeed wealthy patients with PS=0 showed significant lower AUC_{norm} than individuals with PS =1 (p = 0.042). No other correlations were found between PK and gender or age.

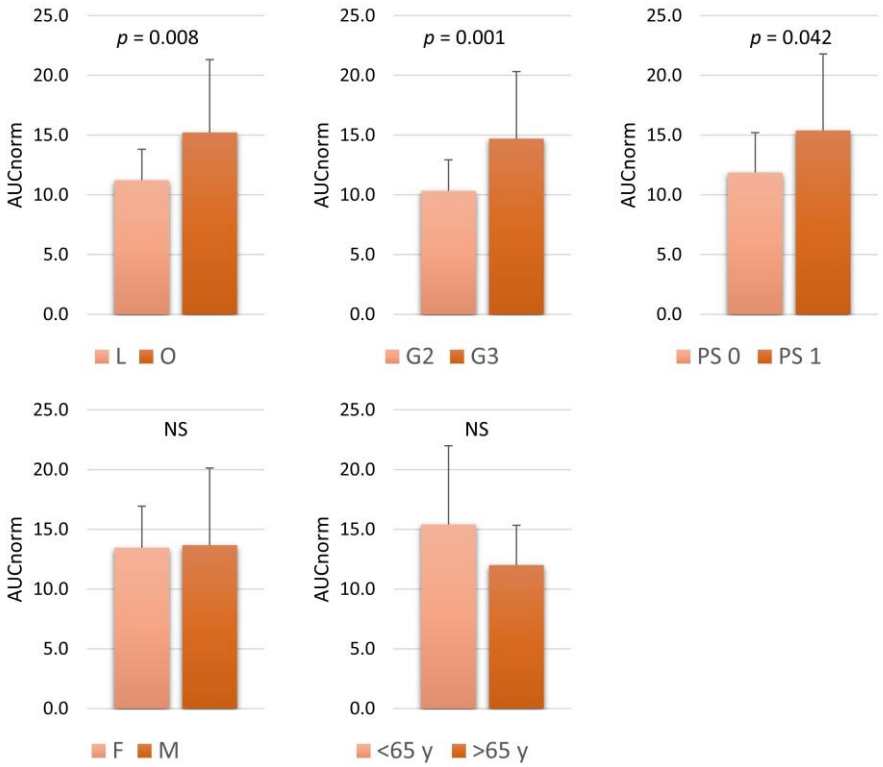

Figure 13. Associations between trabectedin normalized AUC and clinical characteristics such as histotypes, tumour grading, PS, sex and age. AUC data are expressed as mean and SD. Abbreviations: L, leiomyosarcoma and liposarcoma; O, other sarcomas; PS, performance status; F, female; M, male; G2, G3, tumour grade.

3.7 Metabolomics signatures associated with treatment response

Clinical benefit was evaluated on the basis of changes in tumours sizes after three cycles of treatment and patients were accordingly classified as PD (n=20) and SD (n=16). The supervised PLS-DA model clearly distinguished the pre-dose serum metabolomics and clinical data profiles of the two investigated groups (**Figure 14a**) with acceptable model performance (R^2 = 0.57, Q^2 = 0.33) and no risk of overfitting (**Figure 14b**). The variables that mainly contributed to such group classification with a VIP>1 included 15 AAs and derivatives, 3 BAs and 6 clinical parameters (**Figure 14c**).

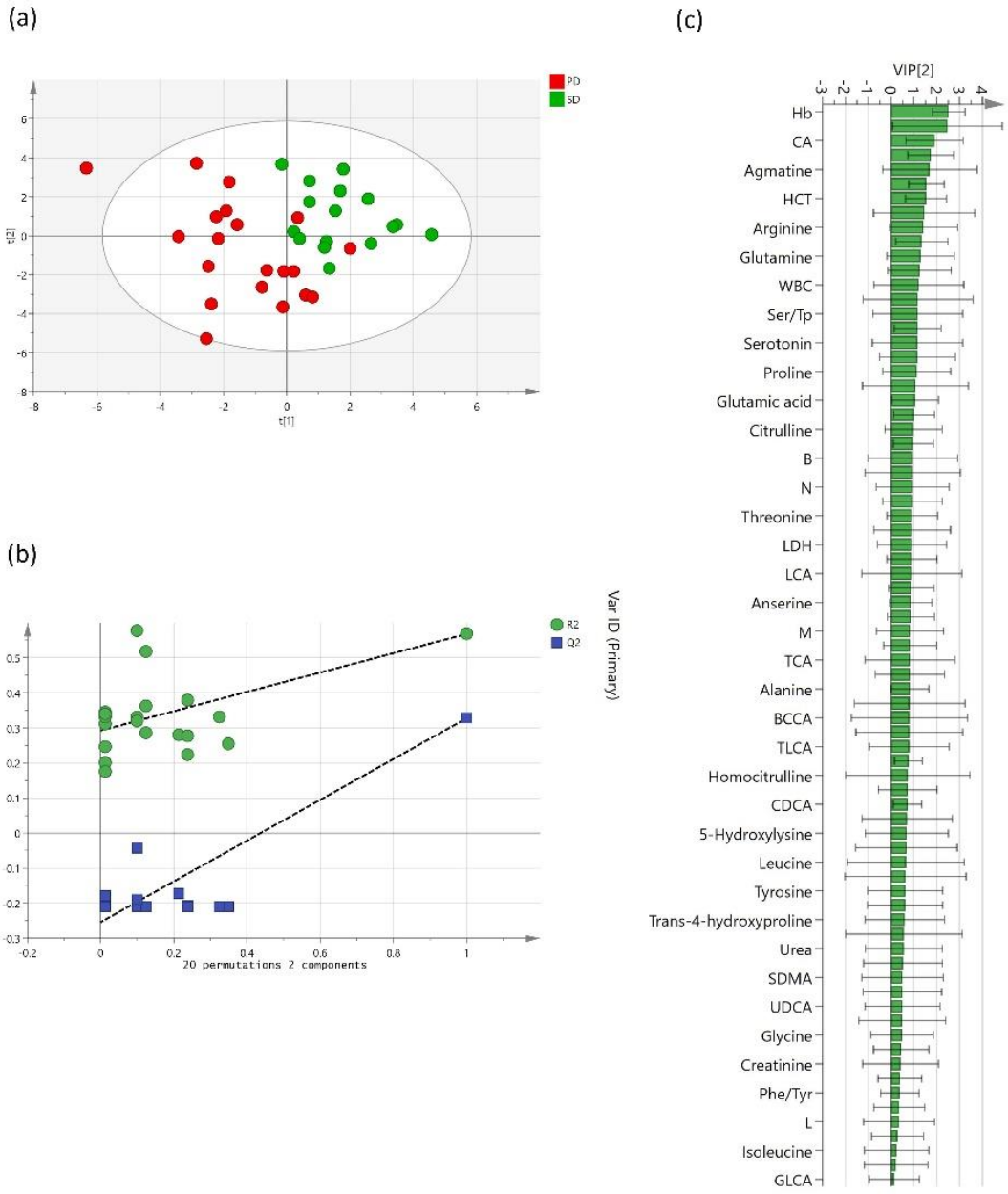

Figure 14. Partial least squares discriminant analysis (PLS-DA) score plot discriminated serum clinical-metabolomics profiles of PD (n = 20, red) and SD patients (n = 16, green) (**a**). Permutation test showed R^2 (green) and Q^2 (blue) validation parameters significantly different between permuted and original models (**b**). Variable importance in projection (VIP) of PLS-DA model ranked by increasing values (**c**).

When t-test was applied only five serum variables resulted to be statistically different, in particular, Hb was significantly lower in PD patients compared to the SD group ($p = 9 \cdot 10^{-4}$), while serum cystathionine ($p = 0.002$), agmatine ($p = 0.03$), and CA ($p = 0.02$) were higher in PD than SD patients. The mean serum concentrations of these compounds together with the relative fold change (mean PD/SD ratio) were depicted in **Figure 15**. Interestingly, the PD group showed also a normalized trabectedin AUC 1.5-fold higher than the counterpart SD group ($p = 5 \cdot 10^{-5}$). Despite the increased drug exposure, the toxicity rate did not result statistically different between groups with G0-2

toxicity occurring in 12 PD and 9 SD patients, while G3-4 toxicity in 8 PD and 9 SD patients (p =0.503, Fisher exact test). Moreover, the high G3 tumour grade and the histotype different from L-sarcomas were also found associated with a bad prognosis (Fisher test, p =0.0017 and p =0.041, respectively). No significant differences were instead present between PD and SD patients in terms of PS, age or gender.

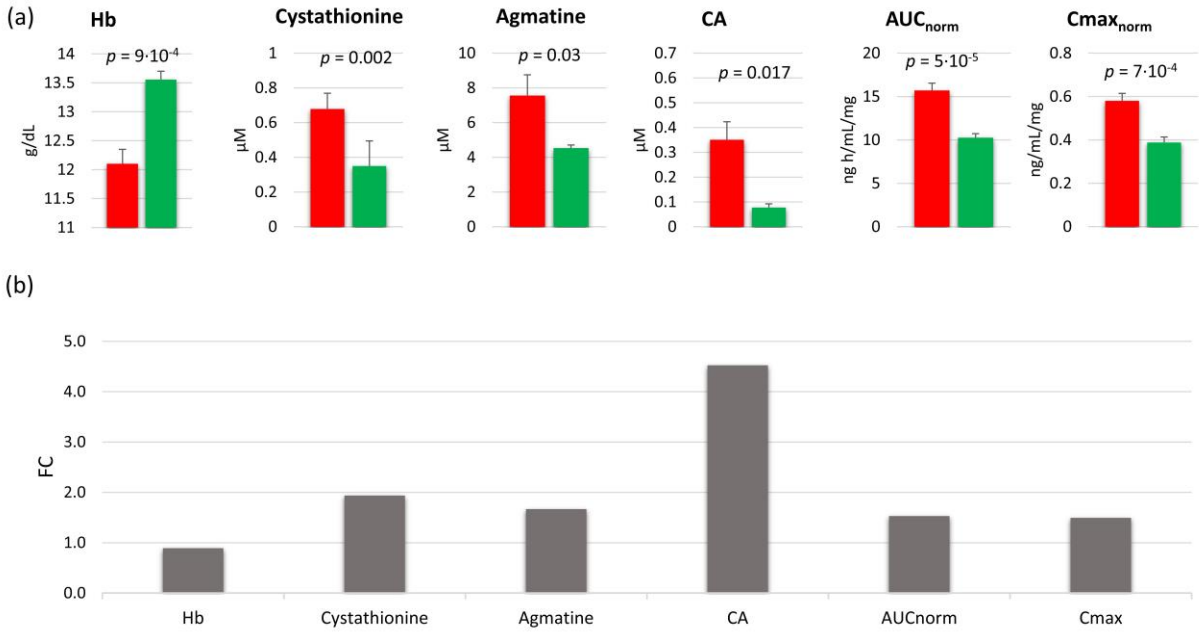

Figure 15. Serum concentrations of variables significantly different between PD (red) and SD patients (green) expressed as mean± SE (**a**) and corresponding fold change (FC) expressed as mean concentration ratio between PD and SD (**b**).

The ROC analysis of each singles variable showed for Hb and cystathionine the highest diagnostic capability in distinguishing PD and SD patients with an AUROC of 0.78 (55% sensitivity, 100% specificity) for Hb and of 0.80 (85% sensitivity, 62.5% specificity) for cystathionine (**Figure 16a,b**). The combination of these variables in a logistic regression model resulted in a better discriminatory power with an AUROC=0.87, a sensitivity of 90%, and a specificity of 75% (**Figure 16c**). Moreover, the integration of the model with the PK parameter $C_{max\,norm}$ further improved the ability of the model in distinguishing SD and PD patients (AUROC=0.92, sensitivity 90%, specificity 81.3%) (**Figure 16d**).

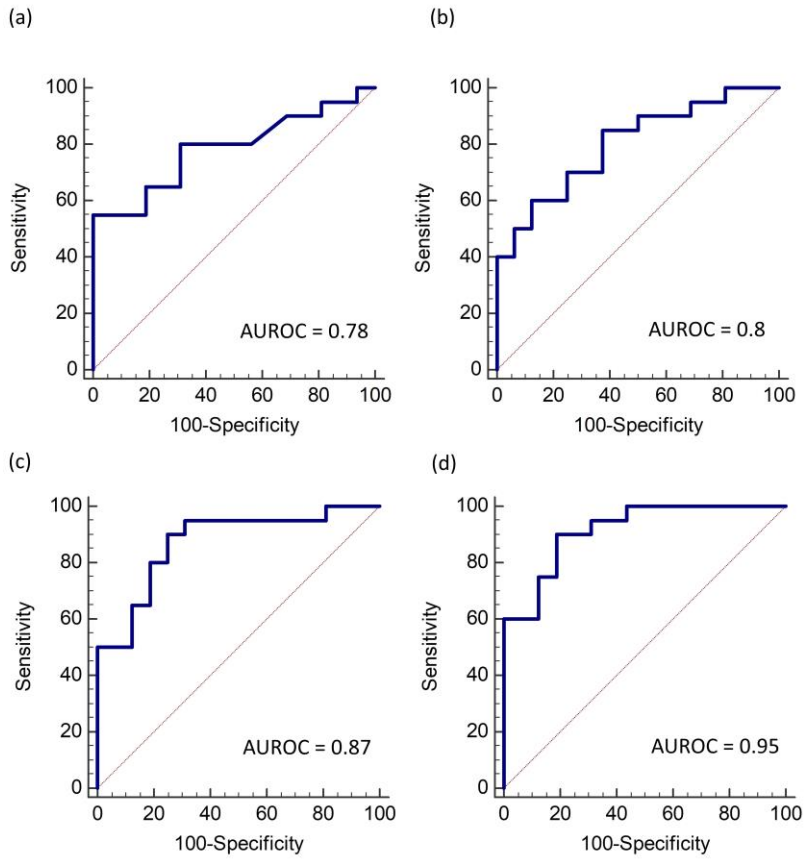

Figure 16. Receiving operator characteristic (ROC) curve for single Hb (**a**), cystathionine (**b**) with an AUROC of 0.78 and 0.8, respectively. The combination of these molecules (**c**) and the integration also with C_{max} (**d**) had higher AUROC of 0.87 (sensitivity, 90%; specificity 75%) and 0.95 (sensitivity, 90%; specificity 81.3%), respectively.

Differences in the baseline metabolomics profiles were investigated also as function of the toxicological response. The PLS-DA analysis showed a modest separation between patients having G0-2 (n= 21) and G3-4 (n= 19) total toxicity (**Figure 17**), however, the model did not pass the internal validation test (R^2 = 0.47, Q^2 = −0.21), not allowing the identification of specific metabolomics signatures of trabectedin toxicological response. The potential association of the toxicity with the PK of the drug was also investigated, however, no differences were found in AUC_{norm} values between G0-2 and G3-4 groups (p = 0.550).

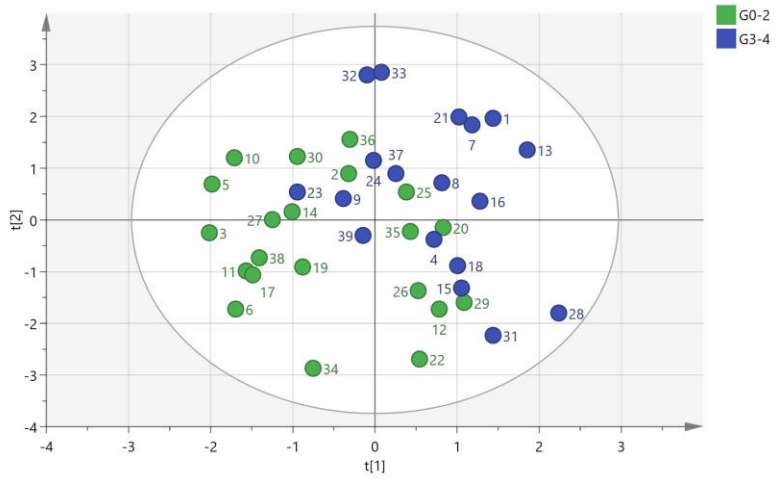

Figure 17. PLS-DA score plot based on serum clinical-metabolomics profiles of patients with G0-2 (n = 21, green) and G3-4 toxicity (n = 19, blue).

3.8 Overall survival prediction by metabolomics

Selection of potential survival predictors

The Kaplan-Meier curve showed a very low survival for metastatic STSs patients, characterized by a median OS of 13.0 months (95% CI, 5.6–23.5) with only 20% of the population surviving more than 1 year (Figure 18).

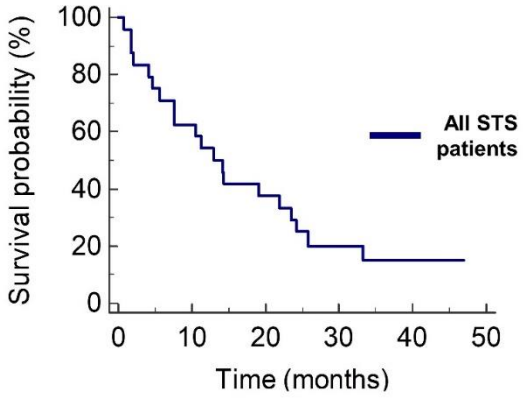

Figure 18. Kaplan–Meier survival analysis in all metastatic STSs patients (n= 24). The censored data included 4 patients, while the other 20 were not censored.

Associations between survival and baseline clinical data analyses indicated that patients with L-sarcoma had a significant longer OS (median, 23.5 months; 95% CI, 4.1–33.2) than patients with other histological types (11.3 months; 95 % CI, 1.7–25.8; p = 0.046 log-rank test) (Figure 19a). Long OS characterized also patients with PS of 0 (23.5 months; 95% CI, 5.6–25.8) compared to those with PS= 1-2 (7.6 months; 95% CI, 2.1–33.2; p = 0.026) (Figure 19b). Conversely, having Hb <12 g/dL was found to be significantly associated with a shorter OS (4.1 months; 95% CI, 0.8–24.2 vs. 21.8 months; 95% CI, 7.6–33.2; p = 0.001) in respect of Hb ≥12 g/dL (Figure 19f). No other associations were

found with tumour grade, age, blood ANC, sodium, albumin, lactate dehydrogenase **(**[**Figure 19c-e, g, h**](#)).

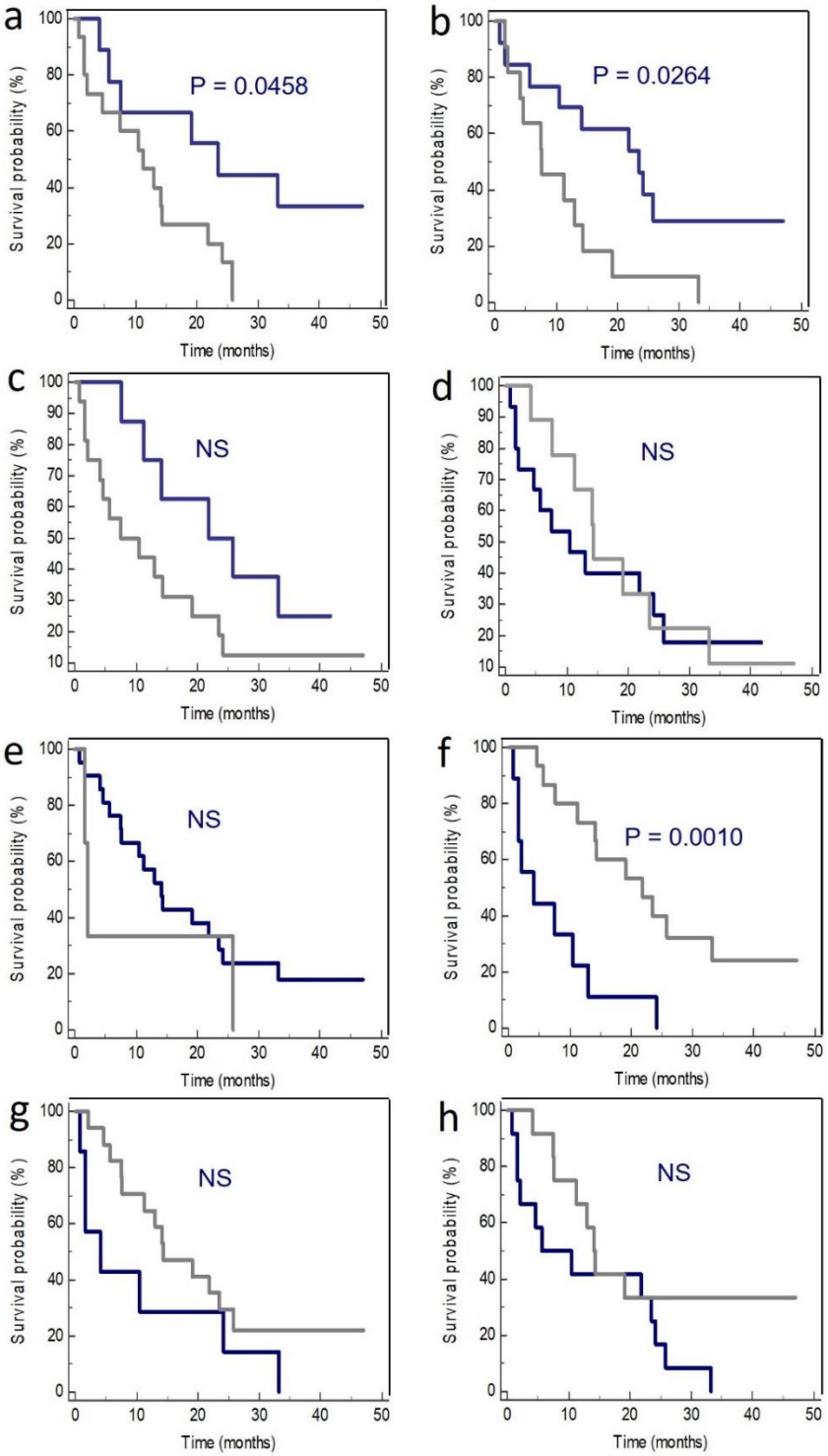

Figure 19. Kaplan-Meier curves of OS in patients stratified for: L-sarcomas (n=9, blue) vs. other histotypes (n=15) (**a**); PS score of 0 (n=13, blue) *vs*. 1 (n=11) (**b**); tumor grade G3 (n=16, blue) *vs*. G2 (n=8) (**c**); age<65 (n=15, blue) *vs*. ≥65 years (n=9)(**d**); absolute neutrophil count <7.5 ·10^9 cells/L (n=21, blue) *vs*. ≥7.5 ·10^9/L (n=3) (**e**); hemoglobin <12 g/dL (n=9, blue) *vs*. ≥12 g/dL (n=15) (**f**); albumin <3.5 g/dL (n=7, blue) *vs*. ≥3.5 g/dL (n=17) (**g**); lactate dehydrogenase <320 U/L (n=12, blue) *vs*. ≥320 U/L (n=12) (**h**).

Correlations between OS and baseline metabolomics data were also investigated by univariate Cox proportional hazards regression (**Table 7**). Four AAs were selected as best predictor variables, however, only citrulline and histidine resulted still significantly correlated after FDR correction (FDR<0.05).

Table 7. Univariate Cox regression analysis of the baseline metabolites.

Covariate	*p*	FDR*	Exp(b)	95% CI
Citrulline	0.001	0.018	0.907	0.86–0.96
Histidine	0.006	0.035	0.942	0.90–0.98
Cystathionine	0.011	0.053	11.343	1.75–73.43
TCA	0.023	0.070	41.431	1.67–1.03·10^3

* *p*-value corrected by Benjamini and Hochberg false discovery rate (FDR) procedure.
Exp(b), relative hazard risk; CI, confidence interval.

The assessment of their predictive ability for OS was further investigated by plotting martingale residuals from the Cox model *vs*. citrulline (Figure 20a) and histidine (Figure 20b) serum levels. Martingale residuals for both AAs were closer to the fitted line indicating a good potential predictivity for OS. In the plot, each point corresponded to patients' residuals, those below zero had a low risk to die, while those above an increased risk. Moreover, the inflexion points of the curves indicated the cut-off values for distinguishing long and short survival patients, in particular, it was about 30 µM for citrulline and 75 µM for histidine.

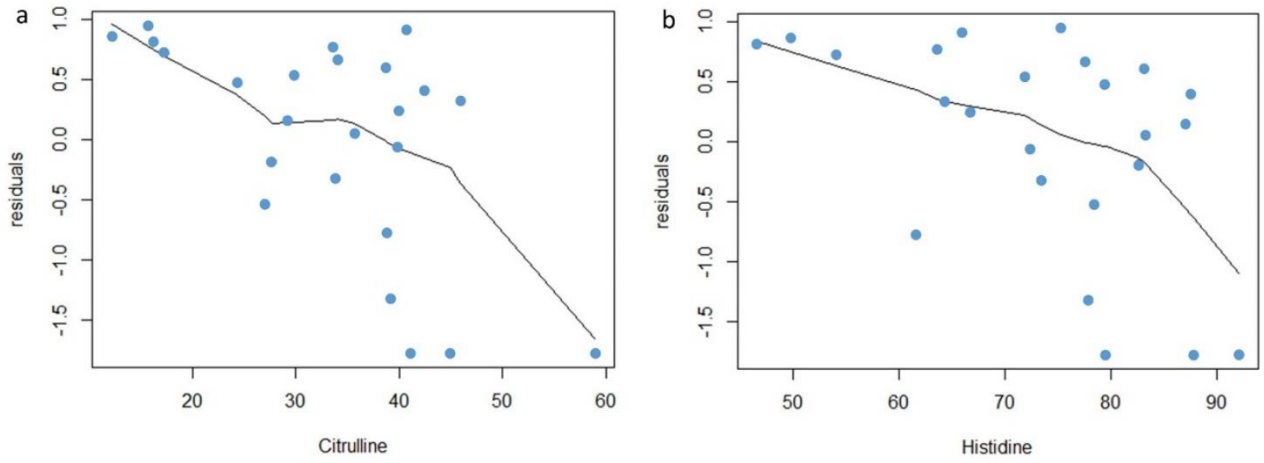

Figure 20. Martingale residuals from null Cox model vs. citrulline (**a**) and histidine (**b**) serum concentrations plotted with locally weighted scatterplot smoothing (LOWESS) fitting line.

The baseline serum levels of citrulline but not histidine were found significantly associated with the tumour grade. Specifically, patients with G3 tumours showed lower citrulline than patients with G2 tumour grade (p = 0.03). with a mean value of 30.7 ± 10.7 and 39.8 ± 9.6 µM, respectively.

Risk prediction model

Metabolites and clinical data (tumour grade, histotypes PS and blood test parameters) selected by univariate Cox regression were subjected to further screening by multivariate Cox proportional hazard regression analysis. Three covariates were identified as significantly associated with OS (**Table 8**) and thus used to build the risk prediction model equated as follows:

$$ln\left(\frac{H(t)}{H0\,(t)}\right) = -0.084 \cdot [\text{Citrulline}] - 0.388 \cdot [\text{Hb}] + 1.117 \cdot [\text{PS}]$$

where H(t)/H0(t) and its natural log represent the hazard ratio and the risk score, respectively. The sign of coefficients indicates the direct or inverse association with the death risk. Therefore, for citrulline and Hb the lowest is the concentration the highest the risk to die, conversely, for PS with a positive coefficient, as its value increases the hazard risk decreases and consequently OS is predicted to be longer.

Table 8. Multivariate Cox regression of significant prognostic factors.

Covariate	*p*	b	Exp(b)	95% CI of Exp(b)
Citrulline	0.010	- 0.084	0.919	0.86–0.98
Hemoglobin	0.009	- 0.388	0.679	0.51–0.91
PS	0.036	1.117	3.056	1.07–8.70

b, regression coefficient; Exp(b), relative hazard risk; CI, confidence interval; PS, performance status.

The predictive ability of the model was successfully assessed by calculating Harrell's C-index, which resulted 0.8. As citrulline showed a relative hazard risk of 0.92, its effective impact on OS prediction was tested removing it from the risk Cox model and recalculating the C-index. The latter was found to decrease from 0.8 to 0.75 ($p = 0.02$) when citrulline was excluded, underlining the good prognostic value of the AA. The risk scores generated by the model ranged from −10.81 to −3.36, with a median of −7.11. Patients with a score ≥ -6.19 fell into the 75th percentile and were classified as high-risk group (H-Risk), while patients with a score ≤ -3.36 constituted the low- to moderate-risk (LM-Risk) group.

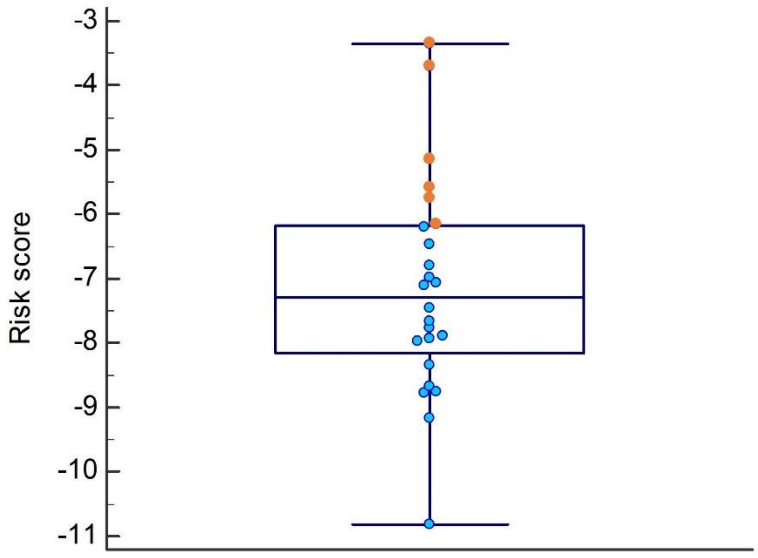

Figure 21. Box-and-whisker plot of the risk score from the Cox regression model. Horizontal lines indicated the median values that separated the lower 25th and the upper 75th quartiles; vertical lines denote the highest and lowest whiskers. Patients with a risk score > the 75th quartile value (-6.19) were included in the H-Risk (orange) while those with a risk score < the 25th quartile into the LM-Risk groups (blue).

The proportional hazard assumption of the multivariate Cox model was validated by plotting the Schoenfeld residuals against the survival time for each selected prognostic variable, citrulline, Hb and PS. Since the fitted lines from the residuals of each predictor resulted to be horizontal (**Figure 22**) and not statistically significant ($p > 0.05$), the proportional hazards assumption was satisfied, thus demonstrating that the log hazard ratio [Beta(t)] remain constant over time.

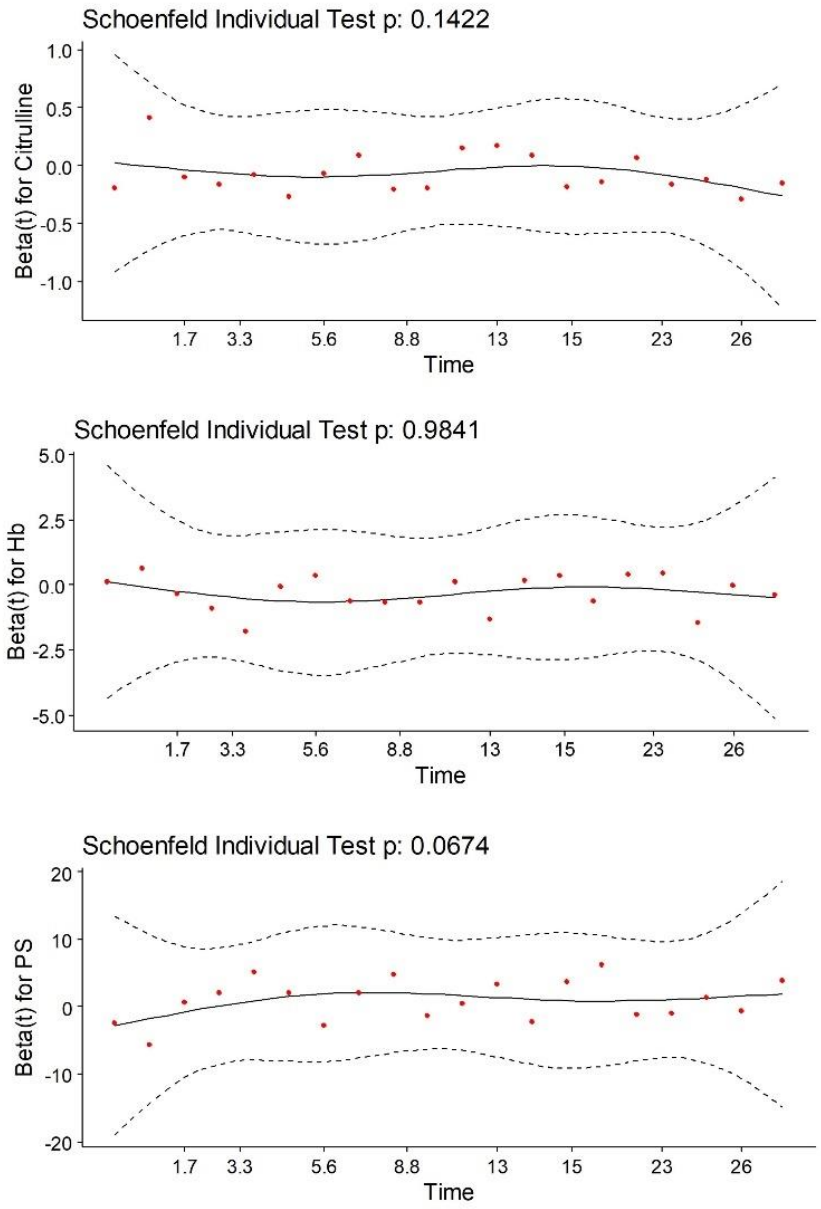

Figure 22. Schoenfeld residuals vs. overall survival time plot for citrulline, Hb and PS. The beta(t) is the log of hazard ratio and the black curve line is the fitted line indicating the time-dependency of covariates. The dashed lines are the confidence interval corresponding to ± two standard errors.

The proportional hazard assumption was also tested by Kaplan-Meier survival analysis (**Figure 23**) by comparison of the two investigated risk groups. The H-Risk patients showed a median OS of 2.1 months (95% CI, 0.8–7.6), significantly lower than that of the LM-Risk group with a median OS of 19.1 months (95% CI, 11.3–25.8). The significant differences between the Kaplan-Meier curve(p <

0.0001, log-rank test) ensured that the Cox proportional assumption was not violated.

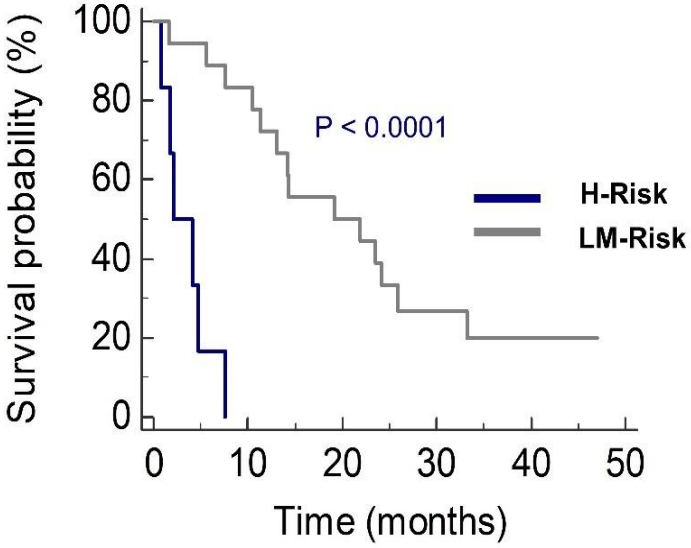

Figure 23. Kaplan–Meier survival analysis for overall survival in the high-risk (H-Risk, *n* = 6) and low- to medium-risk (LM-Risk, *n* = 18) groups identified according to their risk score from Cox regression model based on citrulline, Hb and PS.

The ROC analysis showed a good diagnostic power of the two serum variables of the model, with citrulline found able to discriminate H-Risk and LM-Risk patients with a sensitivity of 100 % and a specificity of 77.8% (AUROC= 0.96; 95% CI, 0.74–0.99) and Hb with a sensitivity of 100%, and specificity was 72.2% (AUROC = 0.87; 95% CI, 0.67–0.97) (**Figure 24**). The cut-off values identified for group classification were 33.7 µM and 12.4 g/dL for citrulline and Hb, respectively.

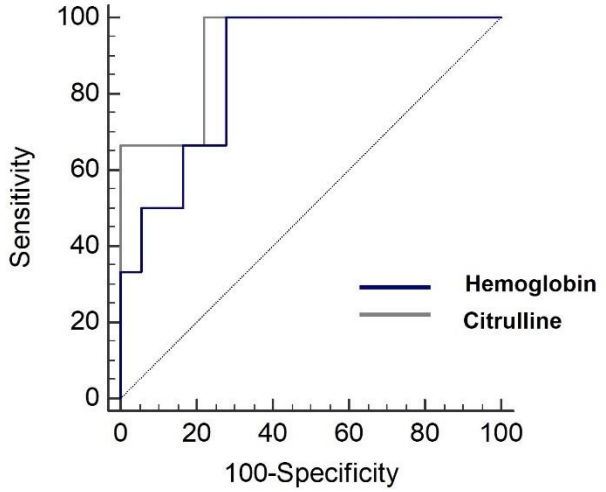

Figure 24. ROC curve analysis of serum citrulline and Hb. The AUC of citrulline was 0.926, with a sensitivity of 100 % and a specificity of 77.8 %. For Hb, the AUC was 0.870, with a sensitivity of 100 % and a specificity of 72.2 %.

The differences between H-Risk and LM-Risk groups in serum levels of citrulline and related AAs involved in its metabolism were investigated. Besides citrulline, ornithine was found 0.43-fold significantly lower in the H-Risk group compared to the LM-risk one (p = 0.02, Student's t test);

however, after normalization for arginine only the citrulline-arginine (CIT/ARG) ratio maintained the statistical significance (p< 0.0001) (**Figure 25**). Moreover, the variability in trabectedin PK was also investigated and high AUC values resulted associated with a worse survival prognosis, indeed the H-risk group showed a median AUC_{norm} of 18.5 compared to 10.4 ng/mL h^{-1} mg^{-1} of the LM-Risk group (p =0.023, Mann-Whitney) as well as a significant higher $C_{max\text{-}norm}$ of 0.7 ng/mL vs. 0.4 of the LM-R group (p =0.019).

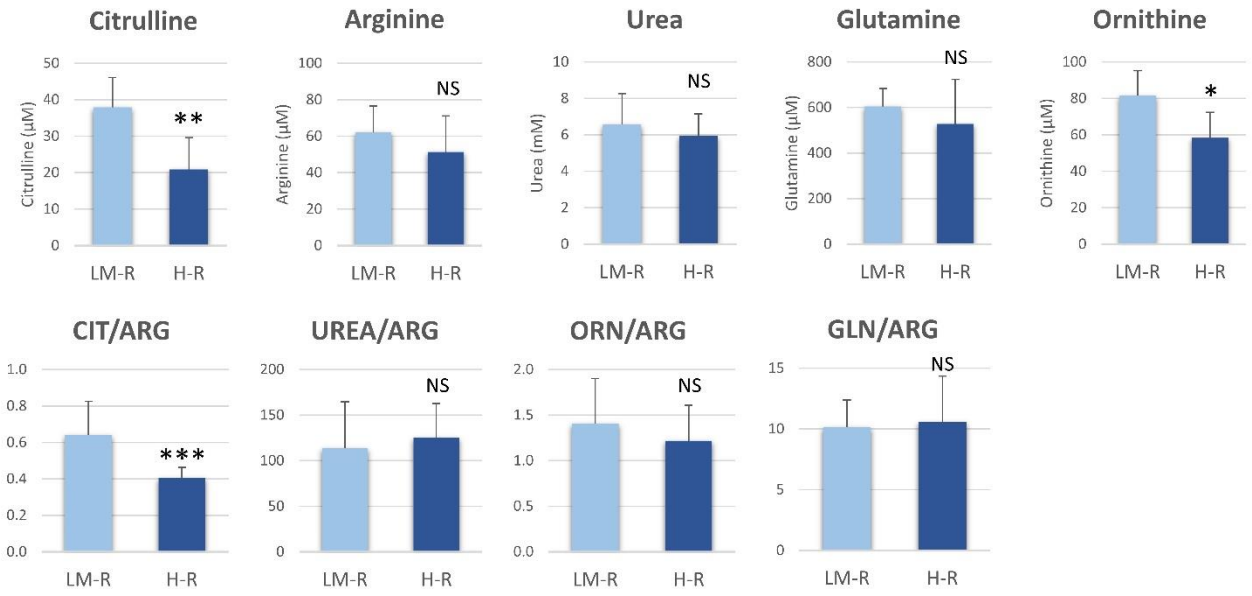

Figure 25. Serum concentrations of metabolites and their ratios involved in citrulline metabolism in H-R and LM-R groups. Values are expressed as mean and SD. *** p < 0.001; ** p < 0.01; * p < 0.05, Student's t-test. LM-R, low- to the medium-risk group; H-R, high-risk group; CIT, citrulline; ARG, arginine; ORN, ornithine; GLN, glutamine; NS, not significant

4. DISCUSSION

Trabectedin has been found to be highly effective in advanced STSs patients, however, a broad variability in the clinical outcome is observed among patients. Several studies evaluating its efficacy, reported a median PFS and OS of 4 and 12 months, respectively, but with only about 8-17% of patients achieving a complete or partial response, and 8% still alive after 4-years of follow-up [94,144–149]. The reasons behind such response variability to the same therapeutic regimen are barely known, making challenging the prediction of the clinical outcome and highlighting the need of predictive markers for trabectedin efficacy. Since the alterations in drug exposure can impact the final clinical effect, in this study we have attempted to explain the inter-individual trabectedin PK variations by metabolomics. The metabolomics profile intrinsically contains information about all those individual genetic and environmental factors that directly or indirectly can affect drug absorption, distribution metabolism and elimination (ADME) and influence the drug response. The trabectedin PK profiles, results of the individual ADME processes, was measured in all enrolled patients by the use of a new developed and validated HILIC-MS/MS method. The derived PK parameters resulted superimposable with those reported in other PK studies [115,145,150] showing the clinical suitability of the novel analytical method. As expected, the drug exposure expressed by AUC, showed a variability of about 34% in the investigated population and such differences were not found associated with age and gender factors, in agreement with literature data [150,151]. Interestingly, the baseline metabolomics profile resulted strongly correlated with the AUC, and the PLS regression model, based on metabolomic pre-dose data, allowed to predict with adequate accuracy the individual PK of trabectedin. However, a PLS model that includes numerous metabolites is not easily applicable in clinical practice, hence it was further resized by narrowing the number of the variables and integrating the clinical parameters. The final model, despite included only five metabolites, maintained a good prediction accuracy of the AUC, thus demonstrating the close relationship between the individual metabolic phenotype and the trabectedin PK. In particular, high drug exposure was associated with low serum levels of citrulline and Hb, and with high cystathionine, TCA and Phe/Tyr ratio. These metabolites could indirectly affect the drug PK by altering the expression and activity of CYP3A, which is the main enzyme responsible for the hepatic biotransformation and clearance of trabectedin [114,152,153]. The metabolite more likely involved in the CYP3A modulation is the TCA, which is a primary BA synthesized from cholesterol in the liver and conjugated with taurine. Different studies demonstrated that BAs, beyond their activity in dietary lipids absorption, can alter the CYP expression through direct interaction with the nuclear farnesoid X receptor (FXR) [154–156]. In particular, high levels of primary free and conjugated BAs can induce FXR activation that enhances CYP3A4 expression in a positive feedback mechanism [156,157]. The concomitant high serum TCA levels and drug AUC observed in this study, may thus result controversial since it would be expected an increased trabectedin metabolism with higher CYP expression. We could speculate that the CYP3A may have a lower affinity for trabectedin compared

to BAs and thus explain the higher drug exposure, but no published literature works evaluated the effect of BAs on trabectedin metabolism not allowing us to support such assumption. However, despite the difficulty to explain the mechanism of PK modulation by BAs, other pharmacometabolomics studies found a positive correlation between serum BAs and drug AUC [74,158,159], supporting the role of BAs as potential predictors of PK interindividual variability. Besides metabolic clearance, the association between TCA and AUC can instead find an explanation in altered drug transport mechanism. Indeed, both BAs and trabectedin are substrates of the ATP Binding Cassette 1-2 (ABCC1-2) also known as multidrug resistance-associated protein 1-2 (MRP1-2) [160–162]. These proteins, mainly localized in the membrane of hepatocytes, kidney and intestine cells, regulate the excretion of organic anions like bilirubin, bile acids and xenobiotics protecting cells from their toxic accumulation [163–169]. In our patients' population, the high baseline TCA levels may act as a competitive antagonist for the ABCC binding of trabectedin thus resulting in raised plasma drug concentration. Moreover, beyond TCA, also other free and conjugated BAs showed to increase proportionally with AUC, thus likely contributing to hamper trabectedin binding. Such potential inhibitory mechanism has led to an increased systemic drug exposure, which may induce acute trabectedin toxicity, as reported in different studies where severe hepatotoxicity was observed in patients and animals with dysfunctional ABCC transporters [170–173]. However, in our series of patients no significant associations between trabectedin AUC and liver toxicity were found, likely because all patients received a pre-treatment with dexamethasone, a potent ABCC inducer [155,174,175], that efficiently decreased the risk of hepatic injuries. Unlike TCA, the other metabolites cystathionine, citrulline, Phe/Tyr and Hb, identified as AUC predictors, did not show any direct link with the ADME processes. These metabolites more likely seemed to delineate a specific cancer patients phenotype characterized by a highly progressive disease. Different studies reported serum cystathionine accumulation in patients with more aggressive tumours [176–178] as well as low serum levels of citrulline were frequently associated with poor outcome [179–181]. In the same way, the Phe/Tyr ratio could reflect a pathophysiological status associated with ongoing inflammation processes being this metabolic ratio value correlated with immune activation markers [182,183]. All together these metabolites may identify a fragile phenotype characterized by a more aggressive tumour disease that may indirectly affect PK processing, predisposing these patients to an increased trabectedin exposure. This is corroborated by the observation that subjects with high AUC presented also a poor PS, a high G3 tumour grade and a non-L-sarcoma histotype, which is, in general, less responsive to trabectedin treatment. Taken all together, these findings showed that baseline metabolomic profile may contain relevant information to unveil differences in the individual phenotypes that in turn, may determine the variability in the drug PK. Hence, the proposed pharmacometabolomics model for trabectedin PK prediction could represent an integrative valuable approach for guiding clinicians in the assessment of the best therapeutic regimen, going toward therapy personalization.

Beyond PK, baseline metabolomics profiling could provide effective biomarkers also for the prediction of trabectedin pharmacodynamics. In this context, we searched for metabolic signatures associated with the inter-patients response variability evaluated as both clinical benefit and OS. The PLS analysis showed that patients in PD could be clearly distinguished from those in SD on the basis of their pre-dose clinical and metabolomics profile. In particular, low serum Hb and high levels of cystathionine, agmatine and CA were identified as negative prognostic factors. Their ability to classify patients according to the response to trabectedin treatment was investigated by ROC analysis, which highlighted cystathionine and Hb as the best classifiers, especially if used in combination. This serum metabolomic signature may be the result of the complex host-tumour metabolic interplay. The tumour metabolic reprogramming can induce modification not only at cellular level but it may involve the entire systemic host metabolism. This would result in changes in blood metabolites concentrations since some metabolites could be consumed to satisfy the cancer energy demand, while others could be synthesized to increase the pool for anabolic reactions necessary to sustain cancer proliferation and diffusion [184].

Cystathionine is an important intermediate of the trans sulphuration pathway consisting of two steps: the homocysteine and serine condensation by cystathionine β-synthase to produce cystathionine, and its hydrolysis by cystathionine γ-lyase into cysteine [185]. The latter is an essential AA for the synthesis of glutathione (GSH), an endogenous antioxidant that protects cells from reactive oxygen species (ROS) damage [186]. The high cystathionine concentrations in the PD group might result from an intensification of such pathway to sustain the pool of cysteine and GSH, which makes cancer cells able to survive also in a highly oxidant environments as those induced by chemotherapeutics [187]. This hypothesis was supported by different studies reporting an association between the high cystathionine β-synthase activity and the tumour progression of drug-resistant phenotype [188–193].

The present study also pointed out that low baseline Hb can be linked with a poor prognosis of STSs patients, in agreement with previous studies [132,194–198]. The presence of anaemia before the anticancer treatment was frequently reported in STSs patients as well as in other tumour types [199–202], suggesting that likely tumour itself can induce such anaemic status. It has been demonstrated that interleukin-6 (IL-6), a pro-inflammatory cytokine often elevated in advanced cancer patients including STSs [203–205], can reduce the gut absorption of iron necessary for erythropoiesis, so resulting in a blood Hb drop [206]. The low Hb found in the series of patients who experience PD, may reflect a more aggressive tumour behaviour with increased systemic inflammation, commonly associated with poor prognosis [203–205]. Moreover, low Hb levels were found to induce tumour hypoxia [207] that in turn can trigger the activation of several molecular pathways promoting angiogenesis, anaerobic metabolism and the transcription of targeted genes implicated in tumour metastasis and proliferation [208–211]. The results of the current investigation, besides confirming the prognostic role of Hb in STSs, underlined the importance of the integration of clinical and

metabolomics data to improve the early identification of patients with a more aggressive disease. However, although Hb and cystathionine could represent potential prognostic biomarkers for overall clinical outcome of STSs, they seemed not specifically predict the response to trabectedin treatment. In this context, since PD group showed a significantly higher trabectedin C_{max}, we integrated the model with this PK parameter, increasing not only their prognostic value, but also their specificity for the evaluation of clinical benefit of trabectedin treatment. The C_{max} can inform about the total drug exposure, being highly correlated with AUC, but compared to the latter, it requires only a blood sample collection, making its use in prognostic model as feasible as common blood biomarkers.

The second clinical endpoint of the study was the identification of specific metabolomics signature associated with the OS [212]. The investigated STSs population showed a median OS of 13 months with a great variability (95% CI, 5.6–23.5) superimposable with results of other similar clinical investigations [144,147,213]. Tumour histology, PS and baseline Hb were confirmed as prognostic factors of STSs OS [132,195,196,214,215], while no associations were found with other reported OS biomarkers, such as blood ANC, albumin and sodium [132,133]. This latter conflicting result was likely due to the more fit patients' population, which showed a better PS compared to those of patients considered in previous studies. The prognostic value based only on such clinical factors resulted limiting to explain the OS variability among patients, hence baseline metabolomics profiles were investigated in attempt to improve the prediction of the clinical outcome of metastatic STSs patients. Two serum AAs, citrulline and histidine, showed positive correlations with OS, indicating that the higher is their serum levels better is the prognosis. However, when Cox regression analysis was performed, only citrulline remained as significant predictor for OS together with Hb and PS [212]. The clinical-metabolomic model allowed the classification of STSs patients according to their mortality risk, identifying a H-Risk group with low OS (median, 2.1 months) and a LM-Risk group with longer OS (median, 19.1 months, $p < 0.0001$). The cut-off values for the discrimination of these two groups were derived from the ROC analysis: having citrulline ≤ 33.7 μM, Hb ≤ 12.4 g/dL and PS ≥ 1 was indicative of poor survival and identified H-Risk patients. The low serum citrulline in the group of H-Risk patients, as mentioned above, may derive from the tumour metabolism reprogramming that induces changes in the whole host metabolome, resulting in blood shortage of those metabolites necessary for cancer growth.

Citrulline is a non-proteogenic AA belonging to arginine metabolism. It is synthesised in the gut from glutamine, while in kidney and liver it participates in the de novo biosynthesis of arginine and in the urea cycle, respectively [216,217] (**Figure26**).

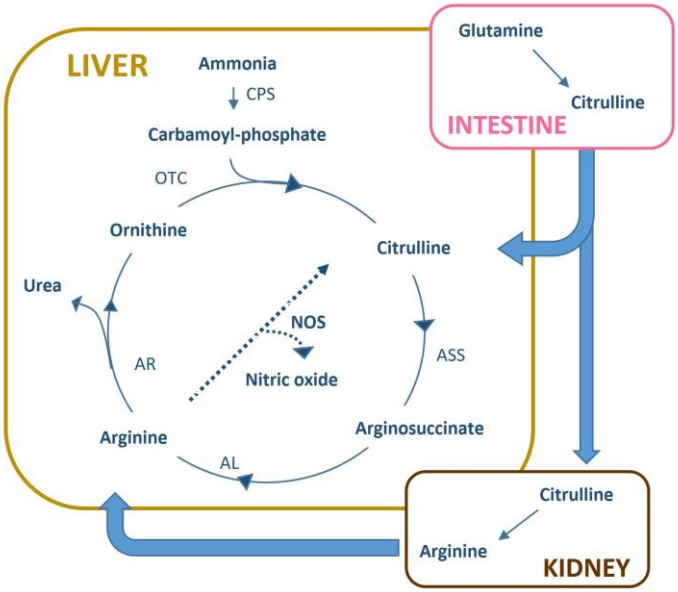

Figure 26. Citrulline metabolism. It is synthesised in enterocytes from glutamine and released into the circulation, reaching the kidneys, where it is used for arginine synthesis or the liver where it entered into the urea cycle for ammonia detoxification. Abbreviation: CPS, carbamoyl phosphate synthetase; ASS, argininosuccinate synthase; AL, argininosuccinate lyase; AR, arginase; OTC, ornithine transcarbamoylase.

Citrulline depletion is generally associated with intestinal injuries as a result of gut inflammation or damage from chemotherapy [217,218]. However, the citrulline shortage observed in the H-Risk patients seemed not associated with altered bowel function or citrulline biosynthesis, since the concentration of the precursor glutamine resulted equal in both LM- and H-Risk groups. Moreover, the bile acids produced by gut microbiome activity did not show any significant differences between groups, excluding the hypothesis of dysbiosis in these patients. Analogously, the serum urea concentrations were similar in the two groups, thus suggesting a normal hepatic functionality for ammonia detoxification by the urea cycle. This result is supported by the urea/arginine and ornithine/arginine ratios that did not significantly differ in the investigated groups. Therefore, the systemic loss of citrulline and ornithine in the H-Risk group may be related to their increased consumption rather than to the altered urea cycle. In the H-Risk patients, the high ornithine use might be liked to an increased polyamine synthesis. However, this assumption could not be confirmed since the polyamines spermine, spermidine and putrescine were not detected in this metabolomics analysis. The high citrulline utilization in the H-Risk patients may be due to an intense host metabolism aimed to maintain a systemic stock of the semi-essential AA arginine. This hypothesis is supported by the observation that the citrulline/arginine ratio was significantly lower in the H-Risk group, suggesting an increased conversion of citrulline into arginine [212]. Furthermore, in STSs it was reported a low expression of arginine metabolism enzyme, in particular of the argininosuccinate synthetase-1 (ASS1), which catalysed the arginine synthesis from citrulline [219,220]. Such

enzymatic loss makes STSs tumours auxotrophic for arginine, therefore the observed citrulline depletion in H-Risk patients may reflect an aggressive STS phenotype with a higher arginine demand to sustain its growth and progression needs. This hypothesis may explain the correlation between the low serum citrulline and short OS observed in the H-Risk patients. However, the relationship between such metabolic features and the trabectedin efficacy remains difficult to explain since arginine metabolism is not directly involved in the antitumor activity of the drug. Likely, such altered arginine metabolism does not influence trabectedin activity, but it may reflect a specific metabolic phenotype and its individual capability to face the deleterious effects of the disease. In this context, citrulline could be considered a prognostic factor independent from the type of chemotherapy and also from the cancer type. This is supported by recent studies reporting reduced citrulline levels in short survival patients with high-grade serous ovarian cancer [180] and with non-small cell lung cancer undergoing immunotherapy treatment [179]. This evidence suggests that the role of citrulline as negative prognostic factor may be applicable in other cancer patients and not only in STSs. However, given the limitation of the study, further investigations are needed to confirm and validate these results. The small number of patients and the lack of an external independent patients' group hindered a full validation of the findings. Moreover, the study involved only metastatic high tumour grade patients, limiting the application of the metabolomics models to STSs patients with advanced disease. Finally, to better assess the relationship between trabectedin efficacy and the identified prognostic biomarkers further studies should include STS patients undergoing different treatments.

5. CONCLUSION

This exploratory study, to our knowledge, is the first to propose a pharmacometabolomics approach for the prediction of individualized trabectedin PK. A metabolic phenotype predictive of drug exposure was identified, allowing to explain the PK inter-patients variability in a metastatic STSs population. The use of this baseline metabolomic profile, based on citrulline, cystathionine, TCA and Hb, may help physicians to predict the drug's fate and manage the safety and efficacy of trabectedin therapy. This study also contributed to the identification of pre-dose metabolomic signature associated with the clinical outcome of STS patients treated with trabectedin. The main findings are that cystathionine and Hb emerged as potential prognostic biomarkers of a poor responsive tumour helping to early individuate patients who would not benefit from the treatment. Moreover, the development of a survival risk model based on citrulline, Hb and PS, further improved the assessment of the clinical outcome, allowing the early identification of high-risk patients.

APPENDIX 1

Table A1. Amino-acids and derivatives included in the LC-MS/MS analysis.

Amino-acids	RT (min)	Selected IS
1-Methyl-L-Histidine	9.3	3-Methylhistidine IS
2-Aminoadipic acid	7.3	L-Serine IS
2-Aminobutyric acid	6.5	gamma-Aminobutyric acid IS
3-Aminoisobutyric acid	5.9	gamma-Aminobutyric acid IS
3-Methyl-L-Histidine	8.6	3-Methylhistidine IS
5-Hydroxylysine	10.3	Lysine IS
ADMA	8.2	ADMA IS
Alanine	7.0	Alanine IS
Arginine	9.3	Arginine IS
Argininosuccinic acid	10.8	Arginine IS
Asparagine	7.9	Asparagine IS
Aspartic acid	8.9	Aspartic acid IS
beta-Alanine	6.7	Alanine IS
Carnosine	9.7	3-Methylhistidine IS
Citrulline	7.9	Citrulline IS
Creatinine	4.3	Creatinine IS
Cystathionine	10.5	Cystathionine IS
Cystine	10.7	Cystine IS
Ethanolamine	5.7	Ethanolamine IS
gamma-Aminobutyric acid	5.7	gamma-Aminobutyric acid IS
Glutamic acid	8.1	Glutamic acid IS
Glutamine	7.6	Glutamine IS
Glycine	7.3	Glycine IS
Histidine	9.2	Histidine IS
Homocitrulline	7.7	Citrulline IS
Homocystine	5.3	Homocystine IS
Isoleucine	5.2	Leucine IS
L-Anserine	9.7	3-Methylhistidine IS
Leucine	4.9	Leucine IS
Lysine	9.7	Lysine IS
Methionine	5.3	Methionine IS
Ornithine	9.7	Ornithine IS
ortho-Phosphorylethanolamine	5.3	Lysine IS
ortho-Phosphoserine	10.5	Lysine IS
Phenylalanine	4.6	Phenylalanine IS
Proline	6.2	Proline IS
Sarcosine	6.6	Sarcosine IS
SDMA	8.2	SDMA IS
Serine	7.8	Serine IS
Serotonin	3.4	Serotonin IS
Taurine	6.0	Taurine IS
Threonine	7.3	Threonine IS
trans-4-Hydroxyproline	6.9	Proline IS
Tryptophan	4.2	Tryptophan IS
Tyrosine	5.4	Tyrosine IS
Urea	4.0	Urea IS
Valine	5.9	Valine IS
Kynurenine	4.4	Kynurenine IS
Agmatine	5.3	Lysine IS

*in red metabolites not detected in plasma samples

APPENDIX 2

Table A2. Compositions of standards mix AAs solutions used to for calibration curves.

	CAL 1	CAL 2	CAL 3	CAL 4	CAL 5
1-Methylhistidine	304.4	152.2	76.1	38.1	19.0
2-Aminoadipic acid	31.3	15.7	7.8	3.9	2.0
2-Aminobutyric acid	59.9	30.0	15.0	7.5	3.7
3-Aminoisobutyric acid	97.0	48.5	24.2	12.1	6.1
3-Methylhistidine	301.5	150.8	75.4	37.7	18.8
5-Hydroxylysine	299.4	149.7	74.9	37.4	18.7
ADMA	0.6	0.3	0.2	0.1	0.04
Alanine	1199.	599.8	299.9	150.0	75.0
Anserine	19.8	9.9	5.0	2.5	1.2
Arginine	304.0	152.0	76.0	38.0	19.0
Argininosuccinic acid	10.0	5.0	2.5	1.3	0.6
Asparagine	171.4	85.7	42.9	21.4	10.7
Aspartic acid	145.6	72.8	36.4	18.2	9.1
Beta-alanine	37.6	18.8	9.4	4.7	2.4
Carnosine	156.9	78.5	39.2	19.6	9.8
Citrulline	70.5	35.3	17.6	8.8	4.4
Creatinine	1000.	500.0	250.0	125.0	62.5
Cystathionine	21.1	10.6	5.3	2.6	1.3
Cystine	190.6	95.3	47.7	23.8	11.9
Ethanolamine	244.4	122.2	61.1	30.6	15.3
Gamma-aminobutyric acid	98.2	49.1	24.5	12.3	6.1
Glutamic acid	611.7	305.9	152.9	76.5	38.2
Glutamine	1219.	609.7	304.8	152.4	76.2
Glycine	1576.	788.3	394.1	197.1	98.5
Histidine	615.7	307.9	153.9	77.0	38.5
Homocitrulline	1585.	792.8	396.4	198.2	99.1
Homocystine	56.0	28.0	14.0	7.0	3.5
Isoleucine	232.1	116.1	58.0	29.0	14.5
Kynurenine	3.0	1.5	0.8	0.4	0.2
Leucine	391.6	195.8	97.9	49.0	24.5
Lysine	377.2	188.6	94.3	47.2	23.6
Methionine	81.1	40.5	20.3	10.1	5.1
O-Phosphorylethanolamin	78.9	39.4	19.7	9.9	4.9
O-Phosphoserine	42.4	21.2	10.6	5.3	2.7
Ornithine	300.7	150.4	75.2	37.6	18.8
Phenylalanine	430.9	215.4	107.7	53.9	26.9
Proline	823.4	411.7	205.9	102.9	51.5
Sarcosine	928.5	464.3	232.1	116.1	58.0
SDMA	0.5	0.2	0.1	0.1	0.0
Serine	761.3	380.7	190.3	95.2	47.6
Serotonin	0.1	0.0	0.0	0.0	0.0
Taurine	391.5	195.8	97.9	48.9	24.5
Threonine	454.6	227.3	113.7	56.8	28.4
Trans-4-hydroxyproline	40.9	20.5	10.2	5.1	2.6
Tryptophan	138.6	69.3	34.6	17.3	8.7
Tyrosine	232.2	116.1	58.1	29.0	14.5
Urea	6000.	3000.	1500.	750.0	375.0
Valine	696.5	348.3	174.1	87.1	43.5

APPENDIX 3

Table A3. Bile acids included in the LC-MS/MS analysis.

Bile acids	RT (min)	Selected IS
TUDCA	3.0	d5-TUDCA
GUDCA	2.9	d4-GUDCA
TCA	3.5	d5-TCA
GCA	3.5	d5-GCA
TCDCA	4.8	d5-TCDCA
TDCA	5.1	d5-TCDCA
GCDCA	4.8	d4-GLCA
GDCA	5.0	d4-GLCA
UDCA	5.6	d4-HDCA
HDCA	5.4	d4-HDCA
CA	5.7	d5-CA
TLCA	6.2	d4-GLCA
GLCA	6.2	d5-CDCA
CDCA	7.1	d4-GLCA
DCA	7.2	d5-CDCA
LCA	8.0	d4-LCA

*in red metabolites not detected in plasma samples

6. ACKNOWLEDGEMENTS

I wish to express my sincere gratitude and respect to my supervisor Giuseppe Corona. I am very appreciative for his precious attention and guidance, continuous support and encouragement during these three years. I want to thank also Dr. Gianmaria Miolo for his kind help and useful suggestion during this project, Dr. Pietro Bulian for sharing his knowledge about statistics, and Dr. Paolo Metus for hosting me in his laboratory and his kind help and patience. I want to acknowledge all colleagues of Immunopathology and Oncological Biomarkers of CRO, for making a friendly and warm working environment.

A special thanks to my PhD schoolmate and friend Albina, for sharing joy and pain over these years and all the friends of Campus CRO for being like a family and making funny the stay in Aviano.

Last but not least, I would like to thank my family who always supported and trusted me, and my life partner Daniele who has been a great source of inspiration for me and gave a lot of encouragement.

7. REFERENCES

1. Fiehn, O. Metabolomics--the Link between Genotypes and Phenotypes. *Plant Mol Biol* **2002**, *48*, 155–171.
2. Nicholson, J.K.; Lindon, J.C.; Holmes, E. "Metabonomics": Understanding the Metabolic Responses of Living Systems to Pathophysiological Stimuli via Multivariate Statistical Analysis of Biological NMR Spectroscopic Data. *Xenobiotica* **1999**, *29*, 1181–1189, doi:10.1080/004982599238047.
3. Wishart, D.S. Metabolomics for Investigating Physiological and Pathophysiological Processes. *Physiological Reviews* **2019**, *99*, 1819–1875, doi:10.1152/physrev.00035.2018.
4. Bao, X.; Wu, J.; Kim, S.; LoRusso, P.; Li, J. Pharmacometabolomics Reveals Irinotecan Mechanism of Action in Cancer Patients. *J Clin Pharmacol* **2019**, *59*, 20–34, doi:10.1002/jcph.1275.
5. Clish, C.B. Metabolomics: An Emerging but Powerful Tool for Precision Medicine. *Cold Spring Harb Mol Case Stud* **2015**, *1*, doi:10.1101/mcs.a000588.
6. Khamis, M.M.; Adamko, D.J.; El-Aneed, A. Mass Spectrometric Based Approaches in Urine Metabolomics and Biomarker Discovery. *Mass Spectrom Rev* **2017**, *36*, 115–134, doi:10.1002/mas.21455.
7. Yang, Q.-J.; Zhao, J.-R.; Hao, J.; Li, B.; Huo, Y.; Han, Y.-L.; Wan, L.-L.; Li, J.; Huang, J.; Lu, J.; et al. Serum and Urine Metabolomics Study Reveals a Distinct Diagnostic Model for Cancer Cachexia. *J Cachexia Sarcopenia Muscle* **2018**, *9*, 71–85, doi:10.1002/jcsm.12246.
8. Zhang, W.-T.; Zhang, Z.-W.; Guo, Y.-D.; Wang, L.-S.; Mao, S.-Y.; Zhang, J.-F.; Liu, M.-N.; Yao, X.-D. Discovering Biomarkers in Bladder Cancer by Metabolomics. *Biomark Med* **2018**, *12*, 1347–1359, doi:10.2217/bmm-2018-0229.
9. Pitt, J.J. Principles and Applications of Liquid Chromatography-Mass Spectrometry in Clinical Biochemistry. *Clin Biochem Rev* **2009**, *30*, 19–34.
10. Schrimpe-Rutledge, A.C.; Codreanu, S.G.; Sherrod, S.D.; McLean, J.A. Untargeted Metabolomics Strategies – Challenges and Emerging Directions. *J Am Soc Mass Spectrom* **2016**, *27*, 1897–1905, doi:10.1007/s13361-016-1469-y.
11. Emwas, A.-H.M. The Strengths and Weaknesses of NMR Spectroscopy and Mass Spectrometry with Particular Focus on Metabolomics Research. *Methods Mol Biol* **2015**, *1277*, 161–193, doi:10.1007/978-1-4939-2377-9_13.
12. Markley, J.L.; Brüschweiler, R.; Edison, A.S.; Eghbalnia, H.R.; Powers, R.; Raftery, D.; Wishart, D.S. The Future of NMR-Based Metabolomics. *Current Opinion in Biotechnology* **2017**, *43*, 34–40, doi:10.1016/j.copbio.2016.08.001.
13. Tsugawa, H.; Cajka, T.; Kind, T.; Ma, Y.; Higgins, B.; Ikeda, K.; Kanazawa, M.; VanderGheynst, J.; Fiehn, O.; Arita, M. MS-DIAL: Data-Independent MS/MS Deconvolution for Comprehensive Metabolome Analysis. *Nat Methods* **2015**, *12*, 523–526, doi:10.1038/nmeth.3393.
14. Anjo, S.I.; Santa, C.; Manadas, B. SWATH-MS as a Tool for Biomarker Discovery: From Basic Research to Clinical Applications. *Proteomics* **2017**, *17*, doi:10.1002/pmic.201600278.
15. Guo, J.; Shen, S.; Xing, S.; Huan, T. DaDIA: Hybridizing Data-Dependent and Data-Independent Acquisition Modes for Generating High-Quality Metabolomic Data. *Anal. Chem.* **2021**, *93*, 2669–2677, doi:10.1021/acs.analchem.0c05022.
16. Roberts, L.D.; Souza, A.L.; Gerszten, R.E.; Clish, C.B. Targeted Metabolomics. *Curr Protoc Mol Biol* **2012**, *CHAPTER*, Unit30.2, doi:10.1002/0471142727.mb3002s98.
17. Cao, G.; Song, Z.; Hong, Y.; Yang, Z.; Song, Y.; Chen, Z.; Chen, Z.; Cai, Z. Large-Scale Targeted Metabolomics Method for Metabolite Profiling of Human Samples. *Analytica Chimica Acta* **2020**, *1125*, 144–151, doi:10.1016/j.aca.2020.05.053.
18. Chen, Y.; Zhou, Z.; Yang, W.; Bi, N.; Xu, J.; He, J.; Zhang, R.; Wang, L.; Abliz, Z. Development of a Data-Independent Targeted Metabolomics Method for Relative Quantification Using Liquid Chromatography Coupled with Tandem Mass Spectrometry. *Anal Chem* **2017**, *89*, 6954–6962, doi:10.1021/acs.analchem.6b04727.

19. Gu, H.; Zhang, P.; Zhu, J.; Raftery, D. Globally Optimized Targeted Mass Spectrometry: Reliable Metabolomics Analysis with Broad Coverage. *Anal Chem* **2015**, *87*, 12355–12362, doi:10.1021/acs.analchem.5b03812.
20. Tautenhahn, R.; Patti, G.J.; Rinehart, D.; Siuzdak, G. XCMS Online: A Web-Based Platform to Process Untargeted Metabolomic Data. *Anal Chem* **2012**, *84*, 5035–5039, doi:10.1021/ac300698c.
21. Beale, D.J.; Pinu, F.R.; Kouremenos, K.A.; Poojary, M.M.; Narayana, V.K.; Boughton, B.A.; Kanojia, K.; Dayalan, S.; Jones, O.A.H.; Dias, D.A. Review of Recent Developments in GC–MS Approaches to Metabolomics-Based Research. *Metabolomics* **2018**, *14*, 152, doi:10.1007/s11306-018-1449-2.
22. Krumpochova, P.; Bruyneel, B.; Molenaar, D.; Koukou, A.; Wuhrer, M.; Niessen, W.M.A.; Giera, M. Amino Acid Analysis Using Chromatography-Mass Spectrometry: An Inter Platform Comparison Study. *J Pharm Biomed Anal* **2015**, *114*, 398–407, doi:10.1016/j.jpba.2015.06.001.
23. Bernardo-Bermejo, S.; Sánchez-López, E.; Tan, L.; Benito-Martínez, S.; Jiang, Z.; Castro-Puyana, M.; Lucio-Cazaña, F.J.; Marina, M.L. Exploratory Metabolomic Analysis Based on Reversed-Phase Liquid Chromatography–Mass Spectrometry to Study an In Vitro Model of Hypoxia-Induced Metabolic Alterations in HK-2 Cells. *International Journal of Molecular Sciences* **2021**, *22*, 7399, doi:10.3390/ijms22147399.
24. Eghlimi, R.; Shi, X.; Hrovat, J.; Xi, B.; Gu, H. Triple Negative Breast Cancer Detection Using LC–MS/MS Lipidomic Profiling. *J. Proteome Res.* **2020**, *19*, 2367–2378, doi:10.1021/acs.jproteome.0c00038.
25. Jaochico, A.; Sangaraju, D.; Shahidi-Latham, S.K. A Rapid Derivatization Based LC-MS/MS Method for Quantitation of Short Chain Fatty Acids in Human Plasma and Urine. *Bioanalysis* **2019**, *11*, 741–753, doi:10.4155/bio-2018-0241.
26. Naser, F.J.; Mahieu, N.G.; Wang, L.; Spalding, J.L.; Johnson, S.L.; Patti, G.J. Two Complementary Reversed-Phase Separations for Comprehensive Coverage of the Semipolar and Nonpolar Metabolome. *Anal Bioanal Chem* **2018**, *410*, 1287–1297, doi:10.1007/s00216-017-0768-x.
27. Virág, D.; Király, M.; Drahos, L.; Édes, A.E.; Gecse, K.; Bagdy, G.; Juhász, G.; Antal, I.; Klebovich, I.; Dalmadi Kiss, B.; et al. Development, Validation and Application of LC-MS/MS Method for Quantification of Amino Acids, Kynurenine and Serotonin in Human Plasma. *J Pharm Biomed Anal* **2020**, *180*, 113018, doi:10.1016/j.jpba.2019.113018.
28. King, A.M.; Mullin, L.G.; Wilson, I.D.; Coen, M.; Rainville, P.D.; Plumb, R.S.; Gethings, L.A.; Maker, G.; Trengove, R. Development of a Rapid Profiling Method for the Analysis of Polar Analytes in Urine Using HILIC–MS and Ion Mobility Enabled HILIC–MS. *Metabolomics* **2019**, *15*, 17, doi:10.1007/s11306-019-1474-9.
29. Nguyen, H.P.; Chandel, N.S.; DeBerardinis, R.J.; Schug, K.A. Hydrophilic Interaction Liquid Chromatography Coupled with MS/MS to Detect and Quantify Dicarboxyethyl Glutathione, a Metabolic Biomarker of the Fumarate Hydratase Deficient Cancer Cell. *J Sep Sci* **2013**, *36*, 3303–3309, doi:10.1002/jssc.201300602.
30. Pavlaki, A.; Begou, O.; Deda, O.; Farmaki, E.; Dotis, J.; Gika, H.; Taparkou, A.; Raikos, N.; Papachristou, F.; Theodoridis, G.; et al. Serum-Targeted HILIC-MS Metabolomics-Based Analysis in Infants with Ureteropelvic Junction Obstruction. *J. Proteome Res.* **2020**, *19*, 2294–2303, doi:10.1021/acs.jproteome.9b00855.
31. Tang, D.-Q.; Zou, L.; Yin, X.-X.; Ong, C.N. HILIC-MS for Metabolomics: An Attractive and Complementary Approach to RPLC-MS. *Mass Spectrom Rev* **2016**, *35*, 574–600, doi:10.1002/mas.21445.
32. Teleki, A.; Takors, R. Quantitative Profiling of Endogenous Metabolites Using Hydrophilic Interaction Liquid Chromatography-Tandem Mass Spectrometry (HILIC-MS/MS). *Methods Mol Biol* **2019**, *1859*, 185–207, doi:10.1007/978-1-4939-8757-3_10.
33. Virgiliou, C.; Gika, H.G.; Theodoridis, G.A. HILIC-MS/MS Multi-Targeted Method for Metabolomics Applications. *Methods Mol Biol* **2018**, *1738*, 65–81, doi:10.1007/978-1-4939-7643-0_5.
34. Buszewski, B.; Noga, S. Hydrophilic Interaction Liquid Chromatography (HILIC)--a Powerful Separation Technique. *Anal Bioanal Chem* **2012**, *402*, 231–247, doi:10.1007/s00216-011-5308-5.

35. Wilm, M. Principles of Electrospray Ionization. *Mol Cell Proteomics* **2011**, *10*, M111.009407, doi:10.1074/mcp.M111.009407.
36. Garcia-Ac, A.; Segura, P.A.; Viglino, L.; Gagnon, C.; Sauvé, S. Comparison of APPI, APCI and ESI for the LC-MS/MS Analysis of Bezafibrate, Cyclophosphamide, Enalapril, Methotrexate and Orlistat in Municipal Wastewater. *J Mass Spectrom* **2011**, *46*, 383–390, doi:10.1002/jms.1904.
37. Gowda, G.A.N.; Djukovic, D. Overview of Mass Spectrometry-Based Metabolomics: Opportunities and Challenges. *Methods Mol Biol* **2014**, *1198*, 3–12, doi:10.1007/978-1-4939-1258-2_1.
38. Kushnir, M.M.; Rockwood, A.L.; Nelson, G.J.; Yue, B.; Urry, F.M. Assessing Analytical Specificity in Quantitative Analysis Using Tandem Mass Spectrometry. *Clinical Biochemistry* **2005**, *38*, 319–327, doi:10.1016/j.clinbiochem.2004.12.003.
39. King, R.; Fernandez-Metzler, C. The Use of Qtrap Technology in Drug Metabolism. *Curr Drug Metab* **2006**, *7*, 541–545, doi:10.2174/138920006777697936.
40. van den Berg, R.A.; Hoefsloot, H.C.; Westerhuis, J.A.; Smilde, A.K.; van der Werf, M.J. Centering, Scaling, and Transformations: Improving the Biological Information Content of Metabolomics Data. *BMC Genomics* **2006**, *7*, 142, doi:10.1186/1471-2164-7-142.
41. Warrack, B.M.; Hnatyshyn, S.; Ott, K.-H.; Reily, M.D.; Sanders, M.; Zhang, H.; Drexler, D.M. Normalization Strategies for Metabonomic Analysis of Urine Samples. *J Chromatogr B Analyt Technol Biomed Life Sci* **2009**, *877*, 547–552, doi:10.1016/j.jchromb.2009.01.007.
42. Worley, B.; Powers, R. Multivariate Analysis in Metabolomics. *Curr Metabolomics* **2013**, *1*, 92–107, doi:10.2174/2213235X11301010092.
43. Triba, M.N.; Le Moyec, L.; Amathieu, R.; Goossens, C.; Bouchemal, N.; Nahon, P.; Rutledge, D.N.; Savarin, P. PLS/OPLS Models in Metabolomics: The Impact of Permutation of Dataset Rows on the K-Fold Cross-Validation Quality Parameters. *Mol Biosyst* **2015**, *11*, 13–19, doi:10.1039/c4mb00414k.
44. Cai, H.-L.; Li, H.-D.; Yan, X.-Z.; Sun, B.; Zhang, Q.; Yan, M.; Zhang, W.-Y.; Jiang, P.; Zhu, R.-H.; Liu, Y.-P.; et al. Metabolomic Analysis of Biochemical Changes in the Plasma and Urine of First-Episode Neuroleptic-Naïve Schizophrenia Patients after Treatment with Risperidone. *J Proteome Res* **2012**, *11*, 4338–4350, doi:10.1021/pr300459d.
45. Derveaux, E.; Thomeer, M.; Mesotten, L.; Reekmans, G.; Adriaensens, P. Detection of Lung Cancer via Blood Plasma and 1H-NMR Metabolomics: Validation by a Semi-Targeted and Quantitative Approach Using a Protein-Binding Competitor. *Metabolites* **2021**, *11*, 537, doi:10.3390/metabo11080537.
46. van der Greef, J.; van Wietmarschen, H.; van Ommen, B.; Verheij, E. Looking Back into the Future: 30 Years of Metabolomics at TNO. *Mass Spectrometry Reviews* **2013**, *32*, 399–415, doi:10.1002/mas.21370.
47. Gates, S.C.; Sweeley, C.C. Quantitative Metabolic Profiling Based on Gas Chromatography. *Clin Chem* **1978**, *24*, 1663–1673.
48. Horning, E.C.; Horning, M.G. Human Metabolic Profiles Obtained by GC and GC/MS. *Journal of Chromatographic Science* **1971**, *9*, 129–140, doi:10.1093/chromsci/9.3.129.
49. Pauling, L.; Robinson, A.B.; Teranishi, R.; Cary, P. Quantitative Analysis of Urine Vapor and Breath by Gas-Liquid Partition Chromatography. *Proc Natl Acad Sci U S A* **1971**, *68*, 2374–2376, doi:10.1073/pnas.68.10.2374.
50. Jellum, E. Profiling of Human Body Fluids in Healthy and Diseased States Using Gas Chromatography and Mass Spectrometry, with Special Reference to Organic Acids. *J Chromatogr* **1977**, *143*, 427–462, doi:10.1016/s0378-4347(00)81792-2.
51. Jellum, E.; Kvittingen, E.A.; Stokke, O. Mass Spectrometry in Diagnosis of Metabolic Disorders. *Biomed Environ Mass Spectrom* **1988**, *16*, 57–62, doi:10.1002/bms.1200160111.
52. Politzer, I.R.; Dowty, B.J.; Laseter, J.L. Use of Gas Chromatography and Mass Spectrometry to Analyze Underivatized Volatile Human or Animal Constituents of Clinical Interest. *Clin Chem* **1976**, *22*, 1775–1788.
53. Putri, S.P.; Nakayama, Y.; Matsuda, F.; Uchikata, T.; Kobayashi, S.; Matsubara, A.; Fukusaki, E. Current Metabolomics: Practical Applications. *Journal of Bioscience and Bioengineering* **2013**, *115*, 579–589, doi:10.1016/j.jbiosc.2012.12.007.

54. Spratlin, J.L.; Serkova, N.J.; Gail Eckhardt, S. Clinical Applications of Metabolomics in Oncology: A Review. *Clin Cancer Res* **2009**, *15*, 431–440, doi:10.1158/1078-0432.CCR-08-1059.
55. Wishart, D.S. Emerging Applications of Metabolomics in Drug Discovery and Precision Medicine. *Nat Rev Drug Discov* **2016**, *15*, 473–484, doi:10.1038/nrd.2016.32.
56. Wang, X.-X.; Yu, P.; Li, J. High-Throughput Metabolomics for Identification of Metabolic Pathways and Deciphering the Effect Mechanism of Dioscin on Rectal Cancer From Cell Metabolic Profiles Coupled With Chemometrics Analysis. *Front. Pharmacol.* **2020**, *11*, doi:10.3389/fphar.2020.00068.
57. Debik, J.; Euceda, L.R.; Lundgren, S.; Gythfeldt, H. von der L.; Garred, Ø.; Borgen, E.; Engebraaten, O.; Bathen, T.F.; Giskeødegård, G.F. Assessing Treatment Response and Prognosis by Serum and Tissue Metabolomics in Breast Cancer Patients. *J Proteome Res* **2019**, *18*, 3649–3660, doi:10.1021/acs.jproteome.9b00316.
58. Chen, Z.; Li, Z.; Li, H.; Jiang, Y. Metabolomics: A Promising Diagnostic and Therapeutic Implement for Breast Cancer. *Onco Targets Ther* **2019**, *12*, 6797–6811, doi:10.2147/OTT.S215628.
59. Corona, G.; Cannizzaro, R.; Miolo, G.; Caggiari, L.; De Zorzi, M.; Repetto, O.; Steffan, A.; De Re, V. Use of Metabolomics as a Complementary Omic Approach to Implement Risk Criteria for First-Degree Relatives of Gastric Cancer Patients. *Int J Mol Sci* **2018**, *19*, doi:10.3390/ijms19030750.
60. Gertsman, I.; Barshop, B.A. Promises and Pitfalls of Untargeted Metabolomics. *J Inherit Metab Dis* **2018**, *41*, 355–366, doi:10.1007/s10545-017-0130-7.
61. Pinu, F.R.; Goldansaz, S.A.; Jaine, J. Translational Metabolomics: Current Challenges and Future Opportunities. *Metabolites* **2019**, *9*, 108, doi:10.3390/metabo9060108.
62. Gika, H.; Theodoridis, G. Sample Preparation Prior to the LC-MS-Based Metabolomics/Metabonomics of Blood-Derived Samples. *Bioanalysis* **2011**, *3*, 1647–1661, doi:10.4155/bio.11.122.
63. Yin, P.; Lehmann, R.; Xu, G. Effects of Pre-Analytical Processes on Blood Samples Used in Metabolomics Studies. *Anal Bioanal Chem* **2015**, *407*, 4879–4892, doi:10.1007/s00216-015-8565-x.
64. Draisma, H.H.M.; Reijmers, T.H.; van der Kloet, F.; Bobeldijk-Pastorova, I.; Spies-Faber, E.; Vogels, J.T.W.E.; Meulman, J.J.; Boomsma, D.I.; van der Greef, J.; Hankemeier, T. Equating, or Correction for between-Block Effects with Application to Body Fluid LC-MS and NMR Metabolomics Data Sets. *Anal Chem* **2010**, *82*, 1039–1046, doi:10.1021/ac902346a.
65. van der Kloet, F.M.; Bobeldijk, I.; Verheij, E.R.; Jellema, R.H. Analytical Error Reduction Using Single Point Calibration for Accurate and Precise Metabolomic Phenotyping. *J. Proteome Res.* **2009**, *8*, 5132–5141, doi:10.1021/pr900499r.
66. Gromski, P.S.; Xu, Y.; Hollywood, K.A.; Turner, M.L.; Goodacre, R. The Influence of Scaling Metabolomics Data on Model Classification Accuracy. *Metabolomics* **2015**, *11*, 684–695, doi:10.1007/s11306-014-0738-7.
67. Monge, M.E.; Dodds, J.N.; Baker, E.S.; Edison, A.S.; Fernández, F.M. Challenges in Identifying the Dark Molecules of Life. *Annu Rev Anal Chem (Palo Alto Calif)* **2019**, *12*, 177–199, doi:10.1146/annurev-anchem-061318-114959.
68. Bini, S.A. Artificial Intelligence, Machine Learning, Deep Learning, and Cognitive Computing: What Do These Terms Mean and How Will They Impact Health Care? *The Journal of Arthroplasty* **2018**, *33*, 2358–2361, doi:10.1016/j.arth.2018.02.067.
69. da Silva, R.R.; Dorrestein, P.C.; Quinn, R.A. Illuminating the Dark Matter in Metabolomics. *Proc Natl Acad Sci U S A* **2015**, *112*, 12549–12550, doi:10.1073/pnas.1516878112.
70. Liebal, U.W.; Phan, A.N.T.; Sudhakar, M.; Raman, K.; Blank, L.M. Machine Learning Applications for Mass Spectrometry-Based Metabolomics. *Metabolites* **2020**, *10*, 243, doi:10.3390/metabo10060243.
71. Pomyen, Y.; Wanichthanarak, K.; Poungsombat, P.; Fahrmann, J.; Grapov, D.; Khoomrung, S. Deep Metabolome: Applications of Deep Learning in Metabolomics. *Computational and Structural Biotechnology Journal* **2020**, *18*, 2818–2825, doi:10.1016/j.csbj.2020.09.033.

72. Clayton, T.A.; Lindon, J.C.; Cloarec, O.; Antti, H.; Charuel, C.; Hanton, G.; Provost, J.-P.; Le Net, J.-L.; Baker, D.; Walley, R.J.; et al. Pharmaco-Metabonomic Phenotyping and Personalized Drug Treatment. *Nature* **2006**, *440*, 1073–1077, doi:10.1038/nature04648.
73. Clayton, T.A.; Baker, D.; Lindon, J.C.; Everett, J.R.; Nicholson, J.K. Pharmacometabonomic Identification of a Significant Host-Microbiome Metabolic Interaction Affecting Human Drug Metabolism. *Proc Natl Acad Sci U S A* **2009**, *106*, 14728–14733, doi:10.1073/pnas.0904489106.
74. Huang, Q.; Aa, J.; Jia, H.; Xin, X.; Tao, C.; Liu, L.; Zou, B.; Song, Q.; Shi, J.; Cao, B.; et al. A Pharmacometabonomic Approach To Predicting Metabolic Phenotypes and Pharmacokinetic Parameters of Atorvastatin in Healthy Volunteers. *J. Proteome Res.* **2015**, *14*, 3970–3981, doi:10.1021/acs.jproteome.5b00440.
75. Kaddurah-Daouk, R.; Hankemeier, T.; Scholl, E.H.; Baillie, R.; Harms, A.; Stage, C.; Dalhoff, K.P.; Jűrgens, G.; Taboureau, O.; Nzabonimpa, G.S.; et al. Pharmacometabolomics Informs About Pharmacokinetic Profile of Methylphenidate. *CPT: Pharmacometrics & Systems Pharmacology* **2018**, *7*, 525–533, doi:10.1002/psp4.12309.
76. Phapale, P.B.; Kim, S.-D.; Lee, H.W.; Lim, M.; Kale, D.D.; Kim, Y.-L.; Cho, J.-H.; Hwang, D.; Yoon, Y.-R. An Integrative Approach for Identifying a Metabolic Phenotype Predictive of Individualized Pharmacokinetics of Tacrolimus. *Clinical Pharmacology & Therapeutics* **2010**, *87*, 426–436, doi:10.1038/clpt.2009.296.
77. Zhang, Z.; Gu, H.; Zhao, H.; Liu, Y.; Fu, S.; Wang, M.; Zhou, W.; Xie, Z.; Yu, H.; Huang, Z.; et al. Pharmacometabolomics in Endogenous Drugs: A New Approach for Predicting the Individualized Pharmacokinetics of Cholic Acid. *J. Proteome Res.* **2017**, *16*, 3529–3535, doi:10.1021/acs.jproteome.7b00218.
78. Muhrez, K.; Benz-de Bretagne, I.; Nadal-Desbarats, L.; Blasco, H.; Gyan, E.; Choquet, S.; Montigny, F.; Emond, P.; Barin-Le Guellec, C. Endogenous Metabolites That Are Substrates of Organic Anion Transporter's (OATs) Predict Methotrexate Clearance. *Pharmacological Research* **2017**, *118*, 121–132, doi:10.1016/j.phrs.2016.05.021.
79. Rahmioglu, N.; Le Gall, G.; Heaton, J.; Kay, K.L.; Smith, N.W.; Colquhoun, I.J.; Ahmadi, K.R.; Kemsley, E.K. Prediction of Variability in CYP3A4 Induction Using a Combined 1H NMR Metabonomics and Targeted UPLC-MS Approach. *J Proteome Res* **2011**, *10*, 2807–2816, doi:10.1021/pr200077n.
80. Shin, K.-H.; Choi, M.H.; Lim, K.S.; Yu, K.-S.; Jang, I.-J.; Cho, J.-Y. Evaluation of Endogenous Metabolic Markers of Hepatic CYP3A Activity Using Metabolic Profiling and Midazolam Clearance. *Clinical Pharmacology & Therapeutics* **2013**, *94*, 601–609, doi:10.1038/clpt.2013.128.
81. Tay-Sontheimer, J.; Shireman, L.M.; Beyer, R.P.; Senn, T.; Witten, D.; Pearce, R.E.; Gaedigk, A.; Gana Fomban, C.L.; Lutz, J.D.; Isoherranen, N.; et al. Detection of an Endogenous Urinary Biomarker Associated with CYP2D6 Activity Using Global Metabolomics. *Pharmacogenomics* **2014**, *15*, 1947–1962, doi:10.2217/pgs.14.155.
82. Miller, H.A.; Yin, X.; Smith, S.A.; Hu, X.; Zhang, X.; Yan, J.; Miller, D.M.; van Berkel, V.H.; Frieboes, H.B. Evaluation of Disease Staging and Chemotherapeutic Response in Non-Small Cell Lung Cancer from Patient Tumor-Derived Metabolomic Data. *Lung Cancer* **2021**, *156*, 20–30, doi:10.1016/j.lungcan.2021.04.012.
83. Burningham, Z.; Hashibe, M.; Spector, L.; Schiffman, J.D. The Epidemiology of Sarcoma. *Clin Sarcoma Res* **2012**, *2*, 14, doi:10.1186/2045-3329-2-14.
84. Choi, J.H.; Ro, J.Y. The 2020 WHO Classification of Tumors of Soft Tissue: Selected Changes and New Entities. *Adv Anat Pathol* **2021**, *28*, 44–58, doi:10.1097/PAP.0000000000000284.
85. Trama, A.; Badalamenti, G.; Baldi, G.G.; Brunello, A.; Caira, M.; Drove, N.; Marrari, A.; Palmerini, E.; Vincenzi, B.; Dei Tos, A.P.; et al. Soft Tissue Sarcoma in Italy: From Epidemiological Data to Clinical Networking to Improve Patient Care and Outcomes. *Cancer Epidemiol* **2019**, *59*, 258–264, doi:10.1016/j.canep.2019.02.012.
86. Mastrangelo, G.; Coindre, J.-M.; Ducimetière, F.; Dei Tos, A.P.; Fadda, E.; Blay, J.-Y.; Buja, A.; Fedeli, U.; Cegolon, L.; Frasson, A.; et al. Incidence of Soft Tissue Sarcoma and Beyond. *Cancer* **2012**, *118*, 5339–5348, doi:10.1002/cncr.27555.

87. Beauchamp, C.P. CORR Insights®: What Is the Success of Repeat Surgical Treatment of a Local Recurrence After Initial Wide Resection of Soft Tissue Sarcomas? *Clin Orthop Relat Res* **2018**, *476*, 1801–1802, doi:10.1097/01.blo.0000533636.35983.b7.
88. Bramwell, V.H.; Anderson, D.; Charette, M.L. Doxorubicin-Based Chemotherapy for the Palliative Treatment of Adult Patients with Locally Advanced or Metastatic Soft-Tissue Sarcoma: A Meta-Analysis and Clinical Practice Guideline. *Sarcoma* **2000**, *4*, 103–112, doi:10.1080/13577140020008066.
89. Cuevas, C.; Francesch, A. Development of Yondelis (Trabectedin, ET-743). A Semisynthetic Process Solves the Supply Problem. *Nat Prod Rep* **2009**, *26*, 322–337, doi:10.1039/b808331m.
90. Barone, A.; Chi, D.-C.; Theoret, M.R.; Chen, H.; He, K.; Kufrin, D.; Helms, W.S.; Subramaniam, S.; Zhao, H.; Patel, A.; et al. FDA Approval Summary: Trabectedin for Unresectable or Metastatic Liposarcoma or Leiomyosarcoma Following an Anthracycline-Containing Regimen. *Clin Cancer Res* **2017**, *23*, 7448–7453, doi:10.1158/1078-0432.CCR-17-0898.
91. Grosso, F.; Jones, R.L.; Demetri, G.D.; Judson, I.R.; Blay, J.-Y.; Le Cesne, A.; Sanfilippo, R.; Casieri, P.; Collini, P.; Dileo, P.; et al. Efficacy of Trabectedin (Ecteinascidin-743) in Advanced Pretreated Myxoid Liposarcomas: A Retrospective Study. *Lancet Oncol* **2007**, *8*, 595–602, doi:10.1016/S1470-2045(07)70175-4.
92. Kawai, A.; Araki, N.; Sugiura, H.; Ueda, T.; Yonemoto, T.; Takahashi, M.; Morioka, H.; Hiraga, H.; Hiruma, T.; Kunisada, T.; et al. Trabectedin Monotherapy after Standard Chemotherapy versus Best Supportive Care in Patients with Advanced, Translocation-Related Sarcoma: A Randomised, Open-Label, Phase 2 Study. *Lancet Oncol* **2015**, *16*, 406–416, doi:10.1016/S1470-2045(15)70098-7.
93. Le Cesne, A.; Cresta, S.; Maki, R.G.; Blay, J.Y.; Verweij, J.; Poveda, A.; Casali, P.G.; Balaña, C.; Schöffski, P.; Grosso, F.; et al. A Retrospective Analysis of Antitumour Activity with Trabectedin in Translocation-Related Sarcomas. *Eur. J. Cancer* **2012**, *48*, 3036–3044, doi:10.1016/j.ejca.2012.05.012.
94. Demetri, G.D.; von Mehren, M.; Jones, R.L.; Hensley, M.L.; Schuetze, S.M.; Staddon, A.; Milhem, M.; Elias, A.; Ganjoo, K.; Tawbi, H.; et al. Efficacy and Safety of Trabectedin or Dacarbazine for Metastatic Liposarcoma or Leiomyosarcoma After Failure of Conventional Chemotherapy: Results of a Phase III Randomized Multicenter Clinical Trial. *J Clin Oncol* **2016**, *34*, 786–793, doi:10.1200/JCO.2015.62.4734.
95. Guirouilh-Barbat, J.; Redon, C.; Pommier, Y. Transcription-Coupled DNA Double-Strand Breaks Are Mediated via the Nucleotide Excision Repair and the Mre11-Rad50-Nbs1 Complex. *MBoC* **2008**, *19*, 3969–3981, doi:10.1091/mbc.e08-02-0215.
96. D'Incalci, M.; Galmarini, C.M. A Review of Trabectedin (ET-743): A Unique Mechanism of Action. *Mol Cancer Ther* **2010**, *9*, 2157–2163, doi:10.1158/1535-7163.MCT-10-0263.
97. Feuerhahn, S.; Giraudon, C.; Martínez-Díez, M.; Bueren-Calabuig, J.A.; Galmarini, C.M.; Gago, F.; Egly, J.-M. XPF-Dependent DNA Breaks and RNA Polymerase II Arrest Induced by Antitumor DNA Interstrand Crosslinking-Mimetic Alkaloids. *Chem Biol* **2011**, *18*, 988–999, doi:10.1016/j.chembiol.2011.06.007.
98. Herrero, A.B.; Martín-Castellanos, C.; Marco, E.; Gago, F.; Moreno, S. Cross-Talk between Nucleotide Excision and Homologous Recombination DNA Repair Pathways in the Mechanism of Action of Antitumor Trabectedin. *Cancer Res* **2006**, *66*, 8155–8162, doi:10.1158/0008-5472.CAN-06-0179.
99. Aune, G.J.; Takagi, K.; Sordet, O.; Guirouilh-Barbat, J.; Antony, S.; Bohr, V.A.; Pommier, Y. Von Hippel-Lindau ^ Coupled and Transcription-Coupled Nucleotide Excision Repair ^ Dependent Degradation of RNA Polymerase II in Response to Trabectedin. *Clin Cancer Res* **2008**, *14*, 6449–6455, doi:10.1158/1078-0432.CCR-08-0730.
100. Bonfanti, M.; La Valle, E.; Fernandez Sousa Faro, J.; Faircloth, G.; Caretti, G.; Mantovani, R.; D'Incalci, M. Effect of Ecteinascidin-743 on the Interaction between DNA Binding Proteins and DNA. *Anti-Cancer Drug Design* **1999**, *14*, 179–186.

101. Di Giandomenico, S.; Frapolli, R.; Bello, E.; Uboldi, S.; Licandro, S.A.; Marchini, S.; Beltrame, L.; Brich, S.; Mauro, V.; Tamborini, E.; et al. Mode of Action of Trabectedin in Myxoid Liposarcomas. *Oncogene* **2014**, *33*, 5201–5210, doi:10.1038/onc.2013.462.
102. Forni, C.; Minuzzo, M.; Virdis, E.; Tamborini, E.; Simone, M.; Tavecchio, M.; Erba, E.; Grosso, F.; Gronchi, A.; Aman, P.; et al. Trabectedin (ET-743) Promotes Differentiation in Myxoid Liposarcoma Tumors. *Mol Cancer Ther* **2009**, *8*, 449–457, doi:10.1158/1535-7163.MCT-08-0848.
103. De Silva, I.U.; McHugh, P.J.; Clingen, P.H.; Hartley, J.A. Defining the Roles of Nucleotide Excision Repair and Recombination in the Repair of DNA Interstrand Cross-Links in Mammalian Cells. *Mol Cell Biol* **2000**, *20*, 7980–7990, doi:10.1128/MCB.20.21.7980-7990.2000.
104. Baghban, R.; Roshangar, L.; Jahanban-Esfahlan, R.; Seidi, K.; Ebrahimi-Kalan, A.; Jaymand, M.; Kolahian, S.; Javaheri, T.; Zare, P. Tumor Microenvironment Complexity and Therapeutic Implications at a Glance. *Cell Communication and Signaling* **2020**, *18*, 59, doi:10.1186/s12964-020-0530-4.
105. Allavena, P.; Signorelli, M.; Chieppa, M.; Erba, E.; Bianchi, G.; Marchesi, F.; Olimpio, C.O.; Bonardi, C.; Garbi, A.; Lissoni, A.; et al. Anti-Inflammatory Properties of the Novel Antitumor Agent Yondelis (Trabectedin): Inhibition of Macrophage Differentiation and Cytokine Production. *Cancer Res* **2005**, *65*, 2964–2971, doi:10.1158/0008-5472.CAN-04-4037.
106. Germano, G.; Frapolli, R.; Belgiovine, C.; Anselmo, A.; Pesce, S.; Liguori, M.; Erba, E.; Uboldi, S.; Zucchetti, M.; Pasqualini, F.; et al. Role of Macrophage Targeting in the Antitumor Activity of Trabectedin. *Cancer Cell* **2013**, *23*, 249–262, doi:10.1016/j.ccr.2013.01.008.
107. Germano, G.; Frapolli, R.; Simone, M.; Tavecchio, M.; Erba, E.; Pesce, S.; Pasqualini, F.; Grosso, F.; Sanfilippo, R.; Casali, P.G.; et al. Antitumor and Anti-Inflammatory Effects of Trabectedin on Human Myxoid Liposarcoma Cells. *Cancer Res* **2010**, *70*, 2235–2244, doi:10.1158/0008-5472.CAN-09-2335.
108. van Kesteren, C.; de Vooght, M.M.M.; López-Lázaro, L.; Mathôt, R. a. A.; Schellens, J.H.M.; Jimeno, J.M.; Beijnen, J.H. Yondelis (Trabectedin, ET-743): The Development of an Anticancer Agent of Marine Origin. *Anticancer Drugs* **2003**, *14*, 487–502, doi:10.1097/00001813-200308000-00001.
109. Forouzesh, B.; Hidalgo, M.; Chu, Q.; Mita, A.; Mita, M.; Schwartz, G.; Jimeno, J.; Gómez, J.; Alfaro, V.; Lebedinsky, C.; et al. Phase I and Pharmacokinetic Study of Trabectedin as a 1- or 3-Hour Infusion Weekly in Patients with Advanced Solid Malignancies. *Clin Cancer Res* **2009**, *15*, 3591–3599, doi:10.1158/1078-0432.CCR-08-2889.
110. Sparidans, R.W.; Rosing, H.; Hillebrand, M.J.; López-Lázaro, L.; Jimeno, J.M.; Manzanares, I.; van Kesteren, C.; Cvitkovic, E.; van Oosterom, A.T.; Schellens, J.H.; et al. Search for Metabolites of Ecteinascidin 743, a Novel, Marine-Derived, Anti-Cancer Agent, in Man. *Anticancer Drugs* **2001**, *12*, 653–666, doi:10.1097/00001813-200109000-00003.
111. Villalona-Calero, M.A.; Eckhardt, S.G.; Weiss, G.; Hidalgo, M.; Campbell, E.; Kraynak, M.; Hoff, D.D.V.; Rowinsky, E.K.; Beijnen, J.H.; Kesteren, C.V.; et al. A Phase I and Pharmacokinetic Study of Ecteinascidin-743 on a Daily × 5 Schedule in Patients with Solid Malignancies. *Clinical cancer research : an official journal of the American Association for Cancer Research* **2002**, *8*, 75–85.
112. Brandon, E.F.A.; Sparidans, R.W.; Guijt, K.-J.; Löwenthal, S.; Meijerman, I.; Beijnen, J.H.; Schellens, J.H.M. In Vitro Characterization of the Human Biotransformation and CYP Reaction Phenotype of ET-743 (Yondelis, Trabectidin), a Novel Marine Anti-Cancer Drug. *Invest New Drugs* **2006**, *24*, 3–14, doi:10.1007/s10637-005-4538-9.
113. Brandon, E.F.A.; Meijerman, I.; Klijn, J.S.; den Arend, D.; Sparidans, R.W.; Lázaro, L.L.; Beijnen, J.H.; Schellens, J.H.M. In-Vitro Cytotoxicity of ET-743 (Trabectedin, Yondelis), a Marine Anti-Cancer Drug, in the Hep G2 Cell Line: Influence of Cytochrome P450 and Phase II Inhibition, and Cytochrome P450 Induction. *Anticancer Drugs* **2005**, *16*, 935–943, doi:10.1097/01.cad.0000180121.16407.38.
114. Machiels, J.-P.; Staddon, A.; Herremans, C.; Keung, C.; Bernard, A.; Phelps, C.; Khokhar, N.Z.; Knoblauch, R.; Parekh, T.V.; Dirix, L.; et al. Impact of Cytochrome P450 3A4 Inducer and Inhibitor on the Pharmacokinetics of Trabectedin in Patients with Advanced Malignancies: Open-Label,

Multicenter Studies. *Cancer Chemother Pharmacol* **2014**, *74*, 729–737, doi:10.1007/s00280-014-2554-1.
115. Perez-Ruixo, J.J.; Zannikos, P.; Hirankarn, S.; Stuyckens, K.; Ludwig, E.A.; Soto-Matos, A.; Lopez-Lazaro, L.; Owen, J.S. Population Pharmacokinetic Meta-Analysis of Trabectedin (ET-743,??Yondelis??) In Cancer Patients: *Clinical Pharmacokinetics* **2007**, *46*, 867–884, doi:10.2165/00003088-200746100-00005.
116. Chu, Q.; Mita, A.; Forouzesh, B.; Tolcher, A.W.; Schwartz, G.; Nieto, A.; Soto-Matos, A.; Alfaro, V.; Lebedinsky, C.; Rowinsky, E.K. Phase I and Pharmacokinetic Study of Sequential Paclitaxel and Trabectedin Every 2 Weeks in Patients with Advanced Solid Tumors. *Clin Cancer Res* **2010**, *16*, 2656–2665, doi:10.1158/1078-0432.CCR-10-0062.
117. Ueda, T.; Kakunaga, S.; Ando, M.; Yonemori, K.; Sugiura, H.; Yamada, K.; Kawai, A. Phase I and Pharmacokinetic Study of Trabectedin, a DNA Minor Groove Binder, Administered as a 24-h Continuous Infusion in Japanese Patients with Soft Tissue Sarcoma. *Invest New Drugs* **2014**, *32*, 691–699, doi:10.1007/s10637-014-0094-5.
118. Kattan, M.W.; Leung, D.H.Y.; Brennan, M.F. Postoperative Nomogram for 12-Year Sarcoma-Specific Death. *JCO* **2002**, *20*, 791–796, doi:10.1200/JCO.2002.20.3.791.
119. Maretty-Nielsen, K.; Aggerholm-Pedersen, N.; Safwat, A.; Jørgensen, P.H.; Hansen, B.H.; Baerentzen, S.; Pedersen, A.B.; Keller, J. Prognostic Factors for Local Recurrence and Mortality in Adult Soft Tissue Sarcoma of the Extremities and Trunk Wall: A Cohort Study of 922 Consecutive Patients. *Acta Orthop* **2014**, *85*, 323–332, doi:10.3109/17453674.2014.908341.
120. Gatta, G.; Capocaccia, R.; Botta, L.; Mallone, S.; De Angelis, R.; Ardanaz, E.; Comber, H.; Dimitrova, N.; Leinonen, M.K.; Siesling, S.; et al. Burden and Centralised Treatment in Europe of Rare Tumours: Results of RARECAREnet—a Population-Based Study. *The Lancet Oncology* **2017**, *18*, 1022–1039, doi:10.1016/S1470-2045(17)30445-X.
121. Eastley, N.C.; Ottolini, B.; Neumann, R.; Luo, J.-L.; Hastings, R.K.; Khan, I.; Moore, D.A.; Esler, C.P.; Shaw, J.A.; Royle, N.J.; et al. Circulating Tumour-Derived DNA in Metastatic Soft Tissue Sarcoma. *Oncotarget* **2018**, *9*, 10549–10560, doi:10.18632/oncotarget.24278.
122. Fricke, A.; Ullrich, P.V.; Heinz, J.; Pfeifer, D.; Scholber, J.; Herget, G.W.; Hauschild, O.; Bronsert, P.; Stark, G.B.; Bannasch, H.; et al. Identification of a Blood-Borne MiRNA Signature of Synovial Sarcoma. *Mol Cancer* **2015**, *14*, 151, doi:10.1186/s12943-015-0424-z.
123. Kohama, I.; Kosaka, N.; Chikuda, H.; Ochiya, T. An Insight into the Roles of MicroRNAs and Exosomes in Sarcoma. *Cancers (Basel)* **2019**, *11*, E428, doi:10.3390/cancers11030428.
124. Kosela-Paterczyk, H.; Paziewska, A.; Kulecka, M.; Balabas, A.; Kluska, A.; Dabrowska, M.; Piatkowska, M.; Zeber-Lubecka, N.; Ambrozkiewicz, F.; Karczmarski, J.; et al. Signatures of Circulating MicroRNA in Four Sarcoma Subtypes. *J Cancer* **2020**, *11*, 874–882, doi:10.7150/jca.34723.
125. Shukla, N.N.; Patel, J.A.; Magnan, H.; Zehir, A.; You, D.; Tang, J.; Meng, F.; Samoila, A.; Slotkin, E.K.; Ambati, S.R.; et al. Plasma DNA-Based Molecular Diagnosis, Prognostication, and Monitoring of Patients with EWSR1 Fusion-Positive Sarcomas. *JCO Precis Oncol* **2017**, *2017*, doi:10.1200/PO.16.00028.
126. Hemming, M.L.; Klega, K.; Rhoades, J.; Ha, G.; Acker, K.E.; Andersen, J.L.; Thai, E.; Nag, A.; Thorner, A.R.; Raut, C.P.; et al. Detection of Circulating Tumor DNA in Patients With Leiomyosarcoma With Progressive Disease. *JCO Precis Oncol* **2019**, *3*, PO.18.00235, doi:10.1200/PO.18.00235.
127. Casadei, L.; Calore, F.; Creighton, C.J.; Guescini, M.; Batte, K.; Iwenofu, O.H.; Zewdu, A.; Braggio, D.A.; Bill, K.L.; Fadda, P.; et al. Exosome-Derived MiR-25-3p and MiR-92a-3p Stimulate Liposarcoma Progression. *Cancer Res* **2017**, *77*, 3846–3856, doi:10.1158/0008-5472.CAN-16-2984.
128. Masaoutis, C.; Korkolopoulou, P.; Theocharis, S. Exosomes in Sarcomas: Tiny Messengers with Broad Implications in Diagnosis, Surveillance, Prognosis and Treatment. *Cancer Letters* **2019**, *449*, 172–177, doi:10.1016/j.canlet.2019.02.025.
129. Braas, D.; Ahler, E.; Tam, B.; Nathanson, D.; Riedinger, M.; Benz, M.R.; Smith, K.B.; Eilber, F.C.; Witte, O.N.; Tap, W.D.; et al. Metabolomics Strategy Reveals Subpopulation of Liposarcomas

Sensitive to Gemcitabine Treatment. *Cancer Discov* **2012**, *2*, 1109–1117, doi:10.1158/2159-8290.CD-12-0197.
130. Lee, P.; Malik, D.; Perkons, N.; Huangyang, P.; Khare, S.; Rhoades, S.; Gong, Y.-Y.; Burrows, M.; Finan, J.M.; Nissim, I.; et al. Targeting Glutamine Metabolism Slows Soft Tissue Sarcoma Growth. *Nat Commun* **2020**, *11*, 498, doi:10.1038/s41467-020-14374-1.
131. Jia, B.; Wang, W.; Lin, S.; Shi, L.; Li, Y.; Gu, Y.; Gao, F.; Qin, Y. The Free Amino Acid Profiles and Metabolic Biomarkers of Predicting the Chemotherapeutic Response in Advanced Sarcoma Patients. *Clin Transl Oncol* **2020**, *22*, 2213–2221, doi:10.1007/s12094-020-02494-5.
132. de Nonneville, A.; Barbolosi, D.; Andriantsoa, M.; El-Cheikh, R.; Duffaud, F.; Bertucci, F.; Salas, S. Validation of Neutrophil Count as An Algorithm-Based Predictive Factor of Progression-Free Survival in Patients with Metastatic Soft Tissue Sarcomas Treated with Trabectedin. *Cancers* **2019**, *11*, 432, doi:10.3390/cancers11030432.
133. Schack, L.H.; Mouritsen, L.S.; Elowsson, C.; Krarup-Hansen, A.; Safwat, A. The Danish Experience with Trabectedin Treatment for Metastatic Sarcoma: Importance of Hyponatremia. *Acta Oncologica* **2015**, *54*, 34–40, doi:10.3109/0284186X.2014.958530.
134. Moura, D.S.; Sanchez-Bustos, P.; Fernandez-Serra, A.; Lopez-Alvarez, M.; Mondaza-Hernandez, J.L.; Blanco-Alcaina, E.; Gavilan-Naranjo, A.; Martinez-Delgado, P.; Lacerenza, S.; Santos-Fernandez, P.; et al. CUL4A, ERCC5, and ERCC1 as Predictive Factors for Trabectedin Efficacy in Advanced Soft Tissue Sarcomas (STS): A Spanish Group for Sarcoma Research (GEIS) Study. *Cancers (Basel)* **2020**, *12*, doi:10.3390/cancers12051128.
135. Italiano, A.; Laurand, A.; Laroche, A.; Casali, P.; Sanfilippo, R.; Le Cesne, A.; Judson, I.; Blay, J.-Y.; Ray-Coquard, I.; Bui, B.; et al. ERCC5/XPG, ERCC1, and BRCA1 Gene Status and Clinical Benefit of Trabectedin in Patients with Soft Tissue Sarcoma. *Cancer* **2011**, *117*, 3445–3456, doi:10.1002/cncr.25925.
136. Tercero, J.C.; Jimeno, J.; Martinez, N.; Montes-Moreno, S.; Rodriguez-Pinilla, S.M.; Sanchez-Beato, M. Predicting Sarcoma-Patients Response to Trabectedin Treatment with Molecular Markers Detected by Immunohistochemistry. *Clin Cancer Res* **2008**, *14*, B8–B8.
137. FDA, C. for D.E. and Bioanalytical Method Validation Guidance for Industry Available online: http://www.fda.gov/regulatory-information/search-fda-guidance-documents/bioanalytical-method-validation-guidance-industry (accessed on 25 November 2019).
138. Van Eeckhaut, A.; Lanckmans, K.; Sarre, S.; Smolders, I.; Michotte, Y. Validation of Bioanalytical LC–MS/MS Assays: Evaluation of Matrix Effects. *Journal of Chromatography B* **2009**, *877*, 2198–2207, doi:10.1016/j.jchromb.2009.01.003.
139. Freedman, K.B.; Back, S.; Bernstein, J. Sample Size and Statistical Power of Randomised, Controlled Trials in Orthopaedics. *THE JOURNAL OF BONE AND JOINT SURGERY* **2001**, *83*, 6.
140. Christensen, E. Multivariate Survival Analysis Using Cox's Regression Model. *Hepatology* **1987**, *7*, 1346–1358, doi:10.1002/hep.1840070628.
141. Dessai, S.; Patil, V. Testing and Interpreting Assumptions of COX Regression Analysis. *Cancer Research, Statistics, and Treatment* **2019**, *2*, 108, doi:10.4103/CRST.CRST_40_19.
142. Chong, J.; Wishart, D.S.; Xia, J. Using MetaboAnalyst 4.0 for Comprehensive and Integrative Metabolomics Data Analysis. *Curr Protoc Bioinformatics* **2019**, *68*, e86, doi:10.1002/cpbi.86.
143. Di Gregorio, E.; Miolo, G.; Steffan, A.; Corona, G. Novel Method for Fast Trabectedin Quantification Using Hydrophilic Interaction Liquid Chromatography and Tandem Mass Spectrometry for Human Pharmacokinetic Studies. *J Pharm Biomed Anal* **2020**, *185*, 113261, doi:10.1016/j.jpba.2020.113261.
144. Demetri, G.D.; Chawla, S.P.; von Mehren, M.; Ritch, P.; Baker, L.H.; Blay, J.Y.; Hande, K.R.; Keohan, M.L.; Samuels, B.L.; Schuetze, S.; et al. Efficacy and Safety of Trabectedin in Patients with Advanced or Metastatic Liposarcoma or Leiomyosarcoma after Failure of Prior Anthracyclines and Ifosfamide: Results of a Randomized Phase II Study of Two Different Schedules. *J. Clin. Oncol.* **2009**, *27*, 4188–4196, doi:10.1200/JCO.2008.21.0088.
145. Garcia-Carbonero, R.; Supko, J.G.; Manola, J.; Seiden, M.V.; Harmon, D.; Ryan, D.P.; Quigley, M.T.; Merriam, P.; Canniff, J.; Goss, G.; et al. Phase II and Pharmacokinetic Study of Ecteinascidin 743 in

Patients with Progressive Sarcomas of Soft Tissues Refractory to Chemotherapy. *J. Clin. Oncol.* **2004**, *22*, 1480–1490, doi:10.1200/JCO.2004.02.098.
146. Kobayashi, H.; Iwata, S.; Wakamatsu, T.; Hayakawa, K.; Yonemoto, T.; Wasa, J.; Oka, H.; Ueda, T.; Tanaka, S. Efficacy and Safety of Trabectedin for Patients with Unresectable and Relapsed Soft-Tissue Sarcoma in Japan: A Japanese Musculoskeletal Oncology Group Study. *Cancer* **2020**, *126*, 1253–1263, doi:10.1002/cncr.32661.
147. Le Cesne, A.; Ray-Coquard, I.; Duffaud, F.; Chevreau, C.; Penel, N.; Bui Nguyen, B.; Piperno-Neumann, S.; Delcambre, C.; Rios, M.; Chaigneau, L.; et al. Trabectedin in Patients with Advanced Soft Tissue Sarcoma: A Retrospective National Analysis of the French Sarcoma Group. *Eur J Cancer* **2015**, *51*, 742–750, doi:10.1016/j.ejca.2015.01.006.
148. Le Cesne, A.; Blay, J.Y.; Judson, I.; Van Oosterom, A.; Verweij, J.; Radford, J.; Lorigan, P.; Rodenhuis, S.; Ray-Coquard, I.; Bonvalot, S.; et al. Phase II Study of ET-743 in Advanced Soft Tissue Sarcomas: A European Organisation for the Research and Treatment of Cancer (EORTC) Soft Tissue and Bone Sarcoma Group Trial. *J. Clin. Oncol.* **2005**, *23*, 576–584, doi:10.1200/JCO.2005.01.180.
149. Schmitt, T.; Keller, E.; Dietrich, S.; Wuchter, P.; Ho, A.D.; Egerer, G. Trabectedin for Metastatic Soft Tissue Sarcoma: A Retrospective Single Center Analysis. *Mar Drugs* **2010**, *8*, 2647–2658, doi:10.3390/md8102647.
150. Grosso, F.; D'Ambrosio, L.; Zucchetti, M.; Ibrahim, T.; Tamberi, S.; Matteo, C.; Rulli, E.; Comandini, D.; Palmerini, E.; Baldi, G.G.; et al. Pharmacokinetics, Safety, and Activity of Trabectedin as First-Line Treatment in Elderly Patients Who Are Affected by Advanced Sarcoma and Are Unfit to Receive Standard Chemotherapy: A Phase 2 Study (TR1US Study) from the Italian Sarcoma Group. *Cancer* **2020**, *126*, 4726–4734, doi:10.1002/cncr.33120.
151. Mehren, M. von; Schilder, R.J.; Cheng, J.D.; Temmer, E.; Cardoso, T.M.; Renshaw, F.G.; Bayever, E.; Zannikos, P.; Yuan, Z.; Cohen, R.B. A Phase I Study of the Safety and Pharmacokinetics of Trabectedin in Combination with Pegylated Liposomal Doxorubicin in Patients with Advanced Malignancies. *Annals of Oncology* **2008**, *19*, 1802–1809, doi:10.1093/annonc/mdn363.
152. Reid, J.M.; Kuffel, M.J.; Ruben, S.L.; Morales, J.J.; Rinehart, K.L.; Squillace, D.P.; Ames, M.M. Rat and Human Liver Cytochrome P-450 Isoform Metabolism of Ecteinascidin 743 Does Not Predict Gender-Dependent Toxicity in Humans. *Clin Cancer Res* **2002**, *8*, 2952–2962.
153. Vermeir, M.; Hemeryck, A.; Cuyckens, F.; Francesch, A.; Bockx, M.; Van Houdt, J.; Steemans, K.; Mannens, G.; Avilés, P.; De Coster, R. In Vitro Studies on the Metabolism of Trabectedin (YONDELIS) in Monkey and Man, Including Human CYP Reaction Phenotyping. *Biochem Pharmacol* **2009**, *77*, 1642–1654, doi:10.1016/j.bcp.2009.02.020.
154. Forman, B.M.; Goode, E.; Chen, J.; Oro, A.E.; Bradley, D.J.; Perlmann, T.; Noonan, D.J.; Burka, L.T.; McMorris, T.; Lamph, W.W.; et al. Identification of a Nuclear Receptor That Is Activated by Farnesol Metabolites. *Cell* **1995**, *81*, 687–693, doi:10.1016/0092-8674(95)90530-8.
155. Martin, P.; Riley, R.; Back, D.J.; Owen, A. Comparison of the Induction Profile for Drug Disposition Proteins by Typical Nuclear Receptor Activators in Human Hepatic and Intestinal Cells. *Br J Pharmacol* **2008**, *153*, 805–819, doi:10.1038/sj.bjp.0707601.
156. Gnerre, C.; Blättler, S.; Kaufmann, M.R.; Looser, R.; Meyer, U.A. Regulation of CYP3A4 by the Bile Acid Receptor FXR: Evidence for Functional Binding Sites in the CYP3A4 Gene. *Pharmacogenetics* **2004**, *14*, 635–645, doi:10.1097/00008571-200410000-00001.
157. Chen, J.; Zhao, K.-N.; Chen, C. The Role of CYP3A4 in the Biotransformation of Bile Acids and Therapeutic Implication for Cholestasis. *Ann Transl Med* **2014**, *2*, doi:10.3978/j.issn.2305-5839.2013.03.02.
158. Lin, Y.S.; Kerr, S.J.; Randolph, T.; Shireman, L.M.; Senn, T.; McCune, J.S. Prediction of Intravenous Busulfan Clearance by Endogenous Plasma Biomarkers Using Global Pharmacometabolomics. *Metabolomics* **2016**, *12*, 161, doi:10.1007/s11306-016-1106-6.
159. Taegtmeyer, A.B.; Haschke, M.; Tchambaz, L.; Buylaert, M.; Tschöpl, M.; Beuers, U.; Drewe, J.; Krähenbühl, S. A Study of the Relationship between Serum Bile Acids and Propranolol Pharmacokinetics and Pharmacodynamics in Patients with Liver Cirrhosis and in Healthy Controls. *PLOS ONE* **2014**, *9*, e97885, doi:10.1371/journal.pone.0097885.

160. König, J.; Nies, A.T.; Cui, Y.; Leier, I.; Keppler, D. Conjugate Export Pumps of the Multidrug Resistance Protein (MRP) Family: Localization, Substrate Specificity, and MRP2-Mediated Drug Resistance. *Biochimica et Biophysica Acta (BBA) - Biomembranes* **1999**, *1461*, 377–394, doi:10.1016/S0005-2736(99)00169-8.
161. Beumer, J.-H.; Buckle, T.; Ouwehand, M.; Franke, N.E.F.; Lopez-Lazaro, L.; Schellens, J.H.M.; Beijnen, J.H.; van Tellingen, O. Trabectedin (ET-743, Yondelis™) Is a Substrate for P-Glycoprotein, but Only High Expression of P-Glycoprotein Confers the Multidrug Resistance Phenotype. *Invest New Drugs* **2006**, *25*, 1, doi:10.1007/s10637-006-7773-9.
162. Beumer, J.H.; Franke, N.E.; Tolboom, R.; Buckle, T.; Rosing, H.; Lopez-Lazaro, L.; Schellens, J.H.M.; Beijnen, J.H.; van Tellingen, O. Disposition and Toxicity of Trabectedin (ET-743) in Wild-Type and Mdr1 Gene (P-Gp) Knock-out Mice. *Invest New Drugs* **2010**, *28*, 145–155, doi:10.1007/s10637-009-9234-8.
163. Lam, P.; Wang, R.; Ling, V. Bile Acid Transport in Sister of P-Glycoprotein (ABCB11) Knockout Mice. *Biochemistry* **2005**, *44*, 12598–12605, doi:10.1021/bi050943e.
164. Kamisako, T.; Leier, I.; Cui, Y.; König, J.; Buchholz, U.; Hummel-Eisenbeiss, J.; Keppler, D. Transport of Monoglucuronosyl and Bisglucuronosyl Bilirubin by Recombinant Human and Rat Multidrug Resistance Protein 2. *Hepatology* **1999**, *30*, 485–490, doi:10.1002/hep.510300220.
165. Paulusma, C.C.; van Geer, M.A.; Evers, R.; Heijn, M.; Ottenhoff, R.; Borst, P.; Oude Elferink, R.P. Canalicular Multispecific Organic Anion Transporter/Multidrug Resistance Protein 2 Mediates Low-Affinity Transport of Reduced Glutathione. *Biochem J* **1999**, *338 (Pt 2)*, 393–401.
166. Huisman, M.T.; Chhatta, A.A.; van Tellingen, O.; Beijnen, J.H.; Schinkel, A.H. MRP2 (ABCC2) Transports Taxanes and Confers Paclitaxel Resistance and Both Processes Are Stimulated by Probenecid. *Int J Cancer* **2005**, *116*, 824–829, doi:10.1002/ijc.21013.
167. Stein, U.; Jürchott, K.; Schläfke, M.; Hohenberger, P. Expression of Multidrug Resistance Genes MVP, MDR1, and MRP1 Determined Sequentially Before, During, and After Hyperthermic Isolated Limb Perfusion of Soft Tissue Sarcoma and Melanoma Patients. *JCO* **2002**, *20*, 3282–3292, doi:10.1200/JCO.2002.01.003.
168. Coley, H.M.; Verrill, M.W.; Gregson, S.E.; Odell, D.E.; Fisher, C.; Judson, I.R. Incidence of P-Glycoprotein Overexpression and Multidrug Resistance (MDR) Reversal in Adult Soft Tissue Sarcoma. *Eur J Cancer* **2000**, *36*, 881–888, doi:10.1016/s0959-8049(00)00032-0.
169. Citti, A.; Boldrini, R.; Inserra, A.; Alisi, A.; Pessolano, R.; Mastronuzzi, A.; Zin, A.; De Sio, L.; Rosolen, A.; Locatelli, F.; et al. Expression of Multidrug Resistance-Associated Proteins in Paediatric Soft Tissue Sarcomas before and after Chemotherapy. *Int J Oncol* **2012**, *41*, 117–124, doi:10.3892/ijo.2012.1433.
170. van Waterschoot, R.A.B.; Eman, R.M.; Wagenaar, E.; van der Kruijssen, C.M.M.; Rosing, H.; Beijnen, J.H.; Schinkel, A.H. ABCC2, ABCC3, and ABCB1, but Not CYP3A, Protect against Trabectedin-Mediated Hepatotoxicity. *Clin Cancer Res* **2009**, *15*, 7616–7623, doi:10.1158/1078-0432.CCR-09-2127.
171. Laurenty, A.-P.; Thomas, F.; Chatelut, E.; Bétrian, S.; Guellec, C.L.; Hennebelle, I.; Guellec, S.L.; Chevreau, C. Irreversible Hepatotoxicity after Administration of Trabectedin to a Pleiomorphic Sarcoma Patient with a Rare ABCC2 Polymorphism: A Case Report. *Pharmacogenomics* **2013**, *14*, 1389–1396, doi:10.2217/pgs.13.124.
172. Maillard, M.; Chevreau, C.; Le Louedec, F.; Cassou, M.; Delmas, C.; Gourdain, L.; Blay, J.-Y.; Cupissol, D.; Bompas, E.; Italiano, A.; et al. Pharmacogenetic Study of Trabectedin-Induced Severe Hepatotoxicity in Patients with Advanced Soft Tissue Sarcoma. *Cancers* **2020**, *12*, 3647, doi:10.3390/cancers12123647.
173. Lee, J.K.; Leslie, E.M.; Zamek-Gliszczynski, M.J.; Brouwer, K.L.R. Modulation of Trabectedin (ET-743) Hepatobiliary Disposition by Multidrug Resistance-Associated Proteins (Mrps) May Prevent Hepatotoxicity. *Toxicol Appl Pharmacol* **2008**, *228*, 17–23, doi:10.1016/j.taap.2007.11.020.
174. Micuda, S.; Fuksa, L.; Brcakova, E.; Osterreicher, J.; Cermanova, J.; Cibicek, N.; Mokry, J.; Staud, F.; Martinkova, J. Zonation of Multidrug Resistance-Associated Protein 2 in Rat Liver after Induction with Dexamethasone. *J Gastroenterol Hepatol* **2008**, *23*, e225-230, doi:10.1111/j.1440-1746.2007.05066.x.

175. Beumer, J.H.; Rademaker-Lakhai, J.M.; Rosing, H.; Hillebrand, M.J.X.; Bosch, T.M.; Lopez-Lazaro, L.; Schellens, J.H.M.; Beijnen, J.H. Metabolism of Trabectedin (ET-743, Yondelis) in Patients with Advanced Cancer. *Cancer Chemother Pharmacol* **2007**, *59*, 825–837, doi:10.1007/s00280-006-0342-2.
176. Stabler, S.; Koyama, T.; Zhao, Z.; Martinez-Ferrer, M.; Allen, R.H.; Luka, Z.; Loukachevitch, L.V.; Clark, P.E.; Wagner, C.; Bhowmick, N.A. Serum Methionine Metabolites Are Risk Factors for Metastatic Prostate Cancer Progression. *PLoS One* **2011**, *6*, e22486, doi:10.1371/journal.pone.0022486.
177. Wróbel, M.; Czubak, J.; Bronowicka-Adamska, P.; Jurkowska, H.; Adamek, D.; Papla, B. Is Development of High-Grade Gliomas Sulfur-Dependent? *Molecules* **2014**, *19*, 21350–21362, doi:10.3390/molecules191221350.
178. Wang, L.; Shi, H.; Liu, Y.; Zhang, W.; Duan, X.; Li, M.; Shi, X.; Wang, T. Cystathionine-γ-lyase Promotes the Metastasis of Breast Cancer via the VEGF Signaling Pathway. *Int J Oncol* **2019**, *55*, 473–487, doi:10.3892/ijo.2019.4823.
179. Ouaknine Krief, J.; Helly de Tauriers, P.; Dumenil, C.; Neveux, N.; Dumoulin, J.; Giraud, V.; Labrune, S.; Tisserand, J.; Julie, C.; Emile, J.-F.; et al. Role of Antibiotic Use, Plasma Citrulline and Blood Microbiome in Advanced Non-Small Cell Lung Cancer Patients Treated with Nivolumab. *J Immunother Cancer* **2019**, *7*, 176, doi:10.1186/s40425-019-0658-1.
180. Bachmayr-Heyda, A.; Aust, S.; Auer, K.; Meier, S.M.; Schmetterer, K.G.; Dekan, S.; Gerner, C.; Pils, D. Integrative Systemic and Local Metabolomics with Impact on Survival in High-Grade Serous Ovarian Cancer. *Clin Cancer Res* **2017**, *23*, 2081–2092, doi:10.1158/1078-0432.CCR-16-1647.
181. Horala, A.; Plewa, S.; Derezinski, P.; Klupczynska, A.; Matysiak, J.; Nowak-Markwitz, E.; Kokot, Z.J. Serum Free Amino Acid Profiling in Differential Diagnosis of Ovarian Tumors—A Comparative Study with Review of the Literature. *Int J Environ Res Public Health* **2021**, *18*, 2167, doi:10.3390/ijerph18042167.
182. Neurauter, G.; Grahmann, A.V.; Klieber, M.; Zeimet, A.; Ledochowski, M.; Sperner-Unterweger, B.; Fuchs, D. Serum Phenylalanine Concentrations in Patients with Ovarian Carcinoma Correlate with Concentrations of Immune Activation Markers and of Isoprostane-8. *Cancer Letters* **2008**, *272*, 141–147, doi:10.1016/j.canlet.2008.07.002.
183. Ploder, M.; Neurauter, G.; Spittler, A.; Schroecksnadel, K.; Roth, E.; Fuchs, D. Serum Phenylalanine in Patients Post Trauma and with Sepsis Correlate to Neopterin Concentrations. *Amino Acids* **2008**, *35*, 303–307, doi:10.1007/s00726-007-0625-x.
184. Vander Heiden, M.G.; DeBerardinis, R.J. Understanding the Intersections between Metabolism and Cancer Biology. *Cell* **2017**, *168*, 657–669, doi:10.1016/j.cell.2016.12.039.
185. Banerjee, R.; Zou, C. Redox Regulation and Reaction Mechanism of Human Cystathionine-β-Synthase: A PLP-Dependent Hemesensor Protein. *Archives of Biochemistry and Biophysics* **2005**, *433*, 144–156, doi:10.1016/j.abb.2004.08.037.
186. Belalcázar, A.D.; Ball, J.G.; Frost, L.M.; Valentovic, M.A.; Wilkinson, J. Transsulfuration Is a Significant Source of Sulfur for Glutathione Production in Human Mammary Epithelial Cells. *ISRN Biochemistry* **2013**, *2013*, e637897, doi:10.1155/2013/637897.
187. Kennedy, L.; Sandhu, J.K.; Harper, M.-E.; Cuperlovic-Culf, M. Role of Glutathione in Cancer: From Mechanisms to Therapies. *Biomolecules* **2020**, *10*, 1429, doi:10.3390/biom10101429.
188. Wang, L.; Han, H.; Liu, Y.; Zhang, X.; Shi, X.; Wang, T. Cystathionine β-Synthase Induces Multidrug Resistance and Metastasis in Hepatocellular Carcinoma. *Curr Mol Med* **2018**, *18*, 496–506, doi:10.2174/1566524019666181211162754.
189. Bhattacharyya, S.; Saha, S.; Giri, K.; Lanza, I.R.; Nair, K.S.; Jennings, N.B.; Rodriguez-Aguayo, C.; Lopez-Berestein, G.; Basal, E.; Weaver, A.L.; et al. Cystathionine Beta-Synthase (CBS) Contributes to Advanced Ovarian Cancer Progression and Drug Resistance. *PLoS One* **2013**, *8*, e79167, doi:10.1371/journal.pone.0079167.
190. Sen, S.; Kawahara, B.; Mahata, S.K.; Tsai, R.; Yoon, A.; Hwang, L.; Hu-Moore, K.; Villanueva, C.; Vajihuddin, A.; Parameshwar, P.; et al. Cystathionine: A Novel Oncometabolite in Human Breast Cancer. *Arch Biochem Biophys* **2016**, *604*, 95–102, doi:10.1016/j.abb.2016.06.010.

191. Ryu, C.S.; Kwak, H.C.; Lee, K.S.; Kang, K.W.; Oh, S.J.; Lee, K.H.; Kim, H.M.; Ma, J.Y.; Kim, S.K. Sulfur Amino Acid Metabolism in Doxorubicin-Resistant Breast Cancer Cells. *Toxicol Appl Pharmacol* **2011**, *255*, 94–102, doi:10.1016/j.taap.2011.06.004.
192. Kawahara, B.; Ramadoss, S.; Chaudhuri, G.; Janzen, C.; Sen, S.; Mascharak, P.K. Carbon Monoxide Sensitizes Cisplatin-Resistant Ovarian Cancer Cell Lines toward Cisplatin via Attenuation of Levels of Glutathione and Nuclear Metallothionein. *J Inorg Biochem* **2019**, *191*, 29–39, doi:10.1016/j.jinorgbio.2018.11.003.
193. Wang, L.; Yang, Z.; Wu, Z.; He, J.; Xu, S.; Li, D.; Zou, Q.; Yuan, Y. Increased Expression of Cystathionine Beta-Synthase and Chemokine Ligand 21 Is Closely Associated with Poor Prognosis in Extrahepatic Cholangiocarcinoma. *Medicine* **2020**, *99*, e22255, doi:10.1097/MD.0000000000022255.
194. Wang, Z.; Shi, N.; Naing, A.; Janku, F.; Subbiah, V.; Araujo, D.M.; Patel, S.R.; Ludwig, J.A.; Ramondetta, L.M.; Levenback, C.F.; et al. Survival of Patients with Metastatic Leiomyosarcoma: The MD Anderson Clinical Center for Targeted Therapy Experience. *Cancer Med* **2016**, *5*, 3437–3444, doi:10.1002/cam4.956.
195. Shi, L.; Wang, Y.; Li, L.; Chou, D.; Zhao, Y.; Zhang, S.; Wang, L.; Zhang, M.; Liu, Y. Prognostic Value of Pretreatment Anemia in Patients with Soft Tissue Sarcoma. *Medicine (Baltimore)* **2021**, *100*, e27221, doi:10.1097/MD.0000000000027221.
196. Szkandera, J.; Gerger, A.; Liegl-Atzwanger, B.; Stotz, M.; Samonigg, H.; Ploner, F.; Stojakovic, T.; Leithner, A.; Pichler, M. Pre-Treatment Anemia Is a Poor Prognostic Factor in Soft Tissue Sarcoma Patients. *PLoS One* **2014**, *9*, doi:10.1371/journal.pone.0107297.
197. Mahyudin, F.; Edward, M.; Basuki, M.H.; Basrewan, Y.; Hernugrahanto, K.D.; Wahyudiputra, A.G. Analysis of Prognostic Factors in Soft Tissue Sarcoma: Cancer Registry from a Single Tertiary Hospital in Indonesia. A Retrospective Cohort Study. *Ann Med Surg (Lond)* **2020**, *57*, 257–263, doi:10.1016/j.amsu.2020.07.053.
198. Nakamura, T.; Grimer, R.; Gaston, C.; Carter, S.; Tillman, R.; Abudu, A.; Jeys, L.; Sudo, A. The Relationship between Pretreatment Anaemia and Survival in Patients with Adult Soft Tissue Sarcoma. *J Orthop Sci* **2013**, *18*, 987–993, doi:10.1007/s00776-013-0454-6.
199. Pergialiotis, V.; Daskalakis, G.; Thomakos, N.; Bellos, I.; Haidopoulos, D.; Loutradis, D.; Rodolakis, A. Prechemotherapy Hemoglobin Levels as a Predictive Factor of Ovarian Cancer Survival: A Systematic Review and Meta-Analysis. *Am J Clin Oncol* **2019**, *42*, 725–731, doi:10.1097/COC.0000000000000570.
200. Huang, X.-Z.; Yang, Y.-C.; Chen, Y.; Wu, C.-C.; Lin, R.-F.; Wang, Z.-N.; Zhang, X. Preoperative Anemia or Low Hemoglobin Predicts Poor Prognosis in Gastric Cancer Patients: A Meta-Analysis. *Dis Markers* **2019**, *2019*, 7606128, doi:10.1155/2019/7606128.
201. Xia, L.; Guzzo, T.J. Preoperative Anemia and Low Hemoglobin Level Are Associated With Worse Clinical Outcomes in Patients With Bladder Cancer Undergoing Radical Cystectomy: A Meta-Analysis. *Clin Genitourin Cancer* **2017**, *15*, 263-272.e4, doi:10.1016/j.clgc.2016.08.017.
202. Abu-Zaid, A.; Alomar, O.; Abuzaid, M.; Baradwan, S.; Salem, H.; Al-Badawi, I.A. Preoperative Anemia Predicts Poor Prognosis in Patients with Endometrial Cancer: A Systematic Review and Meta-Analysis. *Eur J Obstet Gynecol Reprod Biol* **2021**, *258*, 382–390, doi:10.1016/j.ejogrb.2021.01.038.
203. Rutkowski, P.; Kaminska, J.; Kowalska, M.; Ruka, W.; Steffen, J. Cytokine Serum Levels in Soft Tissue Sarcoma Patients: Correlations with Clinico-Pathological Features and Prognosis. *International Journal of Cancer* **2002**, *100*, 463–471, doi:10.1002/ijc.10496.
204. Hagi, T.; Nakamura, T.; Iino, T.; Matsubara, T.; Asanuma, K.; Matsumine, A.; Sudo, A. The Diagnostic and Prognostic Value of Interleukin-6 in Patients with Soft Tissue Sarcomas. *Sci Rep* **2017**, *7*, 9640, doi:10.1038/s41598-017-08781-6.
205. Nakamura, K.; Nakamura, T.; Iino, T.; Hagi, T.; Kita, K.; Asanuma, K.; Sudo, A. Expression of Interleukin-6 and the Interleukin-6 Receptor Predicts the Clinical Outcomes of Patients with Soft Tissue Sarcomas. *Cancers* **2020**, *12*, 585, doi:10.3390/cancers12030585.

206. Nemeth, E.; Rivera, S.; Gabayan, V.; Keller, C.; Taudorf, S.; Pedersen, B.K.; Ganz, T. IL-6 Mediates Hypoferremia of Inflammation by Inducing the Synthesis of the Iron Regulatory Hormone Hepcidin. *J Clin Invest* **2004**, *113*, 1271–1276, doi:10.1172/JCI20945.
207. Vaupel, P.; Mayer, A.; Höckel, M. Impact of Hemoglobin Levels on Tumor Oxygenation: The Higher, the Better? *Strahlenther Onkol* **2006**, *182*, 63–71, doi:10.1007/s00066-006-1543-7.
208. Lv, X.; Li, J.; Zhang, C.; Hu, T.; Li, S.; He, S.; Yan, H.; Tan, Y.; Lei, M.; Wen, M.; et al. The Role of Hypoxia-Inducible Factors in Tumor Angiogenesis and Cell Metabolism. *Genes Dis* **2017**, *4*, 19–24, doi:10.1016/j.gendis.2016.11.003.
209. Park, J.E.; Dutta, B.; Tse, S.W.; Gupta, N.; Tan, C.F.; Low, J.K.; Yeoh, K.W.; Kon, O.L.; Tam, J.P.; Sze, S.K. Hypoxia-Induced Tumor Exosomes Promote M2-like Macrophage Polarization of Infiltrating Myeloid Cells and MicroRNA-Mediated Metabolic Shift. *Oncogene* **2019**, *38*, 5158–5173, doi:10.1038/s41388-019-0782-x.
210. Harrison, L.B.; Chadha, M.; Hill, R.J.; Hu, K.; Shasha, D. Impact of Tumor Hypoxia and Anemia on Radiation Therapy Outcomes. *Oncologist* **2002**, *7*, 492–508, doi:10.1634/theoncologist.7-6-492.
211. Yan, X.; Qu, X.; Tian, R.; Xu, L.; Jin, X.; Yu, S.; Zhao, Y.; Ma, J.; Liu, Y.; Sun, L.; et al. Hypoxia-Induced NAD+ Interventions Promote Tumor Survival and Metastasis by Regulating Mitochondrial Dynamics. *Life Sci* **2020**, *259*, 118171, doi:10.1016/j.lfs.2020.118171.
212. Miolo, G.; Di Gregorio, E.; Saorin, A.; Lombardi, D.; Scalone, S.; Buonadonna, A.; Steffan, A.; Corona, G. Integration of Serum Metabolomics into Clinical Assessment to Improve Outcome Prediction of Metastatic Soft Tissue Sarcoma Patients Treated with Trabectedin. *Cancers* **2020**, *12*, doi:10.3390/cancers12071983.
213. Samuels, B.L.; Chawla, S.; Patel, S.; von Mehren, M.; Hamm, J.; Kaiser, P.E.; Schuetze, S.; Li, J.; Aymes, A.; Demetri, G.D. Clinical Outcomes and Safety with Trabectedin Therapy in Patients with Advanced Soft Tissue Sarcomas Following Failure of Prior Chemotherapy: Results of a Worldwide Expanded Access Program Study. *Ann. Oncol.* **2013**, *24*, 1703–1709, doi:10.1093/annonc/mds659.
214. Lindner, L.H.; Litière, S.; Sleijfer, S.; Benson, C.; Italiano, A.; Kasper, B.; Messiou, C.; Gelderblom, H.; Wardelmann, E.; Le Cesne, A.; et al. Prognostic Factors for Soft Tissue Sarcoma Patients with Lung Metastases Only Who Are Receiving First-line Chemotherapy: An Exploratory, Retrospective Analysis of the European Organization for Research and Treatment of Cancer-Soft Tissue and Bone Sarcoma Group (EORTC-STBSG). *Int J Cancer* **2018**, *142*, 2610–2620, doi:10.1002/ijc.31286.
215. Toulmonde, M.; Bonvalot, S.; Méeus, P.; Stoeckle, E.; Riou, O.; Isambert, N.; Bompas, E.; Jafari, M.; Delcambre-Lair, C.; Saada, E.; et al. Retroperitoneal Sarcomas: Patterns of Care at Diagnosis, Prognostic Factors and Focus on Main Histological Subtypes: A Multicenter Analysis of the French Sarcoma Group. *Ann. Oncol.* **2014**, *25*, 735–742, doi:10.1093/annonc/mdt577.
216. Curis, E.; Nicolis, I.; Moinard, C.; Osowska, S.; Zerrouk, N.; Bénazeth, S.; Cynober, L. Almost All about Citrulline in Mammals. *Amino Acids* **2005**, *29*, 177, doi:10.1007/s00726-005-0235-4.
217. Curis, E.; Crenn, P.; Cynober, L. Citrulline and the Gut. *Curr Opin Clin Nutr Metab Care* **2007**, *10*, 620–626, doi:10.1097/MCO.0b013e32829fb38d.
218. Santarpia, L.; Catanzano, F.; Ruoppolo, M.; Alfonsi, L.; Vitale, D.F.; Pecce, R.; Pasanisi, F.; Contaldo, F.; Salvatore, F. Citrulline Blood Levels as Indicators of Residual Intestinal Absorption in Patients with Short Bowel Syndrome. *ANM* **2008**, *53*, 137–142, doi:10.1159/000170888.
219. Bean, G.R.; Kremer, J.C.; Prudner, B.C.; Schenone, A.D.; Yao, J.-C.; Schultze, M.B.; Chen, D.Y.; Tanas, M.R.; Adkins, D.R.; Bomalaski, J.; et al. A Metabolic Synthetic Lethal Strategy with Arginine Deprivation and Chloroquine Leads to Cell Death in ASS1-Deficient Sarcomas. *Cell Death Dis* **2016**, *7*, e2406, doi:10.1038/cddis.2016.232.
220. Kim, Y.; Kobayashi, E.; Kubota, D.; Suehara, Y.; Mukaihara, K.; Akaike, K.; Ito, A.; Kaneko, K.; Chuman, H.; Kawai, A.; et al. Reduced Argininosuccinate Synthetase Expression in Refractory Sarcomas: Impacts on Therapeutic Potential and Drug Resistance. *Oncotarget* **2016**, *7*, 70832–70844, doi:10.18632/oncotarget.12225.

8. PUBLICATIONS

1. Corona G, **Di Gregorio E**, Vignoli A, Muraro E, Steffan A, Miolo G (2021) 1H-NMR Plasma Lipoproteins Profile Analysis Reveals Lipid Metabolism Alterations in HER2-Positive Breast Cancer Patients. Cancers (Basel) 13:5845. https://doi.org/10.3390/cancers13225845

2. **Di Gregorio, E**., Miolo, G., Saorin, A., Muraro, E., Cangemi, M., Revelant, A., Minatel, E., Trovò, M., Steffan, A., Corona, G., 2021a. Radical Hemithoracic Radiotherapy Induces Systemic Metabolomics Changes That Are Associated with the Clinical Outcome of Malignant Pleural Mesothelioma Patients. Cancers 13, 508. https://doi.org/10.3390/cancers13030508

3. **Di Gregorio, E**., Miolo, G., Saorin, A., Steffan, A., Corona, G., 2021b. From Metabolism to Genetics and Vice Versa: The Rising Role of Oncometabolites in Cancer Development and Therapy. International Journal of Molecular Sciences 22, 5574. https://doi.org/10.3390/ijms22115574

4. **Di Gregorio, E**., Miolo, G., Steffan, A., Corona, G., 2020. Novel method for fast trabectedin quantification using hydrophilic interaction liquid chromatography and tandem mass spectrometry for human pharmacokinetic studies. J Pharm Biomed Anal 185, 113261. https://doi.org/10.1016/j.jpba.2020.113261

5. Miolo, G., **Di Gregorio, E**., Saorin, A., Lombardi, D., Scalone, S., Buonadonna, A., Steffan, A., Corona, G., 2020. Integration of Serum Metabolomics into Clinical Assessment to Improve Outcome Prediction of Metastatic Soft Tissue Sarcoma Patients Treated with Trabectedin. Cancers 12. https://doi.org/10.3390/cancers12071983

6. Saorin, A., **Di Gregorio, E**., Miolo, G., Steffan, A., Corona, G., 2020. Emerging Role of Metabolomics in Ovarian Cancer Diagnosis. Metabolites 10. https://doi.org/10.3390/metabo10100419

7. Vignoli, A., Muraro, E., Miolo, G., Tenori, L., Turano, P., **Di Gregorio, E**., Steffan, A., Luchinat, C., Corona, G., 2020. Effect of Estrogen Receptor Status on Circulatory Immune and Metabolomics Profiles of HER2-Positive Breast Cancer Patients Enrolled for Neoadjuvant Targeted Chemotherapy. Cancers (Basel) 12. https://doi.org/10.3390/cancers12020314

Estratto per riassunto della tesi di dottorato

L'estratto (max. 1000 battute) deve essere redatto sia in lingua italiana che in lingua inglese e nella lingua straniera eventualmente indicata dal Collegio dei docenti.
L'estratto va firmato e rilegato come ultimo foglio della tesi.

Studente: Emanuela Di Gregorio matricola: 956454

Dottorato: Scienze e tecnologie dei bio e nanomateriali

Ciclo: XXXIV

Titolo della tesi[1] : A metabolomics approach to predict trabectedin pharmacokinetics and pharmacodynamic variability in advanced soft tissue sarcoma patients

Abstract (EN):

Trabectedin is successfully used for advanced or metastatic soft tissue sarcomas (STSs) patients. However, great variability in the pharmacological response is still observed, highlighting the need for effective biomarkers of trabectedin efficacy. This study aimed to find pre-dose serum metabolomics signatures able to predict the individual variations in trabectedin pharmacokinetics (PK) as well as the overall clinical response to the treatment. The study enrolled 40 STSs patients undergoing trabectedin. Pre-dose targeted metabolomics profiles and trabectedin PK were determined by LC-MS/MS. Multivariate and univariate analyses were used to find correlations between pre-dose metabolites and PK as well as with the clinical outcome. Individual trabectedin area under the curve (AUC) showed a great variation of 34%. Multiple regression model, based on specific serum metabolites, well predicted AUC (bias of 5.16%; precision 16.85%). Moreover, metabolic signatures of trabectedin response were identified to distinguish patients in stable and progressive disease. A survival model allowed to early identify high-risk patients with low overall survival (OS $\leq$2.1 months). This translation study supports the use of metabolomics as potential tool to explain and manage the trabectedin PK variability in STSs patients and to predict the clinical response to the treatment identifying the patients who may best benefit from the trabectedin treatment.

[1] Il titolo deve essere quello definitivo, uguale a quello che risulta stampato sulla copertina dell'elaborato consegnato.

Abstract (IT):

La trabectidina è utilizzata con successo per i pazienti con sarcomi dei tessuti molli (STS) avanzati o metastatici. Tuttavia, si osserva ancora una grande variabilità nella risposta farmacologica, evidenziando la necessità di accurati biomarcatori della sua efficacia. Lo scopo dello studio è individuare caratteristiche metabolomiche nel siero in grado di prevedere sia le variazioni farmacocinetiche (PK) della trabectidina che la risposta al trattamento. Lo studio ha arruolato 40 pazienti con STS trattati con trabectidina. I profili metabolomici al basale e la farmacocinetica del farmaco sono stati determinati mediante LC-MS/MS. Analisi multivariate e univariate sono state usate per trovare correlazioni tra metaboliti e farmacocinetica nonché con l'esito clinico. L' area sotto la curva (AUC) della trabectidina ha mostrato una grande variazione del 34%. Il modello di regressione multipla, basato su specifici metaboliti sierici, ha predetto l'AUC con un errore del 5,16% e una precisione del 16,85%. Inoltre, sono state identificate caratteristiche metaboliche della risposta alla trabectidina capaci di distinguere i pazienti con malattia stabile o progressiva. Il modello di sopravvivenza ha permesso di identificare precocemente i pazienti ad alto rischio con bassa sopravvivenza (OS <2,1 mesi). Questo studio traslazionale supporta l'uso della metabolomica come potenziale strumento per spiegare e gestire la variabilità farmacocinetica della trabectidina nei pazienti con STS e per prevedere la risposta clinica al trattamento, identificando i pazienti che possono ricevere il miglior beneficio dalla terapia con trabectidina.

Firma dello studente